The Dissertation Committee for Rotimi Ayodele Ojifinni Certifies that this is the approved version of the following dissertation:

The Surface Chemistry of Atomic Oxygen Pre-covered Gold

Committee:

_____

Charles B. Mullins, Supervisor

_____

Graeme Henkelman

_____

Gyeong S. Hwang

_____

Greg O. Sitz

_____

Thomas M. Truskett

The Surface Chemistry of Atomic Oxygen Pre-covered Gold

by

Rotimi Ayodele Ojifinni, B.S.

Dissertation

Presented to the Faculty of the Graduate School of

the University of Texas at Austin

in Partial Fulfillment

of the Requirements

for the Degree of

Doctor of Philosophy

The University of Texas at Austin

May 2008

Dedication

To the three most important people in my life

Dad, Mum and Ibukun

Acknowledgements

I would like to thank Dr. Buddie Mullins (Buddie) for giving me the opportunity to work in his lab. He was magnanimous enough to allow me be the first in the lab in a number of things (the first Material Science and Engineering student and of course the first Nigerian). Buddie patiently taught me and mentored me to become not only a good scientist but a better person in everything I did. Through his affable personality, our interaction has developed over time into a great friendship. Buddie's happy attitude pervaded the lab and this allowed me to bond very well with other colleagues in the lab. I will like to thank Jinlong Gong for being such a true friend and colleague as we both worked on the "middle" chamber. Jinlong and I seemed to have developed a brotherhood as we laughed together always and frowned at the chamber occasionally. I also appreciate the opportunity to interact with the then senior students like Tae-Sang Kim and James Stiehl. They took time in teaching me so many foundational things about this research area. I really enjoyed working with Sean McClure, Minta Akin, David Flaherty, Ming Pan and Ting Yan. Even though I have a weird accent, they tried to understand me and got used to how I talked. I am really grateful for the time I spent with Dr. J.M. White of the Chemistry Department before he passed away. He motivated me to think and work hard.

I would like to thank my friends outside of the lab. Cliff Holubec became my American Dad through his fatherly love and care. Teh-Sheng Ma my brother from

Taiwan and all members of the International Students Connection (ISC). Even though they did not understand what research I was doing, they cared enough to ask how I was doing and they prayed for me all the time. Azubuike Egwuenu (even though he left me and went to make money at ExxonMobil), Babatunde Oyenekan, Babatunde Oguntade, Michael Ehiwario, Fadesola Olanegan, the McKnellys (Wayne, Rosa Lee, Melissa, Amy, James and little North), Claudia Torres-Garibay, Ezra Uzosike, Enitan Pecku, Femi Oyebola, Pastor Biodun Oladimeji, Pastor Dapo Oyewole, all encouraged me when the chips were down and the going got tough. I am so glad to have such wonderful friends who were always cheering me on to the finish line.

My deepest gratitude goes to the Almighty God for blessing me with a wonderful family who did everything to make sure that I achieve this feat. My dad and mum for their unconditional love and support. Their words of encouragement and exemplary lives of hard work are so etched in my memory that even though they were all the way in Nigeria, I feel their presence with me all through. My fiancée and best friend, Ibukunoluwa deserves this Ph.D. as much as I do because of her unwavering support. Her kind words helped me through many of the difficult times. Despite the long distance, she stuck with me without complaining. What could I have done without her? I would like to thank my aunt, Mrs. Olofinlua and her family for believing in me and urging me to start the Ph.D. I can never forget my Uncle, Dr. Lawrence Ojo for being a wonderful mentor. Finally I will like to thank my brothers, sisters, sister-in-law, brother-in-law and my nephew, Tope for always asking me when I was going to finish the Ph.D. Their asking constantly reminded me that some people cared about my finishing the Ph.D.

The Surface Chemistry of Atomic Oxygen Pre-covered Gold

Rotimi Ayodele Ojifinni, Ph.D.

The University of Texas at Austin, 2008

Supervisor: Charles B. Mullins

Gold used to be regarded as catalytically inert until about 20 years ago when it was shown that supported gold clusters < 5 nm in diameter exhibited some unique catalytic properties. Based on this revelation, several studies have demonstrated the feasibility of reactions previously thought of as impossible on gold. The ability of gold to oxidize CO below ambient temperatures at rates higher than conventional CO oxidation catalysts (Pd and Pt) has been shown to hold potentials for technological applications. Extensive past and on-going research are geared towards elucidating the mechanistic details of this reaction. The nature of the active sites, the effect of the supports and the effect of moisture are still debated in literature. I therefore present some experimental results supported with density functional theory calculations to shed additional light on some of the issues concerning gold catalysis in general, and low temperature CO oxidation in particular.

Previous studies of the effect of moisture on oxide-supported gold reported that although water promotes CO oxidation on this surface by as much as two orders of magnitude, it is only a spectator molecule on the surface. I present here evidence for strong water-oxygen interactions when water is co-adsorbed with atomic oxygen on Au(111). Impinging a CO beam on the surface co-adsorbed with oxygen and water produces water-enhanced CO oxidation. Based on these results, I propose that CO reacts with hydroxyls formed from water-oxygen interactions to form CO_2, similar to a previous observation on Pt(111).

Exposing a Au(111) surface pre-covered with ^{16}O to isotopically labeled carbon dioxide ($C^{18}O_2$) showed that $^{16}O^{18}O$ (m/e = 34) was produced from carbonate formation and decomposition. Estimates of reaction probability and activation energy gave ~ 10^{-4} - 10^{-5} and -0.15 eV respectively.

The effect of annealing on the reactivity of oxygen pre-covered Au(111) was investigated using water, carbon monoxide and carbon dioxide as probe molecules. Pre-covering Au(111) with atomic oxygen followed by annealing resulted in surfaces that were less reactive towards water, CO and CO_2. Annealing is believed to stabilize the reactive metastable oxygen thereby increasing the barrier to reaction similar to what is reported on other surfaces.

Table of Contents

List of Figures

Chapter 1: Introduction

Gold's interesting chemistry compared to other metals is evidenced by its resistance to oxidation and corrosion. It is also the most electronegative metal and it is only slightly more electropositive than non-metals such as sulfur and iodine. The extremely high ionization potential (9.22 eV) and electron affinity (2.31 eV) also differentiates gold from all other metals. Gold is the only transition metal without a stable oxide and it possesses a unique ability to interact with itself (aurophilic ability), thereby forming superstructures of gold-containing molecules. Therefore it comes as no surprise that gold has a unique chemistry with respect to catalysis and surface reactions.

The first consideration in understanding the exceptional chemistry of gold (Z = 79) is its electronic configuration. Gold has the electronic configuration $[Xe]4f^{14}5d^{10}6s^{1}$ and it is a Group 11 (1B) element, same group as copper and silver. The 5d band is regarded as the focal point of gold's chemistry as a result of relativistic effects.[1-4] Due to the large nuclear charge of gold, the s and the p orbitals (p orbitals to a lesser extent) contract while the d and f orbitals expand. The energy difference between the 5d and 6s orbitals of gold shrinks by more than 60%[2] when compared to the theoretically modeled non-relativistic case.[5] Another effect of gold's relativistic contraction is the strength of binding of the 6s electrons, which accounts for its extremely high electronegativity and innertness.[1-4]

Therefore, gold compared to other transition metals used to be universally regarded as catalytically inert or a poor catalyst at best until about 20 years ago when a Japanese scientist, Masatake Haruta showed[6] that well-prepared gold nanoparticles (NPs) are capable of some interesting catalytic reactions. Since then, there has been a growing

effort at exploiting some of this unique chemistry of gold for fundamental and industrial applications. Several reactions[7-12] have been reported in literature such as low temperature CO oxidation,[11-16] propylene epoxidation,[17-20] the water-gas shift reaction,[17,21-23] NO reduction[24], ammonia oxidation[25], hydrogenation of carbon oxides[10] and, hydrochlorination of acetylene.[26,27]

Among all these reactions, CO oxidation has received the most attention due to the exceptional activity of gold NPs at temperatures as low as 65 K.[11] Although it is generally accepted that gold clusters 2-5 nm in diameter supported on metal oxides exhibit the greatest activity,[16] many other details about this reaction are far from being completely understood. In particular, the reaction mechanism, details about the oxidation state of active gold, the effect of the metal oxide support, whether atomic or molecular oxygen is the reactive species and, the role of moisture have drawn attention from both fundamental research and technological applications point of view.

Concerning the oxidation state of gold, some authors assert that Au^{o} is the only active oxidation state[28-30] but Fu et al. proposed that Au^{x+} is responsible[17] for gold's activity while others proposed that both states may be simultaneously present.[1,31,32] Au^{x-} has also been proposed as resulting from charge transfer to gold from defect sites (on the metal oxide support).[8,33,34] Another highly debated issue is the influence of support on gold's reactivity. The interface between the gold and the metal oxide has been suggested as active site for CO oxidation[28,35-37] while other studies claim that the low-coordination sites on gold particles are the active sites for CO oxidation.[8,38]

The origin of the oxygen species responsible for CO oxidation can provide a clue to understanding the mechanism of this reaction. There are three different opinions about

the origin of the oxygen species in CO oxidation. The reaction according to the first idea [37,39] begins by molecular oxygen dissociation on low-coordination gold sites followed by CO oxidation while the metal oxide acts as a passive support for the gold NPs. The second school of thought[36,40] contends that molecular oxygen adsorbs on the support then dissociates and spills over to the gold NPs where it oxidizes CO. The third group[41,42] proposes that molecular oxygen reacts directly with CO to form an adsorbed carbonate, which later reacts with CO to form two CO_2 molecules. Previous studies from our research group have shown evidence that both atomic oxygen and molecularly chemisorbed oxygen are present during CO oxidation on TiO_2-supported gold NPs.[12,43-46]

Water plays an important role in many chemical reactions either when added intentionally or when present as moisture due to humidity in ambient reaction conditions. In either case, understanding the role of water in CO oxidation on gold has been a subject of recent research efforts. Date and co-workers[47,48] have reported that water promotes CO oxidation on Au/TiO_2 by close to two orders of magnitude. They proposed that water plays two possible roles in enhancing CO oxidation.[47,48]. The first role is the activation of molecular oxygen on gold NPs to produce atomic oxygen followed by CO oxidation by the activated oxygen. [47,48] The second role is the decomposition of carbonates formed during the reaction of CO with molecular oxygen. [47,48] Both possibilities point to the fact that water is indirectly involved in CO oxidation. However, recent studies[14,49] have emerged confirming that water enhances CO oxidation on gold but also showing that water is directly involved in the reaction.

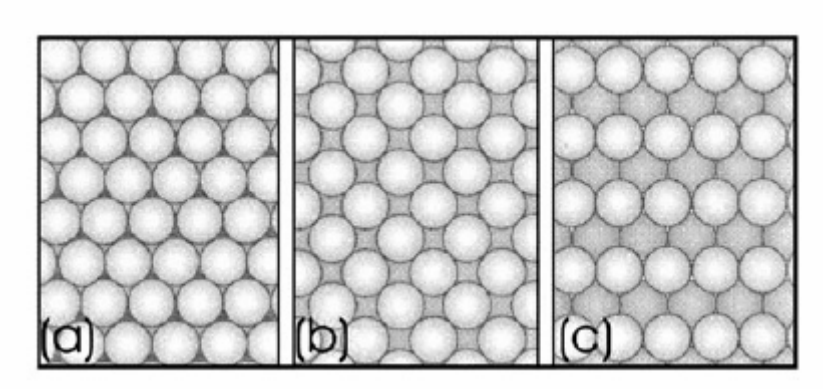

Figure 1.1: Crystal structure of the (a) (111), (b) (100) and (c) (110) of fcc gold.[5]

In light of all these controversial issues regarding CO oxidation on gold, this dissertation is a collection of studies aimed at providing more clarity on a variety of the aforementioned issues. Using a well prepared single crystal Au(111), it is possible to circumvent the support effects as well as the problem of agglomeration of gold NPs earlier reported on metal oxide supported gold NPs.[16] Another desirable characteristic of the (111) surface is that it is the most stable and by extension, the predominant surface of fcc metal NPs supported on metal oxides. Since the model system for low temperature CO oxidation is the Au/TiO_2 system, studying the single crystal Au(111) surface will provide a wealth of information that can aid in better understanding this reaction both from fundamental and technological points of view.

Figure 1.1 shows the (111), (110) and (100), the three low Miller index surfaces of face centered cubic (fcc) gold. The clean (111) surface has been well studied and it is reputed to undergo lattice reconstruction in UHV.[50] This reconstruction produces the herringbone structure, shown as a zigzag pattern that results from joining of 120^0 rotated domains (Figure 1.2).[5,50] It comprises a complex-stacking-fault domain in which both fcc and hexagonal close packed (hcp) domains are present on the surface with narrow

transition regions between them.[5,50] Although the reconstructed surface is reportedly stable up to 865 K, the extreme conditions (annealing for several hours at over 800 ^{0}C in 1 bar O_2) necessary for it to be generated makes it highly unlikely in catalytically active systems.[5] As such, I will be talking about the Au(111) surface in this work as being the unreconstructed surface.

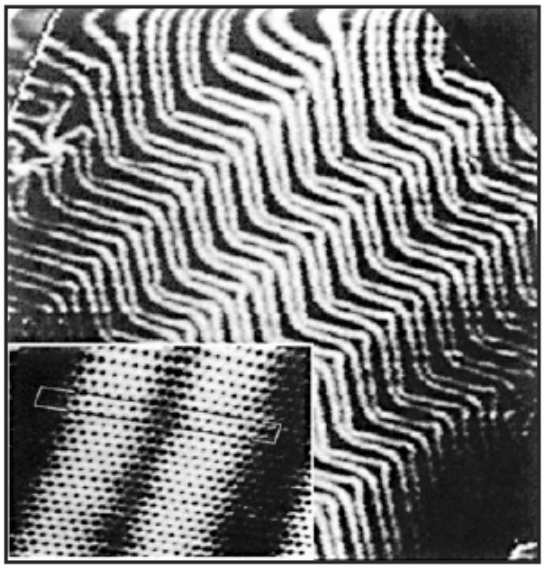

Figure 1.2: STM image of the herringbone reconstruction of Au(111)[5]

Atomic oxygen pre-covered Au(111) surfaces used for the experiments reported in this dissertation were prepared by oxygen atom deposition using a radio frequency (RF) generated plasma-jet source that produces a supersonic beam of O atoms from an 8% (vol.) O_2 in Ar gas mixture.[51-53] An oxygen dissociation fraction of ~40%, as measured by time of flight techniques, was achieved. Ions were deflected from the O-atom beam by a charged plate (biased negatively at 3000 V) located below the beam line in one of the differential pumping stages of the UHV chamber. We have previously shown that very small surface concentrations [less than 0.02 ML] of adsorbed oxygen

molecules $O_{2,a}$ are produced on the Au(111) surface from exposure to our O-atom beam source, however we reasonably neglect this species in this study because its' presence is nearly undetectable.[12,43]

Chapter 2 presents a detailed study of the role of water in the low temperature CO oxidation on atomic oxygen pre-covered Au(111). It presents both experimental results and DFT calculations **[in collaboration with Nathan S. Froemming and Dr. Graeme Henkelman]** showing that water not only acts as a promoter during CO oxidation on gold, it is directly involved in the CO oxidation reaction. It begins by presenting three experiments for water-oxygen interactions and reaction on Au(111). The first experiment shows that water thermally desorbs from the oxygen covered Au(111) at ~ 175 K (compared to desorption from clean gold at ~ 155 K). This shift in desorption temperature is indicative of the stronger binding of water on oxygen pre-covered Au(111). According to supporting DFT results, water binds to oxygen pre-covered Au(111) with a binding energy of 0.29 eV which is almost double the binding energy (0.15 eV) of water to clean Au(111). This first observation is similar to results earlier reported by Lazaga et. al. on Au(111)[54] as well as the results of a study by Outka and Madix on Au(110)[55]. The second experiment shows TPD spectra of water where a new feature in the water desorption emerges showing oxygen exchange between adsorbed atomic oxygen and adsorbed water. For instance, water TPD spectra from a Au(111) surface on which ^{18}O and $D_2{}^{16}O$ were co-adsorbed showed a new water feature ($D_2{}^{18}O$) in addition to $D_2{}^{16}O$. DFT results show very facile hydroxyl formation followed by rapid and reversible hydroxyl recombination on oxygen pre-covered Au(111). The third experiment regards the water-oxygen interaction and shows oxygen scrambling between water and adsorbed

oxygen adatoms as shown by oxygen TPD upon heating the surface. In further support of these experimental findings, DFT calculations indicate rapid diffusion of surface hydroxyl groups at temperatures as low as 75 K. The second part of Chapter 2 provides results to unambiguously show the direct involvement and promoting role of water in CO oxidation on oxygen covered Au(111) at low temperatures. Based on experimental results and DFT calculations, it is proposed that water dissociates to form hydroxyls (OH and OD) and these hydroxyls react with CO to produce CO_2. The later part of Chapter 2 addresses observed differences in water-oxygen interactions and oxygen scrambling between $^{18}O/H_2{}^{16}O$ and $^{18}O/D_2{}^{16}O$ with the "heavy" water producing less scrambling. Similar differences were also observed in water reactivity towards CO oxidation in which less CO_2 was produced with $^{16}O/D_2{}^{16}O$ than with $^{16}O/H_2{}^{16}O$.

Chapter 3 presents experimental evidence of carbonate formation and decomposition on atomic oxygen pre-covered Au(111). Results are presented showing oxygen mixing in temperature programmed desorption (TPD) measurements when a Au(111) pre-covered with ^{16}O was exposed to isotopically labeled CO_2 ($C^{18}O_2$). $^{16}O^{18}O$ production was observed when a Au(111) surface pre-covered with atomic oxygen is exposed to $C^{18}O_2$ (3-30 L) at surface temperatures ranging from 77 K to 400 K. A reaction probability on the order of 10^{-4} - 10^{-5} and an activation energy of -0.15 eV were obtained for this reaction. This low reaction probability was also alluded to as possible reasons why previous studies on Au(111)[54] and Au(110)[56] showed no appreciable surface carbonate formation and reaction.

In chapter 4, results are presented to show the effect of annealing on the reactivity of oxygen pre-covered Au(111). Although previous studies on some other surfaces.[57-61]

have shown that the reactivity of oxygen species can be characterized by its reactivity towards probe molecules, such studies have not been done on gold. The reactivity of different atomic oxygen states on Au(111) was therefore studied using isotopically labeled water ($H_2{}^{18}O$ and $D_2{}^{16}O$), carbon monoxide (CO), and oxygen-labeled carbon dioxide ($C^{18}O_2$), as probe molecules inside an ultra high vacuum (UHV) chamber. Experimental results were presented from molecular beam scattering and temperature programmed desorption (TPD) measurements showing a significant difference in reactivity at 77 K between annealed and unannealed atomic oxygen pre-covered Au(111) surfaces. The annealed surface was prepared by dosing atomic oxygen (^{16}O and ^{18}O) at 77 K, then annealing to temperatures ranging from 100 – 420 K before dosing probe molecules ($H_2{}^{18}O$, $D_2{}^{16}O$,CO and $C^{18}O_2$) at 77 K. The reactivity of oxygen with water was observed to diminish drastically due to annealing. This was observed as a reduction in the higher temperature (~ 175 K) desorption peak of water as well as a decrease in the oxygen exchange products ($^{18}O^{16}O$ and $^{18}O_2$ in the case of $^{16}O/H_2{}^{18}O$ and, $^{18}O^{16}O$ and $^{16}O_2$ in the $^{18}O/D_2{}^{16}O$ system). Progressively lower CO_2 evolution was also observed with annealing of an oxygen pre-covered Au(111) surface to higher temperatures before impinging a CO beam at 77 K. The decrease in CO_2 production was most pronounced at the highest annealing temperatures. Subsequent O_2 TPD spectra after CO titration experiments show that the oxygen adlayer becomes more unreactive towards CO as annealing temperature increases. The effect of annealing on the reaction probability for surface carbonate formation on Au(111) was also investigated. A noticeable decrease in reaction probability was observed when a Au(111) surface pre-covered with ^{16}O was pre-annealed before exposure to 30 L $C^{18}O_2$ exposure at 77 K. The reaction probability

decreased with increasing annealing temperatures with the highest decrease (a factor of ~ 10 decrease relative to the unannealed surface) observed for a surface annealed to 400 K. Chapter 4 also presents conclusions that metastable oxygen species are responsible for the reactivity observed on the unannealed surface and that annealing stabilizes these metastable oxygen species thereby reducing their reactivity.

Chapter 5 summarizes the major findings of my work and discusses their relevance to current understanding of gold catalysis in general but with particular reference to low temperature CO oxidation. I also present recommendations for future research work in these areas.

REFERENCES

(1) Bond, G. C.; Thompson, D. T. *Gold Bull.* **2000**, *33*, 41.

(2) Pitzer, K. S. *Acc. Chem. Res.* **1979**, *12*, 272.

(3) Pyykko, P. *Angew. Chem.-Int. Ed.* **2002**, *41*, 3573.

(4) Pyykko, P.; Desclaux, J. P. *Acc. Chem. Res.* **1979**, *12*, 276.

(5) Meyer, R.; Lemire, C.; Shaikhutdinov, S. K.; Freund, H. *Gold Bull.* **2004**, *37*, 72.

(6) Haruta, M.; Kobayashi, T.; Sano, H.; Yamada, N. *Chem. Lett.* **1987**, 405.

(7) Bond, G. C.; Thompson, D. T. *Catal. Rev.-Science and Engineering* **1999**, *41*, 319.

(8) Chen, M. S.; Goodman, D. W. *Science* **2004**, *306*, 252.

(9) Chen, M. S.; Kumar, D.; Yi, C. W.; Goodman, D. W. *Science* **2005**, *310*, 291.

(10) Haruta, M. *Catal. Today* **1997**, *36*, 153.

(11) Kim, T. S.; Stiehl, J. D.; Reeves, C. T.; Meyer, R. J.; Mullins, C. B. *J. Am. Chem. Soc.* **2003**, *125*, 2018.

(12) Stiehl, J. D.; Kim, T. S.; McClure, S. M.; Mullins, C. B. *J. Am. Chem. Soc.* **2004**, *126*, 13574.

(13) Gong, X. Q.; Hu, P.; Raval, R. *J. Chem.Phys.* **2003**, *119*, 6324.

(14) Kim, T. S.; Gong, J.; Ojifinni, R. A.; White, J. M.; Mullins, C. B. *J. Am. Chem. Soc.* **2006**, *128*, 6282.

(15) Min, B. K.; Wallace, W. T.; Goodman, D. W. *Surf. Sci.* **2006**, *600*, L7.

(16) Valden, M.; Lai, X.; Goodman, D. W. *Science* **1998**, *281*, 1647.

(17) Fu, Q.; Saltsburg, H.; Flytzani-Stephanopoulos, M. *Science* **2003**, *301*, 935.

(18) Hayashi, T.; Tanaka, K.; Haruta, M. *J. Catal.* **1998**, *178*, 566.

(19) Mul, G.; Zwijnenburg, A.; van der Linden, B.; Makkee, M.; Moulijn, J. A. *J. Catal.* **2001**, *201*, 128.

(20) Stangland, E. E.; Stavens, K. B.; Andres, R. P.; Delgass, W. N. *J. Catal.* **2000**, *191*, 332.

(21) Andreeva, D.; Idakiev, V.; Tabakova, T.; Ilieva, L.; Falaras, P.; Bourlinos, A.; Travlos, A. *Catal. Today* **2002**, *72*, 51.

(22) Liu, Z.-P.; Jenkins, S. J.; King, D. A. *Phys. Rev. Lett.* **2005**, *94*, 196102.

(23) Rodriguez, J. A.; Ma, S.; Liu, P.; Hrbek, J.; Evans, J.; Perez, M. *Science* **2007**, *318*, 1757.

(24) Ueda, A.; Haruta, M. *Gold Bull.* **1999**, *32*, 3.

(25) Gong, J. L.; Ojifinni, R. A.; Kim, T. S.; White, J. M.; Mullins, C. B. *J. Am. Chem. Soc.* **2006**, *128*, 9012.

(26) Nkosi, B.; Coville, N. J.; Hutchings, G. J.; Adams, M. D.; Friedl, J.; Wagner, F. E. *J. Catal.* **1991**, *128*, 366.

(27) Nkosi, B.; Adams, M. D.; Coville, N. J.; Hutchings, G. J. *J. Catal.* **1991**, *128*, 378.

(28) Bollinger, M. A.; Vannice, M. A. *Appl. Catal. B* **1996**, *8*, 417.

(29) Boyen, H. G.; Kastle, G.; Weigl, F.; Koslowski, B.; Dietrich, C.; Ziemann, P.; Spatz, J. P.; Riethmuller, S.; Hartmann, C.; Moller, M.; Schmid, G.; Garnier, M. G.; Oelhafen, P. *Science* **2002**, *297*, 1533.

(30) Lopez, N.; Norskov, J. K. *J. Am. Chem. Soc.* **2002**, *124*, 11262.

(31) Guzman, J.; Gates, B. C. *J. Phys. Chem. B* **2002**, *106*, 7659.

(32) Burke, L. D.; Nugent, P. F. *Gold Bull.* **1998**, *31*, 39.

(33) Goodman, D. W. *Catal. Lett.* **2005**, *99*, 1.

(34) Yoon, B.; Hakkinen, H.; Landman, U.; Worz, A. S.; Antonietti, J. M.; Abbet, S.; Judai, K.; Heiz, U. *Science* **2005**, *307*, 403.

(35) Ajo, H. M.; Bondzie, V. A.; Campbell, C. T. *Catal. Lett.* **2002**, *V78*, 359.

(36) Grunwaldt, J. D.; Baiker, A. *J. Phys. Chem. B* **1999**, *103*, 1002.

(37) Schubert, M. M.; Hackenberg, S.; van Veen, A. C.; Muhler, M.; Plzak, V.; Behm, R. J. *J. Catal.* **2001**, *197*, 113.

(38) Liu, Z. P.; Hu, P.; Alavi, A. *J. Am. Chem. Soc.* **2002**, *124*, 14770.

(39) Bondzie, V. A.; Parker, S. C.; Campbell, C. T. *J. Vac. Sci. Tech. A* **1999**, *17*, 1717.

(40) Bondzie, V. A.; Parker, S. C.; Campbell, C. T. *Catal Lett.* **1999**, *63*, 143.

(41) Hakkinen, H.; Landman, U. *J. Am. Chem. Soc.* **2001**, *123*, 9704.

(42) Konova, P.; Naydenov, A.; Venkov, C.; Mehandjiev, D.; Andreeva, D.; Tabakova, T. *J. Mol. Catal. A* **2004**, *213*, 235.

(43) Stiehl, J. D.; Gong, J. L.; Ojifinni, R. A.; Kim, T. S.; McClure, S. M.; Mullins, C. B. *J. Phys. Chem. B* **2006**, *110*, 20337.

(44) Stiehl, J. D.; Kim, T. S.; McClure, S. M.; Mullins, C. B. *J. Am. Chem. Soc.* **2004**, *126*, 1606.

(45) Stiehl, J. D.; Kim, T. S.; McClure, S. M.; Mullins, C. B. *J. Phys. Chem. B* **2005**, *109*, 6316.

(46) Stiehl, J. D.; Kim, T. S.; Reeves, C. T.; Meyer, R. J.; Mullins, C. B. *J. Phys. Chem. B* **2004**, *108*, 7917.

(47) Date, M.; Haruta, M. *J. Catal.* **2001**, *201*, 221.

(48) Daté, M.; Okumura, M.; Tsubota, S.; Haruta, M. *Angew. Chem. Int. Edit* **2004**, *43*, 2129.

(49) Gong, J. L.; Ojifinni, R. A.; Kim, T. S.; Stiehl, J. D.; McClure, S. M.; White, J. M.; Mullins, C. B. *Top. Catal.* **2007**, *44*, 57.

(50) Barth, J. V.; Brune, H.; Ertl, G.; Behm, R. J. *Phys. Rev. B* **1990**, *42*, 9307.

(51) Pollard, J. E. *Rev. Sci. Instru.* **1992**, *63*, 1771.

(52) Wheeler, M. C.; Reeves, C. T.; Seets, D. C.; Mullins, C. B. *J. Chem. Phys.* **1998**, *108*, 3057.

(53) Wheeler, M. C.; Seets, D. C.; Mullins, C. B. *J. Chem. Phys.* **1997**, *107*, 1672.

(54) Lazaga, M. A.; Wickham, D. T.; Parker, D. H.; Kastanas, G. N.; Koel, B. E. *ACS Symposium Series* **1993**, *523*, 90.

(55) Outka, D. A.; Madix, R. J. *J. Am. Chem. Soc.* **1987**, *109*, 1708.

(56) Outka, D. A.; Madix, R. J. *Surf. Sci.* **1987**, *179*, 351.

(57) Carley, A. F.; Davies, P. R.; Roberts, M. W. *Curr. Opin. Solid St. Mat. Sci.* **1997**, *2*, 525.

(58) Carley, A. F.; Davies, P. R.; Roberts, M. W.; Shukla, N.; Song, Y.; Thomas, K. K. *Appl. Surf. Sci.* **1994**, *81*, 265.

(59) Carley, A. F.; Davies, P. R.; Roberts, M. W.; Thomas, K. K. *Surf. Sci.* **1990**, *238*, L467.

(60) Carley, A. F.; Roberts, M. W. Unpublished results.

(61) Carley, A. F. R., S.; and Roberts, M.W. *Surf. Sci.* **1983**, *135*, 35.

Chapter 2: Water-Enhanced Low-Temperature CO Oxidation and Isotopes Effects on Atomic Oxygen Covered Au(111)

INTRODUCTION

Catalysis on gold has become increasingly more studied as a result of Haruta's pioneering work on the reactivity of gold nanoparticles (NPS).[1] Since then, several studies have shed additional light on the catalytic activity of gold.[2-48] These studies have reported interesting results regarding low temperature oxidation of carbon monoxide, propylene epoxidation, the water-gas shift reaction and the selective oxidation of ammonia as well as other important surface chemical reactions. Among these, low temperature CO oxidation is quite unique because the activity of gold catalysts cannot be matched by other metals. This low temperature activity has generated great interest and much research in metal oxide supported gold NPS. Although it is widely accepted that gold particles 2-5 nm in diameter exhibit the greatest activity,[43] research continues on the nature of the active sites for these catalysts and on details of the reaction mechanism. While some studies suggest that the perimeter interface of gold particles with the metal oxide support acts as the active site for CO oxidation, [2,4,37,49]others based on theory and gas phase cluster experiments[27,31,50] point to low coordination sites on small gold particles. The oxidation state of the active form of gold is also under debate. Some studies suggest that metallic gold[6,29] is the active form while others claim oxidic gold[18,20] is responsible for gold's chemical activity. Thus, several issues are in need of resolution to fully understand CO oxidation on gold catalysts. The {111} facet is the most stable and most prevalent configuration of most supported metal nanoparticles, therefore an

understanding of CO oxidation on Au(111) will be very useful in understanding this reaction on supported Au NPS.

This work presents both experimental results and density functional theory (DFT) calculations showing the effect of adsorbed water on CO oxidation on Au(111) pre-covered with atomic oxygen at temperatures as low as 77 K. The interaction of water with several clean single crystal metal surfaces has been reported, and a number of those systems have been shown to irreversibly dissociate water.[13,52-56] Studies of co-adsorbed water and oxygen on metal surfaces have also been reported. These latter investigations can be divided into two broad categories: those in which water does not dissociate in the presence of oxygen on the surface and those in which oxygen induces water dissociation. For those metal surfaces known to demonstrate water dissociation in the presence of co-adsorbed oxygen, it is commonly believed that the oxygen adatom abstracts a hydrogen atom from the adsorbed water molecule to form two OH groups.[57-61] In some studies, a stable water-oxygen complex was observed to be present before forming OH groups.[62-65] In most cases, OH groups adsorbed on noble metal surfaces react with sufficient heating to form water, leaving an oxygen atom on the surface. However, unless water dissociates on the *clean* metal surface, OH groups that have formed from the water-oxygen interaction do not dissociate further to adsorbed hydrogen and oxygen.[66]

While many metal surfaces exhibit oxygen induced water dissociation, there are a few cases, including Ni(111) and Ru(0001), in which water dissociation does not occur with chemisorbed oxygen atoms on the surface.[67-72] These studies have commonly noted stabilization of the molecular water by preadsorbed oxygen as evidenced by an upward shift in the water desorption temperature, but no reaction or isotopic scrambling between

water and oxygen atoms on the surface was observed. Until recently, Au(111) was also regarded as a surface upon which water did not dissociate in the presence of oxygen adatoms and, as with the other metals mentioned above, water was considered to desorb from the oxygen covered surface without reaction, leaving the original oxygen on the surface.[25] However, in an earlier, brief account[21] of some of this work, we showed evidence suggesting that oxygen covered Au(111) might dissociate water.

Addition of moisture in the feed stream to a high surface area supported Au/TiO_2 catalyst at atmospheric pressure is believed to enhance the CO oxidation reaction by as much as two orders of magnitude.[15,16] Date and Haruta[15,16] suggested that water has two possible roles during CO oxidation. First, it may promote the reaction by activating molecular oxygen on the surface to enhance CO_2 production, a fact supported by related DFT calculations by Liu et al[17]. The second possible role of water is assisting in the decomposition of carbonates that may accumulate on the surface in order to accommodate additional reactants on the surface during CO oxidation. All these hypotheses propose that water promotes CO oxidation but is not directly involved in the reaction.

Here we present evidence of oxygen exchange when water is added to an atomic oxygen pre-covered Au(111) surface, resulting in oxygen scrambling on the surface as determined via temperature programmed desorption employing isotopically labeled oxygen in select reactants. We also show that water is directly involved in CO oxidation on a Au(111) surface populated with atomic oxygen and water. We also investigate isotope effects on CO oxidation and water-oxygen interactions from using both $D_2{}^{16}O$ and $H_2{}^{16}O$.

EXPERIMENTAL

The experiments reported here were performed in an ultrahigh vacuum (UHV) molecular beam surface scattering apparatus that has been previously described in detail[22,73] but is briefly summarized here. The apparatus consists of a UHV scattering/analysis chamber and a quadruply differentially-pumped molecular beam source chamber. The scattering/analysis chamber (base pressure less than 2.0×10^{-10} Torr) is equipped with an Auger electron spectrometer (AES), low energy electron diffraction optics (LEED), and a quadrupole mass spectrometer (QMS).

The sample is a Au(111) single crystal (11mm in diameter, 1.5 mm thick) mounted to a tantalum plate that can be resistively heated and which is in thermal contact with a liquid nitrogen bath for cooling. The temperature of the surface was monitored with a type K thermocouple spot-welded to the tantalum plate. Oxygen atoms were deposited on the Au(111) surface using a radio frequency (RF) generated plasma-jet source that produces a supersonic beam of O atoms from an 8% (vol.) O_2 in Ar gas mixture.[74-76] An oxygen dissociation fraction of ~40%, as measured by time of flight techniques, was achieved. Ions were deflected from the O-atom beam by a charged plate (biased negatively at 3000 V) located below the beam line in one of the differential pumping stages. We have previously shown that very small surface concentrations [less than 0.02 ML] of adsorbed oxygen molecules $O_{2,a}$ are produced on the Au(111) surface from exposure to our O-atom beam source, however we reasonably neglect this species in this study because its' presence is nearly undetectable.[40,41]

Research purity, isotopically-labeled water [Isotec®, 97.1% $H_2{}^{18}O$ and Spectra®, 99.9% $D_2{}^{16}O$] was employed to distinguish the oxygen atom in water from oxygen atoms

used in O-atom doses [^{16}O and ^{18}O (from Matheson Trigas™ 99.999% $^{16}O_2$ and Isotec® 99.7% $^{18}O_2$ respectively)]. A typical value for the CO beam flux was ~9×10^{13} molecules / cm^2.

All of the beams (oxygen, water, and CO) were expanded from the same nozzle through the same apertures to ensure that the beam illumination "spots" on the gold sample were the same in size and coincident. Gas lines were flushed to pressures less than 3 x 10^{-2} Torr before switching gases during these experiments. This pressure allows complete purging of the line after dosing gases as determined experimentally in our laboratory. In most cases, it took about 2 - 3 minutes to purge our gas lines. Purging the line after a water dose took about 10 – 12 minutes and control experiments were performed in which we were able to determine that there was no appreciable loss of adsorbed oxygen on the gold surface during this purging time. For accuracy, we kept the same purging time between doses in all our experiments both with and without water.

The RF generator was switched on only when it was necessary to dose atomic oxygen through the nozzle. The beam spot (~3 mm in diameter) was much smaller than the sample size to minimize the effects due to other surfaces in the chamber. When necessary, the Au(111) surface was cleaned by argon ion (1 keV, 6 μA) sputtering, followed by annealing in UHV (850 K for 10 minutes), a procedure which produces a carbon-free surface as verified by AES. More routine cleaning with atomic oxygen is performed after virtually every experiment. Surface crystallinity was verified by LEED.

Oxygen coverages were estimated from the ratio of the dN(E)/dE peak heights, O(503eV)/Au(239eV) AES ratio compared to the O/Pt AES ratio of 0.3 observed for a p(2 × 2) oxygen adlayer on Pt(111) which corresponds to 3.9×10^{14} O atoms/cm^2. Using

a Au(239eV)/Pt(237eV) AES ratio of 0.95 as a conversion factor,[35] a O/Au AES ratio of 0.3 corresponds to 4.1×10^{14} oxygen atoms cm^{-2} (0.29 ML). Here, 1ML of oxygen is defined as 1.39×10^{15} atoms/cm^2 and refers to a single atomic layer of close-packed gold.

Water coverages were calculated using a mass balance on experiments in which a CO beam impinged on a water and atomic oxygen pre-covered surface and for which CO_2, H_2O, and O_2 were all accounted. For example when $H_2{}^{16}O$ was dosed for 6 seconds through the nozzle (at a pressure of 1.0 Torr) on a Au(111) surface at 77 K, the area W_1 underneath the subsequent water TPD could be integrated. The companion experiment involved precovering the Au(111) surface with 0.08 ML of ^{16}O followed by an identical 6 sec $H_2{}^{16}O$ dose with the sample at 77 K and a 30 sec $C^{16}O$ dose at 140 K, and the amount of CO_2 produced was recorded as A_1. A subsequent TPD showed that there was no atomic oxygen remaining on the surface but a small amount (~25% of the initial coverage) of $H_2{}^{16}O$ was left on the surface (the area underneath this water TPD is referred to as W_2). The same CO oxidation experiment was performed without precovering the surface with $H_2{}^{16}O$ and the amount of CO_2 produced was recorded as A_2. The quantity (A_1-A_2) represents the amount of CO_2 produced by (W_1-W_2) amount of $H_2{}^{16}O$. The value of the coverage of water represented by W_1-W_2 can be determined by multiplying the ratio (A_1-A_2)/A_2 by 0.08 ML (the O-atom coverage in both experiments). This quantity can then be multiplied by the ratio W_1/(W_1-W_2) to obtain the coverage of water corresponding to the TPD area W_1 amount of $H_2{}^{16}O$. This method produced a water coverage of 0.08 ML for a 6 sec water exposure (sample temperature of 77 K) with a nozzle pressure of 1.0 Torr.

DFT CALCULATIONS (all DFT calculations were performed by Dr. Graeme Henkelman and Nathan S. Froemming)

Calculations of the elementary steps of CO oxidation on Au(111) were performed at the density functional level of theory (DFT) using the Perdew-Wang-91 generalized gradient approximation function.[77] The core electrons of each atom were described with pseudopotentials within the projector augmented wave framework[78] as implemented in the VASP code. Kohn-Sham single-electron wavefunctions were expanded in a plane wave basis set up to a cut-off energy of 274 eV, appropriate for the pseudopotentials. Spin-polarized calculations were tested on each system, and used when required. In our slab calculations, the Au(111) surface was modeled with 4 layers, in which the bottom two layers were frozen in the equilibrium bulk face-centered-cubic (fcc) lattice positions with a lattice constant of 4.173 Å, and the top two layers were relaxed. A vacuum gap of 10 Å was used to separate the periodic slabs. Convergence with respect to the number of layers in the slab, k-point sampling, and the energy cut-off for the plane wave basis set were all checked and found to be sufficient. Coverage dependence was tested by comparing a p(2x2) slab with 4 atoms per layer, and a larger p(3x3) slab with 9 atoms per layer. A Monkhorst-Pack grid[79] of 8×8×1 for the p(2x2) and 4×4×1 for the p(3x3) slab was used to sample the Brillouin zone. Energy barriers and saddle points were calculated using the climbing-image Nudged Elastic Band [80,81] and dimer min-mode following[82,83] methods.

RESULTS

Oxygen and water interaction on Au(111)

Figure 2.1 displays TPD spectra of water [$H_2{}^{18}O$ and $D_2{}^{16}O$] from the Au(111) surface. Figure 2.1 (a) shows 0.53 ML of water [$H_2{}^{18}O$, m/e=20 and $H_2{}^{16}O$, m/e=18] desorbing from the clean Au(111) surface with a desorption peak temperature near 155 K. Water exhibits zero-order desorption kinetics from the Au(111) surface, and sub-monolayer and multilayer water cannot be clearly distinguished from each other.[84] The water desorption spectra from the clean Au(111) surface shown in Figure 2.1 (a) are similar to spectra previously reported by Kay et al.[84] Figure 2.1 (b) shows TPD spectra after exposure of 0.53 ML of $H_2{}^{18}O$ to Au(111) pre-covered by 0.18 ML of ^{16}O at 77 K. A new feature appears, at a higher temperature (near 175 K) than for the clean Au(111) surface and there is a visible decrease in intensity in the lower temperature peak. The corresponding oxygen TPD from the surface (not shown) shows mixing of the oxygen isotopes and will be discussed in detail later. Similar experiments to those in Figures 2.1(a) and (b) were performed using deuterated water ($D_2{}^{16}O$) and labeled oxygen (^{18}O) adatoms. As shown in Figures 2.1(c) and (d), the $D_2{}^{16}O/^{18}O$ results show the same general trends as the earlier results obtained using the $H_2{}^{18}O/^{16}O$ combination. We observed the formation of features at comparable temperatures for m/e=22 in Figure 2.1(d) and there is a hint of this shown in Figure 2.1(b) but the m/e=18 signal is much noisier. These features are $D_2{}^{18}O$ (m/e=22) which was formed as a result of oxygen exchange in the $^{18}O/D_2{}^{16}O$ system and $H_2{}^{16}O$ in the $^{16}O/H_2{}^{18}O$ system. The m/e=22 feature is obviously not observed in Figure 2.1(c) in which there was no adsorbed ^{18}O on

the surface prior to adding $D_2{}^{16}O$. Again, the corresponding oxygen TPD for Figure 2.1 (d) shows oxygen exchange and this will be discussed in detail immediately below.

In order to solely populate the higher temperature (175 K) water desorption peak feature, a smaller exposure (0.08 ML) of $D_2{}^{16}O$ was added to Au(111) pre-covered by 0.18 ML of oxygen of ^{18}O at 77 K as shown in figure 2.2. Interestingly, there is no water desorption from the lower temperature peak feature (155 K) in Figure 2.2 (a) which suggests that all adsorbed water molecules are interacting strongly with adsorbed atomic oxygen. The corresponding oxygen TPD is shown in Figure 2.2 (b) and will be discussed in detail later. Similar observations to those reported in Figure 2.2 were seen with the $H_2{}^{18}O/{}^{16}O$ system at comparable coverages. Figure 2.3 shows the oxygen TPD spectra from our Au(111) surface populated with (a) 0.37 ML of ^{16}O and (b) 0.53 ML of isotopically labeled water ($H_2{}^{18}O$) co-adsorbed with 0.37 ML of ^{16}O. With the oxygen atom pre-coverage alone, only $^{16}O_2$ oxygen (m/e=32) desorbs from the surface. However, when 0.53 ML of $H_2{}^{18}O$ was added to the ^{16}O covered Au(111) surface, $^{16}O^{18}O$ (m/e=34) and $^{18}O_2$ (m/e=36) both desorb from the surface in addition to mass 32. The only possible source of ^{18}O is the isotopically labeled water, $H_2{}^{18}O$. We again pre-covered the surface with 0.37 ML ^{18}O followed by TPD as shown in Figure 2.3(c). As expected, the dominant desorption feature is $^{18}O_2$ (m/e=36) with a small amount of $^{16}O^{18}O$ (m/e=34). This mass 34 is due to some oxygen exchange in our alumina (Al_2O_3) nozzle and it will be properly accounted for when quantitatively discussing oxygen scrambling on ^{18}O covered surfaces. On adding 0.53 ML $D_2{}^{16}O$ to a Au(111) surface pre-covered with 0.37 ML ^{18}O as shown in Figure 2.1d, masses 36, 34 and 32 were all produced. TPD spectra (not shown) for

higher oxygen coverages [as high as 1.3 ML] do not show any additional water desorption features.

Mass balance calculations were done to account for all the adsorbed water and oxygen. In the case of water, the area underneath the TPD spectra in each of the above [Figures 2.1-2.3] were compared with the area underneath the water TPD spectra from clean Au(111) for similar coverages. Similar mass balance calculations were done for oxygen by comparing the oxygen TPD spectra from a surface to which water was not added with the sum of the TPD areas of all oxygen-containing species (masses 32, 34 and 36) for surfaces with co-adsorbed water and oxygen. We obtained agreement within 10% for all the water-oxygen experiments reported in this work.

Our DFT calculations show that a single H_2O molecule binds to the clean Au(111) surface with a binding energy of 0.15 eV and that it is highly mobile (thus, the activation barrier for surface diffusion must be less than 0.15 eV), so that it can readily find stronger binding sites if they exist (e.g., on the O covered surface). On an oxygen pre-covered surface, H_2O forms a hydrogen-bond with the adsorbed oxygen adatom with an energy of 0.29 eV as shown in Figure 2.4 (A). From this initial state, the adsorbed atomic oxygen abstracts a hydrogen atom from the H_2O to form two hydroxyl groups on the surface. Figure 2.4 shows the mechanism of this reaction with a barrier of 0.11 eV (45 K activation temperature). The final state of this reaction is only 0.05 eV higher in energy than the initial state, so that hydroxyl formation will be very rapid and reversible between nearby H_2O and O atoms on the surface. Figure 2.5 shows the results of our computations regarding the mechanism and barrier for surface diffusion of hydroxyls on the Au(111) surface indicating rapid mobility above ~ 75 K.

CO oxidation by co-adsorbed water and atomic oxygen on Au(111)

We have recently studied and reported preliminary results from an investigation of low temperature CO oxidation on Au(111) with co-adsorbed water.[21] This expansion of our studies of low temperature CO oxidation[21,22,41] by including water as a surface coadsorbate was inspired by results in which moisture enhanced low temperature CO oxidation on metal oxide supported gold nanoclusters.[15,16]

Figure 2.6 demonstrates how CO reacts with oxygen originating from adsorbed water on Au(111) at 77 K. In Figure 2.6 (a), a beam of CO is impinged between 10 and 20 sec on a surface pre-covered by 0.11 ML of ^{16}O and, as expected, only mass 44 $C^{16}O^{16}O$ is observed during the CO impingement. In Figure 2.6 (b), the CO beam is impinged on Au(111) covered only by 0.11 ML of isotopically labeled $H_2{}^{18}O$. Without preadsorbed oxygen, CO does not interact with the adsorbed water to form carbon dioxide. In Figure 2.6 (c), 0.11 ML of $H_2{}^{18}O$ is dosed on a 0.11 ML precoverage of ^{16}O on Au(111), followed by impingement of the CO beam. In this case, in addition to mass 44 $^{16}O\ C^{16}O$, which is created from CO reacting with ^{16}O on the surface, a small amount (26% of the total CO_2 produced) of mass 46 $^{16}OC^{18}O$ is observed, indicating that oxygen (in this case, ^{18}O) originating from water is directly involved in CO oxidation (no mass 48 $^{18}OC^{18}O$ is observed). A notable feature of these QMS spectra is that the CO_2 signal decays quickly (within 2-3 sec), although the CO beam continues to strike the surface for 10 sec. Based on TPD measurements following these experiments, a considerable amount of surface oxygen remains on the surface, as well as CO. This rapid decay of CO_2 production is due to unreacted CO covering the surface, which limits further reaction at 77 K. Figures 2.6 (d) to (f) display similar results for CO oxidation with $D_2{}^{16}O$ and ^{18}O.

As expected, only mass 46 $^{18}OC^{16}O$ is produced on the surface populated with only ^{18}O prior to the CO dose [Figure 2.6 (d)] while there was no CO_2 produced from the surface populated with only $D_2{}^{16}O$ prior to the CO dose [Figure 2.6 (e)]. Figure 2.6 (f) shows that in addition to mass 46 $^{18}OC^{16}O$, mass 44 $^{16}OC^{16}O$ is produced from the surface pre-covered with both ^{18}O and $D_2{}^{16}O$ prior to the CO dose, indicating that adsorbed $D_2{}^{16}O$ or fragments of this molecule supplied oxygen (^{16}O) to oxidize CO to CO_2.

Figure 2.7 shows CO_2 evolution from gas phase CO impinging on a Au(111) surface with co-adsorbed oxygen (^{16}O) and water ($H_2{}^{18}O$)at a temperature of 77 K with various oxygen coverages. Again, the CO beam was impinged on the sample between 10 and 20 sec in these experiments. Oxygen coverages were (a) 0.08 ML, (b) 0.18 ML, (c) 0.37 ML, and (d) 0.50 ML, with 0.08 ML of water in all cases. As seen in Figure 2.7, both mass 44 and mass 46 CO_2 were produced from impinging CO on the surface. On the right, in the bar chart, the amount of CO_2 produced is shown beside the corresponding CO_2 QMS signal. The ratio of mass 46/44 CO_2 produced are shown as labels on the bar charts for each experiment. Initially, as the ^{16}O coverage increases, the mass 44 CO_2 production increases, as more oxygen becomes available on the surface. However, as the oxygen coverage reaches higher values (higher than 0.18 ML in this case), the mass 44 CO_2 production decreases with increasing oxygen coverage. The mass 46 CO_2 production demonstrates similar behavior where the CO_2 production peaks (at 0.18 ML oxygen coverage) and decreases as the amount of preadsorbed oxygen increases. With 0.50 ML of preadsorbed oxygen, very little mass 46 CO_2 is produced. With increasing oxygen pre-coverage, the ratio of mass 46/44 CO_2 decreases until it reaches 0.12 for 0.50 ML of oxygen pre-coverage. We initially attributed the trend in CO_2 production to site blocking

as the oxygen coverage increases limiting the availability of open adsorption sites on the surface for water and CO adsorption. In order to test our site blocking hypothesis, we measured the initial adsorption probability of CO on identical surfaces to the ones used for the experiments shown in Figure 2.7. Figure 2.8 (a) shows a plot of the initial CO adsorption probability as a function of varying oxygen coverages while keeping the water coverage (0.08 ML of $H_2{}^{18}O$) the same. The initial adsorption probability of CO increases with oxygen coverage at low coverages, peaks at 0.50 ML, and then decreases with further increases in coverage. In Figure 2.8 (b), 0.37 ML ^{16}O was used in all cases while varying the $H_2{}^{18}O$ coverages. The CO adsorption probability again increases with $H_2{}^{18}O$ coverage, peaks at 0.13 ML $H_2{}^{18}O$ coverage and subsequently decreases. Points 1, 2 and 3 in Figure 2.8 show a comparison of CO adsorption on clean Au(111), oxygen-covered Au(111) (0.18 ML of ^{16}O) without water, and a surface covered with both oxygen (0.18 ML) and water (0.08 ML). We observed that the initial sticking probability was greatly enhanced compared to the clean surface by precovering the surface with solely oxygen (74% increase) and even more so by precovering with both oxygen and water (94% increase) in the low coverage regime. It appears from the initial adsorption probability measurement that the observed CO oxidation trends reported in Figure 2.7 are not due to site blocking. A possible explanation for the change in reactivity at higher oxygen coverages is the formation of 3-D oxygen clusters as earlier reported by Min et al.[32] Additionally, we have measured reductions in the reactivity of oxygen overlayers on Au(111) after annealing.[85]

In order to further explore the direct involvement of water in CO_2 production, we compared the total amount of CO_2 produced from a solely oxygen covered Au(111)

surface with that of a Au(111) surface covered with both atomic oxygen and water. These experiments (shown in Figure 2.9) were performed at 140 K to prevent accumulation of adsorbed CO. This temperature is well below the maximum desorption peak temperature (175 K) for water on oxygen covered Au(111), but above the desorption peak temperature (108 K) for CO. This kept the surface coverage of CO very low by reducing the residence time of CO on the surface. Although not shown here, we note that adsorbed water alone will not oxidize CO at 140 K just as we noted for a surface temperature of 77 K as shown in Figure 2.6 (b).

In Figure 2.9 (a), a CO beam is impinged on 0.11 ML of ^{16}O at 140 K. The area underneath the curve between 10 and 40 seconds represents the amount of mass 44 CO_2 produced, as shown in the inset. As expected, no mass 46 CO_2 is detected in this case. In Figure 2.9 (b), both masses 44 CO_2 and 46 CO_2 were produced when a CO beam was impinged on the surface covered by 0.11 ML of ^{16}O and 0.14 ML of $H_2{}^{18}O$. The inset shows the total amount of CO_2 produced for each case in a bar chart, with the red bar representing mass 44 CO_2 and the blue bar representing mass 46 CO_2. Much more CO_2 [91% more in Figure 2.9(b) than in Figure 2.9 (a)] is produced when water is added to the oxygen layer on the surface prior to CO impingement. TPD experiments (not shown) following the experiment in Figure 2.9 (b) showed that ~ 0.04 ML of the initially adsorbed $H_2{}^{18}O$ is left unreacted on the surface. Similar results are obtained with the Au(111) surface pre-covered by 0.11 ML of ^{18}O and 0.14 ML of $D_2{}^{16}O$ as shown in Figures 2.9 (c) and (d).

Isotope effects on water-oxygen interactions and water enhanced CO oxidation

We investigated isotope effects in water-oxygen interactions by using atomic oxygen (^{18}O) with both water ($H_2{}^{16}O$) and deuterated water ($D_2{}^{16}O$). Figure 2.10 (a) shows water TPD spectra from a 0.18 ML ^{18}O pre-covered Au(111) surface to which a 0.27 ML of $H_2{}^{16}O$ was added at 77 K while Figure 2.10 (c) shows the corresponding oxygen TPD spectra from this surface. Both $H_2{}^{16}O$ (m/e=18) and $H_2{}^{18}O$ (m/e=20) are produced as seen in Figure 2.10 (a). 0.18 ML ^{18}O was again dosed on Au(111) at 77 K followed by the addition of 0.27 ML $D_2{}^{16}O$ with subsequent TPD producing both $D_2{}^{16}O$ (m/e=20) and $D_2{}^{18}O$ (m/e=22) as shown in Figure 2.10 (b). Figure 2.10 (d) shows the corresponding oxygen TPD spectra for this $^{18}O/D_2{}^{16}O$ case. In order to make a comparison between $H_2{}^{16}O$ and $D_2{}^{16}O$, we used water coverages that were within 6% of each other as determined by TPD and the oxygen dose experiments were in agreement to within 1%. Quantitative analysis of the TPD data in Figure 2.10 shows that $H_2{}^{18}O$ (m/e=20) accounted for 36% of the total amount of water produced in the $^{18}O/H_2{}^{16}O$ case compared to only 6% $D_2{}^{18}O$ (m/e=22) in the $^{18}O/D_2{}^{16}O$ case. Another measure of this isotope effect is the relative amount of unscrambled $^{18}O_2$ (m/e = 36) compared to the total amount of molecular oxygen on the surface during the water-oxygen interaction. The $^{18}O/H_2{}^{16}O$ case had 16% unscrambled mass 36, with most of the initial ^{18}O ending up in $H_2{}^{18}O$. However, in the $^{18}O/D_2{}^{16}O$ case, 31% unscrambled mass 36 was produced as less of the initial ^{18}O ended up in $D_2{}^{18}O$.

To investigate isotope effects in CO oxidation, three complementary CO oxidation experiments were performed. The first experiment is a precoverage of 0.08 ML ^{16}O on Au(111) at 77 K (without any pre-adsorbed water) followed by CO impingement for 30 seconds, the second experiment involved the addition of 0.08 ML of $H_2{}^{16}O$ to a 0.08 ML ^{16}O covered surface at 77 K followed by CO impingement for 30 seconds at 140 K and, the third in which 0.08 ML of $D_2{}^{16}O$ was added to a 0.08 ML ^{16}O covered surface at 77 K prior to a 30 second CO dose at 140 K as shown in Figure 2.11. We determined the amount of CO_2 produced in each case by integrating the area underneath the corresponding CO_2 QMS signal and observed that the surface with co-adsorbed $H_2{}^{16}O$ produced 24% more CO_2 than the surface with co-adsorbed $D_2{}^{16}O$. Additionally, subsequent water TPD spectra showed that 75% of the adsorbed $H_2{}^{16}O$ reacted on the surface while only 38% reacted in the case of $D_2{}^{16}O$. This could be anticipated since the experiments shown earlier in Figure 2.10 showed that less $D_2{}^{16}O$ (compared to $H_2{}^{16}O$) reacts with the adsorbed oxygen overlayer, thus making fewer adsorbed hydroxyl groups with which impinging CO can react. Comparing both cases in which water was added, we see more CO_2 produced than the surface without water. Figure 2.11 shows that 70% more CO_2 (compared with the surface without water added) is produced when $H_2{}^{16}O$ is added and 27% more CO_2 (compared with the surface without water added) is produced when $D_2{}^{16}O$ is added.

DISCUSSION

In the previous section, we presented experimental results pertaining to water strongly reacting with adsorbed atomic oxygen to produce OH groups as well as water (or OH) directly reacting with CO to produce CO_2 on the Au(111) surface. We observed an upward shift in the water desorption temperature and oxygen scrambling when atomic oxygen and water were co-adsorbed on the surface. The direct involvement of water was observed in CO oxidation by the production of $^{16}OC^{18}O$ (in addition to $^{16}OC^{16}O$) during CO impingement on a surface covered by both $H_2{}^{18}O$ and ^{16}O. We therefore present the following to further elucidate the foregoing results:

1. **Water interacts with adsorbed atomic oxygen to form either hydroxyls or a water-oxygen complex and** w**ater-oxygen interactions produce oxygen exchange between water and adsorbed oxygen.**

The formation of stable H_2O-O complexes on the surface results in an upward shift in the water desorption peak temperature [Figure 2.1 (b)] compared to water desorption from the pristine single crystal metal surface [Figure 2.1 (a)]. As alluded to previously, for the Au(111) surface, the metal-water interaction is comparable to the water-water interaction and there is no distinct monolayer water TPD feature.[84] In contrast, with the oxygen pre-covered surface, one can imagine water forming hydrogen bonds with the oxygen adlayer and binding more strongly than on the clean Au(111) surface. This observation was supported by results from our DFT calculations in which hydroxyl formation is favorable even at 45 K due to the low activation energy (0.11 eV), as seen in Figure 2.4. This higher desorption temperature feature was also observed by Lazaga *et al.*,[25] on the oxygen pre-covered Au(111) surface and it was attributed to oxygen stabilized water or recombination and disproportionation of OH groups. They

proposed that during the TPD of this surface, the H_2O-O complex decomposes to evolve water, thereby leaving the original oxygen atom on the surface.[25]

The absence of the lower temperature feature (near 155 K) with 0.08 ML $D_2{}^{16}O$ coverage in addition to 0.18 ML ^{18}O coverage as shown in Figure 2.2 (a) indicates that all adsorbed water molecules are interacting with adsorbed atomic oxygen. Similar observations (not shown) were seen with the $H_2{}^{18}O/{}^{16}O$ system at similar coverages. We propose here that all the water molecules readily formed hydroxyls on interacting with the oxygen overlayer on the Au(111) surface. However, we observed $H_2{}^{16}O$ [m/e=18 in Figure 2.1 (b) from co-adsorbed ^{16}O and $H_2{}^{18}O$] and $D_2{}^{18}O$ [m/e=22 in Figure 2.1 (d) from co-adsorbed ^{18}O and $D_2{}^{16}O$] both from the *low* temperature water desorption peak (155 K) an observation that might be explained, as mentioned earlier, by the rapid diffusion of OH groups above 75 K as determined by our DFT calculations (Figure 2.5).

A strong water-oxygen interaction resulting in oxygen scrambling between water and adsorbed oxygen atoms is shown in Figures 2.3 (a) and (b). We attribute this to OH recombination after oxygen had activated water or perhaps abstracted hydrogen from water to create OH groups. Upon heating, OH groups recombine to form water, leaving an oxygen atom on the surface. In the process, oxygen scrambling occurs just as on many other metal surfaces. We note that with only water on Au(111) (i.e., no preadsorbed oxygen), there was no indication of water dissociation or recombinative oxygen desorption near 535 K. This molecular adsorption of water without dissociation on clean Au(111) has also been previously reported in XPS and TPD experiments.[25] Outka and co-workers also observed isotope mixing when they coadsorbed ^{18}O and $H_2{}^{16}O$ on Au(110) during TPD measurements[35] and also ascribed this oxygen scrambling to either

decomposition of oxygen-stabilized water or disproportionation of surface hydroxyls. They suggest that the Brønsted base character of oxygen adatoms is sufficient to abstract an acidic hydrogen atom from the adsorbed water molecule on the group 1B metals.[35]

The presence of $^{16}O^{18}O$ in all the oxygen TPD spectra following water and oxygen ($^{16}O/H_2{}^{18}O$ and $^{18}O/D_2{}^{16}O$) exposures on Au(111) surface clearly demonstrates that the water is reacting with the oxygen overlayer. In this surface reaction, oxygen atoms in the original pre-coverage preparation get scrambled with oxygen atoms that originate in water ending up as surface atoms on Au(111) and vice-versa, and subsequently desorbing to produce $^{16}O^{18}O$. Corresponding DFT calculations indicate that there is rapid diffusion of hydroxyls at temperatures as low as 75 K (Figure 2.5), which helps explain the facile oxygen exchange between water and adsorbed oxygen atoms observed in both water desorption peaks and in the oxygen desorption.

2. Water directly enhances CO oxidation on the oxygen pre-covered Au(111) surface to produce more CO_2 than without water:

As stated in the results section, our experiments involving CO oxidation on an atomic oxygen (^{16}O) and water ($H_2{}^{18}O$) co-adsorbed Au(111) surface produced both $C^{16}O_2$ and $^{18}OC^{16}O$ [the same for the case of $^{18}O/D_2{}^{16}O$] as seen in Figure 2.6. We propose that this is due to CO reacting with either activated water or hydroxyls on the surface. Although we cannot confirm the exact nature of the activated water on the surface, we note that formation of hydroxyl groups by adding water to an oxygen overlayer on a transition metal surface at low temperature is not uncommon. Sueyoshi et al. have shown with HREELS on Cu(100), oxygen atoms can abstract hydrogen from water to form hydroxyls at temperatures as low as 100 K[86] and similar reactions may take place on Au(111). We also noted that by impinging CO directly on a Au(111) surface covered with only water,

there was no CO_2 produced further supporting the notion that water does not dissociate on clean Au(111).[25]

To further investigate water-enhanced CO oxidation, we carried out DFT calculations on reactions involving CO, O, and H_2O on the Au(111) surface. We find that there are three distinct possible reaction pathways resulting in the formation of CO_2. The CO oxidation mechanism is similar for each pathway, but they differ in regards to if and when a hydrogen atom is abstracted from the H_2O molecule by the adsorbed O atom as it oxidizes CO.

In reaction pathway I, adsorbed oxygen adatoms are hydrogen-bonded to H_2O (a spectator molecule) as they react with CO. The mechanism of this reaction, which has a barrier of 0.33 eV is depicted in Figure 2.12. This process is very similar to the oxidation of CO by an O adatom which has a somewhat lower barrier of 0.25 eV. With H_2O present, the initial state is stabilized, and the reaction barrier is increased. This pathway is consistent with the prompt but slower [than without adsorbed water] reaction of water and oxygen with CO at temperatures as low as 77 K However, this pathway does not allow for more CO_2 to be produced as is observed experimentally.

In reaction pathway II we allow adsorbed OH to be formed prior to CO oxidation [pathway II is different than pathway I in which there was no OH formation]. From the calculation graphically displayed in Figure 2.4, we know that adsorbed H_2O will react with a chemisorbed O atom, donating a hydrogen atom to form two adsorbed hydroxyl groups. The barrier for this reaction is low (0.11 eV) so that when H_2O is deposited on an oxygen pre-covered surface, adsorbed OH species are expected to form [which is consistent with our experimental observations]. Once surface OH groups are formed,

they can subsequently react with CO as shown in Figure 2.13. Formation of an OCOH intermediate occurs spontaneously when CO and isolated OH meet. The OCOH molecule is firmly bound to the surface with an energy of 1.84 eV. In order for CO_2 to form, the H atom must be transferred to the surface or to another molecule on the surface. We considered the following two possibilities:

1. The OCOH molecule undergoes a cis-trans isomerism [Figure 2.14 (A-C)] and then the hydrogen atom is abstracted by the gold surface [Figure 2.14 (D-F)]. Both processes have high barriers (0.44 eV and 0.93 eV respectively).

2 A second possibility is that the OCOH molecule transfers the hydrogen to an existing molecule on the surface. We considered a hydroxyl acceptor as shown in Figure 2.15. The OH molecule near the OCOH is shown in Figure 2.15 (A). The hydrogen transfer to OH, Figure 2.15 (B), has a much lower barrier (0.28 eV) than hydrogen transfer to the surface (0.93 eV) because the transfer distance is reduced and the products (H_2O and CO_2) are lower in energy [Figure 2.15 (C)].

Pathway III starts the same way as pathway II, with hydrogen transfer between a H_2O molecule and an oxygen adatom. The resulting two OH adspecies are held together by a hydrogen bond, so they are unlikely to diffuse away from each other at low temperature. Then, if a CO molecule diffuses to one of the OH molecules, a concerted hydrogen-transfer CO-oxidation reaction occurs as seen in Figure 2.16. The barrier for the reaction, 0.11 eV, is actually due to CO diffusion. As CO meets one of the OH adspecies, a long OCOHOH intermediate geometry is formed [Figure 2.16(C)]. Here, the middle OH dissociates to simultaneously form H_2O and CO_2. Another way of describing this

reaction is that CO oxidation with OH takes place to form CO_2 as the hydrogen from the OH transfers to a neighboring OH to form H_2O. However, this pathway cannot exclusively account for all the chemistry taking place on the surface since this mechanism is inconsistent with more CO_2 being produced with the addition of water as is observed experimentally.

The energy landscape for the above three pathways is shown in Figure 2.17. Each process has the same initial state, with O, H_2O and CO adsorbed on Au(111) in that order. The zero of energy is a clean surface and CO, $\frac{1}{2}O_2$, and H_2O in the gas phase. In both pathways I and II, the molecules get trapped in intermediate minima from which barriers of 0.33 eV and 0.28eV respectively, must be overcome to form CO_2. In pathway III, no such low-energy intermediate is formed and the overall CO oxidation reaction has a barrier of 0.11 eV and can occur at temperatures as low as 45 K. This is consistent with our experimental observation in which CO oxidation in the presence of water readily occurs at T_s=77 K. It is also worthwhile to state here that our observed experimental results are likely occurring due to a combination of two or more of the above reaction pathways described by DFT calculations.

It may be useful to compare the chemistry reported here with the water-gas-shift reaction (WGS). The WGS is a reversible, exothermic reaction of carbon monoxide and water. Two possible mechanisms have been proposed for this reaction.[87] The first mechanism is the associative mechanism,[88-90] with the following reaction steps:

$$CO_{gas} \rightarrow CO_{ads} \quad (1)$$
$$H_2O_{gas} \rightarrow H_2O_{ads} \quad (2)$$
$$H_2O_{ads} \rightarrow OH_{ads} + H_{ads} \quad (3)$$
$$CO_{ads} + OH_{ads} \rightarrow HCOO_{ads} \quad (4)$$
$$HCOO_{ads} \rightarrow CO_{2,gas} + H_{ads} \quad (5)$$
$$2H_{ads} \rightarrow H_{2,gas} \quad (6)$$

The process indicates that the hydroxyl group from water dissociation combines with CO to form a formate intermediate, which then decomposes into CO_2 and hydrogen. Formate dissociation is regarded as the rate-determining step in the associative mechanism of the water-gas shift reaction. The second mechanism is the redox mechanism[91,92] in which CO directly reacts with adsorbed oxygen to form CO_2 following the complete dissociation of water into atomic oxygen and molecular hydrogen as follows:

$$CO_{gas} \rightarrow CO_{ads} \quad (1)$$
$$H_2O_{gas} \rightarrow H_2O_{ads} \quad (2)$$
$$H_2O_{ads} \rightarrow H_{2,gas} + O_{ads} \quad (3)$$
$$CO_{ads} + O_{ads} \rightarrow CO_{ads} \quad (4)$$
$$HOCO_{ads} \rightarrow CO_{2,gas} \quad (5)$$

A recent study[93] has reported the high performance of TiO_2-x/Au(111) and CeO_2-x/Au(111) catalysts in the water-gas shift (WGS) reaction. This study claims that although clean Au(111) is not catalytically active for the WGS, Au(111) surfaces that are 20 to 30% covered by ceria or titania nanoparticles have activities comparable to those of good WGS catalysts such as Cu(111) or Cu(100).[93] The reaction is said to occur by water dissociating on O vacancies of the oxide nanoparticles while CO adsorbs on Au sites located nearby, and subsequent reaction steps take place at the metal-oxide interface.[93] The following was proposed[93] as the reaction mechanism based on DFT calculations:

$$CO_{gas} \rightarrow CO_{ads} \quad (1)$$
$$H_2O_{gas} \rightarrow H_2O_{ads} \quad (2)$$
$$H_2O_{ads} \rightarrow OH_{ads} + H_{ads} \quad (3)$$
$$CO_{ads} + OH_{ads} \rightarrow HOCO_{ads} \quad (4)$$
$$HOCO_{ads} \rightarrow CO_{2,gas} + H_{ads} \quad (5)$$
$$2H_{ads} \rightarrow H_{2,gas} \quad (6)$$

Erdohelyi and co-workers' infrared spectroscopy study of the reaction of CO with water over catalysts composed of iridium supported on oxides (MgO, Al_2O_3, SiO_2 and TiO_2) revealed that formate, in agreement with the associative mechanism above is the reaction intermediate.[94] Formate ions were observed as new IR bands at 1590cm^{-1} and 1380 cm^{-1} (at 473 K) and were assigned to the asymmetric and symmetric O-C-O stretching vibrations of the absorbed formate ion.[94] A recent density functional theory calculation of CO reaction with water on $Pt_2Mo(111)$ showed that water dissociation into H_{ad} and OH_{ad} was followed by CO reaction with the hydroxyl to form COOH which later decomposes to CO_2 and H_{ad} in the forward reaction or CO and OH_{ad} in the reverse reaction.[95] The associative mechanism with a COOH intermediate is a plausible reaction on Au(111) as well with the only difference being reaction step 2 where atomic oxygen abstracts a hydrogen from water to form surface hydroxyls. The redox mechanism is very unlikely on Au(111) because it is not known to completely dissociate water to hydrogen and oxygen.[66]

The reaction of CO and OH to form CO_2 is widely studied in gas phase chemistry, due to the pivotal role of OH radicals in atmospheric chemistry.[96,97] Many other investigations of CO and OH reactions on metal surfaces are motivated by electrochemistry.[98-100] One relevant study regarding the reaction of adsorbed CO and OH on Pt(111) under UHV conditions performed by Bergeld et al.[98] showed that water can promote CO oxidation on oxygen covered Pt(111). They observed that a new CO_2 desorption feature near 200 K appears when water is co adsorbed prior to temperature programmed reaction of a Pt(111) surface populated with CO and atomic oxygen. This new peak occurs at a much lower temperature than does the CO_2 desorption peak (~300

K) for a typical surface reaction between CO and oxygen adatoms on Pt(111), and it has been attributed to CO reacting with OH groups on the surface. A similar reaction may occur on Au(111), in which hydroxyls are formed from water splitting and reacting with CO to form CO_2 at 77 K. Related calculations performed by Gong et al. demonstrated that on Pt(111), CO_2 formation is likely to follow a mechanism in which CO first reacts with OH to form surface COOH, followed by this COOH reacting with OH to form CO_2 and H_2O.[101]

Our observation that much more CO_2 is produced when water is added to the oxygen layer on the surface (Figure 2.9 insets) is similar to what Bergeld et al. observed on Pt(111),where they demonstrated the promotional effect of water on CO oxidation.[98] Based on our TPD measurements after CO impingement at 140 K (not shown here), no detectable amount of oxygen remained on the surface. However, a small amount (~ 0.04 ML of the initial $H_2{}^{18}O$) was observed during the reaction. CO oxidation on a surface covered with ^{18}O and $D_2{}^{16}O$ showed similar observations [Figures 2.9 (c) and (d)] and again we speculate that activated water or OD from $D_2{}^{16}O$ is responsible for CO oxidation. We might expect a difference in the rate of CO_2 production due to a kinetic isotope effect on CO oxidation as a result of the OH versus OD bond, and this is discussed later in this paper. As mentioned earlier, the total amount of CO_2 produced when water is added to the oxygen pre-covered surface increases. This is a clear indication that water contributes some additional oxygen for CO oxidation and that water does not simply exchange oxygen atoms with adsorbed oxygen on the surface. A simple oxygen exchange would result in the same CO_2 production on both surfaces (i.e. with and without water) since there would be the same amount of adsorbed oxygen atoms.

It is also possible to argue that this additional CO_2 is produced from additional oxygen atoms created by complete dissociation of water on the oxygen covered surface. In this case, water may lose a hydrogen atom to a nearby oxygen atom and the resulting OH groups further dissociate on the surface to leave oxygen atoms on the surface. However, it is well known that on metals that do not dissociate water on their clean surfaces [and this group includes the Au(111) surface], OH dissociation is not favored over two OH groups recombining to form one water leaving an oxygen atom on the surface.[66] Consequently we rule out the likelihood of additional oxygen on the surface due to complete dissociation of water as being responsible for the additional CO_2 produced on the surface. This is consistent with our DFT calculations showing that the dissociation of OH on Au(111) is endothermic by 1.33 eV, and hence not activated below room temperature. However, in our attempts to account for all the adsorbed species, we did not detect molecular hydrogen or hydrogen containing species, such as H_2CO, HCOOH, during CO impingement reaction or subsequent TPD measurements. A residual gas analysis during one of the experiments did not show molecular hydrogen or any other hydrogen containing species different from those in the UHV background. Previous works[15,16,98] have also reported that no molecular hydrogen was detected in water assisted CO oxidation reactions. We speculate that hydrogen atoms released on the surface during reaction recombine and desorb at a rate that is undetectable.

3. Differences in reactivity of $H_2{}^{16}O$ and $D_2{}^{16}O$ with oxygen (^{18}O), and the relative CO_2 production with H_2O and $D_2{}^{16}O$ are indicative of kinetic isotope effects.

The observed decrease in oxygen scrambling in the $^{18}O/D_2{}^{16}O$ system compared to the $^{18}O/H_2{}^{16}O$ system (Figure 2.10) is likely due to a kinetic isotope effect in water-

oxygen interactions during the formation of hydroxyls or a water-oxygen complex. Formation of $H_2{}^{18}O$ will be favored over $D_2{}^{18}O$ under identical reaction conditions since the O-H bond is weaker than O-D bond due to zero-point energy differences. There was a higher degree of oxygen scrambling when ^{18}O and $H_2{}^{16}O$ were co-adsorbed on the surface with only 16% of the total $^{18}O_2$ remaining unscrambled compared to 31% unscrambled $^{18}O_2$ when ^{18}O and $D_2{}^{16}O$ were co-adsorbed on the surface.

The fact that CO oxidation on the surface with the $^{16}O/H_2O$ ad-mixture produced ~24% more CO_2 than the one with the $^{16}O/D_2{}^{16}O$ ad-mixture also suggest kinetic isotope effects in water-enhanced CO_2 production as shown in Figure 2.11. As mentioned earlier, the surface with OH groups produced 70% more CO_2 than the surface without any water while the surface with OD groups produced only 27% more CO_2 than the surface without any water added, also shown in Figure 2.11. However, it is likely that there are fewer OD species on the surface than OH species based on the observation that 75% of the initial H_2O coverage reacted on the $^{16}O/H_2O$ surface while only 38% of the initial $D_2{}^{16}O$ reacted in the case of the $^{16}O/D_2{}^{16}O$ ad-mixture as seen from water TPD data (not shown) following the experiments in Figure 2.11. Thus, it is difficult to construct a consistent experiment with which the CO reactivity of adsorbed OH could be compared with OD.

Kinetic isotope effects were observed by Wieckowski[102] between H_2O and D_2O in HCOOH and CH_3OH adsorption and oxidation on platinum electrodes in a sulfuric acid electrolyte. This study attributed the observed kinetic isotope effects in the oxidation of methanol and formic acid to adsorbed water ($H_2{}^{16}O$ and $D_2{}^{16}O$) molecules being the direct source of oxygen-containing species involved in the oxidation of methanol.[102] Based on transition state theory, the observation of a kinetic isotope effect in a reaction is

suggestive that the isotopic specie is directly involved in the rate determining step.[103] Our current results provide strong evidence that water interacts with adsorbed oxygen to form OH and OD groups, which then reacts with impinging CO molecules to form CO_2.

CONCLUSIONS

Previous studies have proposed that although water promotes CO oxidation, it is not directly involved in the reaction. However, we have presented unambiguous experimental evidence supported by DFT results that water promotes CO oxidation on Au(111) by directly reacting with adsorbed oxygen adatoms to form OH groups followed by OH reacting with CO to form CO_2.

The initial step in this reaction is the interaction of water with oxygen atoms preadsorbed on Au(111). We observed that water strongly interacts with oxygen atoms leading to the activation of water to form a water-oxygen complex or hydroxyls as evidenced by a new TPD feature with its' peak near 175 K, in addition to the water desorption feature at 155K characteristic of water desorption without oxygen pre-adsorbed on the Au(111) surface. Supporting evidence from DFT calculations show that hydroxyls are readily formed by water on oxygen pre-covered Au(111) due to the small activation barrier of 0.11 eV. Water-oxygen interactions also produce oxygen scrambling on the Au(111) surface as evidenced from isotopic mixing in the oxygen evolution in TPD measurements. Here oxygen atoms from adsorbed water exchange with adsorbed oxygen adatoms on the Au(111) surface likely due to rapid diffusion of OH groups with subsequent reversible reactions between two nearby adsorbed hydroxyl groups to adsorbed water and oxygen.

We noted that labeled oxygen from water, for example $H_2{}^{18}O$, is observed as evolving $^{18}OC^{16}O$ after $C^{16}O$ impingement on a Au(111) surface covered with both oxygen and isotopically labeled water suggesting that water is directly involved in the oxidation of CO on this surface. DFT calculations also showed that in the presence of

H_2O, the barrier for CO oxidation for a select pathway is reduced to 0.11 eV compared to 0.25 eV for CO oxidation on oxygen pre-covered Au(111) without H_2O. This reduction is attributed to a concerted hydrogen transfer from one hydroxyl to another that acts to stabilize the transition state for CO oxidation, and promote CO oxidation at temperatures as low as 45 K. However, DFT calculations suggest that more than one reaction pathway is involved in the oxidation of CO by Au(111) with co-adsorbed oxygen adatoms and water since experimentally we observe that 70-80% of that water is consumed in this reaction.

Finally, kinetic isotope effects were observed in water-oxygen interactions as well as in water enhanced CO oxidation with $H_2{}^{16}O$ showing higher reactivity in both cases than $D_2{}^{16}O$. Based on all these results, we propose that OH or OD groups formed from water interacting with atomic oxygen on Au(111) are responsible for the promotional effect in oxidizing CO to produce CO_2 on the surface.

REFERENCES

All DFT calculations used in this paper were performed by Dr. Graeme Henkelman and Nathan S. Froemming.

(1) Haruta, M.; Kobayashi, T.; Sano, H.; Yamada, N. *Chem. Lett.* **1987**, 405.
(2) Ajo, H. M.; Bondzie, V. A.; Campbell, C. T. *Catal. Lett.* **2002**, *V78*, 359.
(3) Andreeva, D.; Idakiev, V.; Tabakova, T.; Ilieva, L.; Falaras, P.; Bourlinos, A.; Travlos, A. *Catal. Today* **2002**, *72*, 51.
(4) Bollinger, M. A.; Vannice, M. A. *Appl. Catal. B* **1996**, *8*, 417.
(5) Bond, G. C.; Thompson, D. T. *Catal. Rev.* **1999**, *41*, 319.
(6) Boyen, H. G.; Kastle, G.; Weigl, F.; Koslowski, B.; Dietrich, C.; Ziemann, P.; Spatz, J. P.; Riethmuller, S.; Hartmann, C.; Moller, M.; Schmid, G.; Garnier, M. G.; Oelhafen, P. *Science* **2002**, *297*, 1533.
(7) Chen, M. S.; Goodman, D. W. *Science* **2004**, *306*, 252.
(8) Chen, M. S.; Goodman, D. W. *Acc. Chem. Res.* **2006**, *39*, 739.
(9) Chen, M. S.; Kumar, D.; Yi, C. W.; Goodman, D. W. *Science* **2005**, *310*, 291.
(10) Choudhary, T. V.; Goodman, D. W. *Top. Catal.* **2002**, *21*, 25.
(11) Choudhary, T. V.; Goodman, D. W. *App. Catal. A* **2005**, *291*, 32.
(12) Chusuei, C. C.; Lai, X. F.; Davis, K. A.; Bowers, E. K.; Goodman, D. W.; Omary, M. A.; Rawashdeh-Omary, M. A.; Fackler, J. P.; Bagus, P. S. *Abstracts of Papers of the American Chemical Society* **2000**, *220*, U237.
(13) Crowell, J. E.; Chen, J. G.; Hercules, D. M.; Yates, J. J. T. *J. Chem. Phys.* **1987**, *86*, 5804.
(14) Daniells, S. T.; Makkee, M.; Moulijn, J. A. *Catal. Lett.* **2005**, *100*, 39.
(15) Date, M.; Haruta, M. *J. Catal.* **2001**, *201*, 221.
(16) Daté, M.; Okumura, M.; Tsubota, S.; Haruta, M. *Angew. Chem. Int. Edit* **2004**, *43*, 2129.
(17) Liu, L. M.; McAllister, B.; Ye, H. Q.; Hu, P. *J. Am. Chem. Soc.* **2006**, *128*, 4017.
(18) Fu, Q.; Saltsburg, H.; Flytzani-Stephanopoulos, M. *Science* **2003**, *301*, 935.
(19) Hayashi, T.; Tanaka, K.; Haruta, M. *J. Catal.* **1998**, *178*, 566.
(20) Hodge, N. A.; Kiely, C. J.; Whyman, R.; Siddiqui, M. R. H.; Hutchings, G. J.; Pankhurst, Q. A.; Wagner, F. E.; Rajaram, R. R.; Golunski, S. E. *Catal. Today* **2002**, *72*, 133.
(21) Kim, T. S.; Gong, J.; Ojifinni, R. A.; White, J. M.; Mullins, C. B. *J. Am. Chem. Soc.* **2006**, *128*, 6282.
(22) Kim, T. S.; Stiehl, J. D.; Reeves, C. T.; Meyer, R. J.; Mullins, C. B. *J. Am. Chem. Soc.* **2003**, *125*, 2018.
(23) Kolmakov, A.; Goodman, D. W. *Catal. Lett.* **2000**, *70*, 93.
(24) Kolmakov, A.; Goodman, D. W. *Surf. Sci.* **2001**, *490*, L597.
(25) Lazaga, M. A.; Wickham, D. T.; Parker, D. H.; Kastanas, G. N.; Koel, B. E. *ACS Symposium Series* **1993**, *523*, 90.
(26) Lin, S. D.; Bollinger, M.; Vannice, M. A. *Catal. Lett.* **1993**, *17*, 245.
(27) Liu, Z. P.; Hu, P.; Alavi, A. *J. Am. Chem. Soc.* **2002**, *124*, 14770.
(28) Liu, Z.-P.; Jenkins, S. J.; King, D. A. *Phys. Rev. Lett.* **2005**, *94*, 196102.
(29) Lopez, N.; Norskov, J. K. *J. Am. Chem. Soc.* **2002**, *124*, 11262.
(30) Luo, K.; Kim, D. Y.; Goodman, D. W. *J. Mol. Catal. A-Chem* **2001**, *167*, 191.

(31) Mills, G.; Gordon, M. S.; Metiu, H. *J. Chem. Phys.* **2003**, *118*, 4198.
(32) Min, B. K.; Alemozafar, A. R.; Pinnaduwage, D.; Deng, X.; Friend, C. M. *J. Phys. Chem. B* **2006**, *110*, 19833.
(33) Min, B. K.; Wallace, W. T.; Goodman, D. W. *Surf. Sci.* **2006**, *600*, L7.
(34) Mul, G.; Zwijnenburg, A.; van der Linden, B.; Makkee, M.; Moulijn, J. A. *J. Catal.* **2001**, *201*, 128.
(35) Outka, D. A.; Madix, R. J. *J. Am. Chem. Soc.* **1987**, *109*, 1708.
(36) Outka, D. A.; Madix, R. J. *Surf. Sci.* **1987**, *179*, 351.
(37) Schubert, M. M.; Hackenberg, S.; van Veen, A. C.; Muhler, M.; Plzak, V.; Behm, R. J. *J. Catal.* **2001**, *197*, 113.
(38) Schumacher, B.; Plzak, V.; Kinne, M.; Behm, R. J. *Catal. Lett.* **2003**, *V89*, 109.
(39) Stangland, E. E.; Stavens, K. B.; Andres, R. P.; Delgass, W. N. *J. Catal.* **2000**, *191*, 332.
(40) Stiehl, J. D.; Gong, J. L.; Ojifinni, R. A.; Kim, T. S.; McClure, S. M.; Mullins, C. B. *J. Phys. Chem. B* **2006**, *110*, 20337.
(41) Stiehl, J. D.; Kim, T. S.; McClure, S. M.; Mullins, C. B. *J. Am. Chem. Soc.* **2004**, *126*, 13574.
(42) Tsubota, S.; Cunningham, D. A. H.; Bando, Y.; Haruta, M. Preparation of nanometer gold strongly interacted with TiO2 and the structure sensitivity in low-temperature oxidation of CO. In *Preparation of Catalysts Vi*, 1995; Vol. 91; pp 227.
(43) Valden, M.; Lai, X.; Goodman, D. W. *Science* **1998**, *281*, 1647.
(44) Wallace, W. T.; Min, B. K.; Goodman, D. W. *J. Mol. Catal. A* **2005**, *228*, 3.
(45) Wang, Z. L.; Gao, R. P.; Nikoobakht, B.; El-Sayed, M. A. *J. Phys. Chem. B* **2000**, *104*, 5417.
(46) Yan, Z.; Chinta, S.; Mohamed, A. A.; Fackler, J. P.; Goodman, D. W. *Catal. Lett.* **2006**, *111*, 15.
(47) Meyer, R.; Lemire, C.; Shaikhutdinov, S. K.; Freund, H. *Gold Bull.* **2004**, *37*, 72.
(48) Gong, J. L.; Ojifinni, R. A.; Kim, T. S.; White, J. M.; Mullins, C. B. *J. Am. Chem. Soc.* **2006**, *128*, 9012.
(49) Grunwaldt, J. D.; Baiker, A. *J. Phys. Chem. B* **1999**, *103*, 1002.
(50) Xu, Y.; Mavrikakis, M. *J. Phys. Chem. B* **2003**, *107*, 9298.
(51) Baltrusaitis, J.; Schuttlefield, J. D.; Zeitler, E.; Jensen, J. H.; Grassian, V. H. *J. Phys. Chem. C* **2007**, *111*, 14870.
(52) Baro, A. M.; Erley, W. *J. Vac. Sci. Tech.* **1982**, *20*, 580.
(53) Callen, B. W.; Griffiths, K.; Norton, P. R.; Harrington, D. A. *J. Phys. Chem. B* **1992**, *96*, 10905.
(54) Jiang, P.; Zappone, M. W.; Bernasek, S. L.; Robertson, J. A. *J. Vac. Sci. Tech. A* **1996**, *14*, 2372.
(55) Shao, Y.; Paul, J. *Appl. Surf. Sci.* **1993**, *72*, 113.
(56) Spitzer, A.; Luth, H. *Surf. Sci.* **1985**, *160*, 353.
(57) Au, C. T.; Carley, A. F.; Pashuski, A.; Read, S.; Roberts, M. W.; Zeini-Isfahan, A. *Springer Series in Surface Sciences* **1993**
33, 241.
(58) Bedurftig, K.; Volkening, S.; Wang, Y.; Wintterlin, J.; Jacobi, K.; Ertl, G. *J. Chem. Phys.* **1999**, *111*, 11147.
(59) Creighton, J. R.; White, J. M. *Surf. Sci.* **1984**, *136*, 449.

(60) Klaua, M.; Madey, T. E. *Surf. Sci.* **1984**, *136*, L42.
(61) Seitsonen, A. P.; Zhu, Y.; Bedurftig, K.; Over, H. *J. Am. Chem. Soc.* **2001**, *123*, 7347.
(62) Bange, K.; Madey, T. E.; Sass, J. K.; Stuve, E. M. *Surf. Sci.* **1987**, *183*, 334.
(63) Fisher, G. B.; Sexton, B. A. *Phys. Rev. Lett.* **1980**, *44*, 683.
(64) Kubota, J.; Kondo, J.; Domen, K.; Hirose, C. *Surf. Sci.* **1993**, *295*, 169.
(65) Nyberg, C.; Tengstl, C. G. *J. Chem. Phys.* **1984**, *80*, 3463.
(66) Henderson, M. A. *Surf. Sci. Rep.* **2002**, *46*, 1.
(67) Doering, D. L.; Madey, T. E. *Surf. Sci.* **1982**, *123*, 305.
(68) Kretzschmar, K.; Sass, J. K.; Hofmann, P.; Ortega, A.; Bradshaw, A. M.; Holloway, S. *Chem. Phys. Lett.* **1981**, *78*, 410.
(69) Madey, T. E.; Yates, J. J. T. *Chem. Phys. Lett.* **1977**, *51*, 77.
(70) Pache, T.; Steinruck, H. P.; Huber, W.; Menzel, D. *Surf. Sci.* **1989**, *224*, 195.
(71) Schulze, M.; Reißner, R.; Bolwin, K.; Kuch, W. *Fresenius J. Anal. Chem.* **1995**, *V353*, 661.
(72) Thiel, P. A.; Hoffmann, F. M.; Weinberg, W. H. *Phys. Rev. Lett.* **1982**, *49*, 501.
(73) Wheeler, M. C.; Seets, D. C.; Mullins, C. B. *J. Chem. Phys.* **1996**, *105*, 1572.
(74) Pollard, J. E. *Rev. Sci. Instru.* **1992**, *63*, 1771.
(75) Wheeler, M. C.; Reeves, C. T.; Seets, D. C.; Mullins, C. B. *J. Chem. Phys.* **1998**, *108*, 3057.
(76) Wheeler, M. C.; Seets, D. C.; Mullins, C. B. *J. Chem. Phys.* **1997**, *107*, 1672.
(77) Perdew, J. P. *Electronic structure of solids*Berlin, 1991.
(78) Kresse, G.; Joubert, D. *Phys. Rev. B* **1999**, *59*, 1758.
(79) Monkhorst, H. J.; Pack, J. D. *Phys. Rev. B* **1976**, *13*, 5188.
(80) Henkelman, G.; Jonsson, H. *J. Chem. Phys.* **2000**, *113*, 9978.
(81) Henkelman, G.; Uberuaga, B. P.; Jonsson, H. *J. Chem. Phys.* **2000**, *113*, 9901.
(82) Henkelman, G.; Jonsson, H. *J. Chem. Phys.* **1999**, *111*, 7010.
(83) Olsen, R. A.; Kroes, G. J.; Henkelman, G.; Arnaldsson, A.; Jonsson, H. *J. Chem. Phys.* **2004**, *121*, 9776.
(84) Kay, B. D.; Lykke, K. R.; Creighton, J. R.; Ward, S. J. *J. Chem. Phys.* **1989**, *91*, 5120.
(85) Ojifinni, R. A.; Gong, J. L.; Kim, T. S.; Mullins, C. B. *In preparation*.
(86) Sueyoshi, T.; Sasaki, T.; Iwasawa, Y. *J. Phys. Chem. B* **1997**, *101*, 4648.
(87) Gorte, R. J.; Zhao, S. *Catal. Today* **2005**, *104*, 18.
(88) Grenoble, D. C.; Estadt, M. M.; Ollis, D. F. *J. Catal.* **1981**, *67*, 90.
(89) Salmi, T.; Hakkarainen, R. *Appl. Catal.* **1989**, *49*, 285.
(90) Vanherwijnen, T.; Dejong, W. A. *J. Catal.* **1980**, *63*, 83.
(91) Bunluesin, T.; Gorte, R. J.; Graham, G. W. *Appl. Catal. B* **1998**, *15*, 107.
(92) Chinchen, G. C.; Spencer, M. S. *J. Catal.* **1988**, *112*, 325.
(93) Rodriguez, J. A.; Ma, S.; Liu, P.; Hrbek, J.; Evans, J.; Perez, M. *Science* **2007**, *318*, 1757.
(94) Erdohelyi, A.; Fodor, K.; Suru, G. *App. Catal. A* **1996**, *139*, 131.
(95) Wang, J. G.; Hammer, B. *J. Catal.* **2006**, *243*, 192.
(96) Lester, M. I.; Pond, B. V.; Anderson, D. T.; Harding, L. B.; Wagner, A. F. *J. Chem. Phys.* **2000**, *113*, 9889.

(97) Rockmann, T.; Brenninkmeijer, C. A. M.; Saueressig, G.; Bergamaschi, P.; Crowley, J. N.; Fischer, H.; Crutzen, P. J. *Science* **1998**, *281*, 544.
(98) Bergeld, J.; Kasemo, B.; Chakarov, D. V. *Surf. Sci.* **2001**, *495*, L815.
(99) Hayden, B. E.; Rendall, M. E.; South, O. *J. Am. Chem. Soc.* **2003**, *125*, 7738.
(100) Lei, T.; Zei, M. S.; Ertl, G. *Surf. Sci.* **2005**, *581*, 142.
(101) Gong, X. Q.; Hu, P.; Raval, R. *J. Chem.Phys.* **2003**, *119*, 6324.
(102) Wieckowski, A. *J. Electroanal. Chem.* **1977**, *78*, 229.
(103) Melander, L.; Saunders, W. H. J. *Reaction Rates of Isotopic Molecules*, 2nd ed.; Wiley, New York, 1980.

Figure 2.1

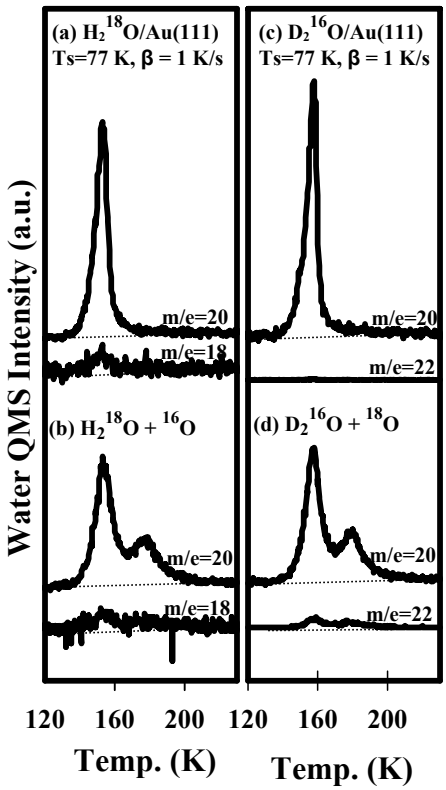

Figure 2.1: TPD of $H_2{}^{18}O$ (m/e=20) and $H_2{}^{16}O$ (m/e=18) from (a) 0.53 ML of $H_2{}^{18}O$ on clean Au(111) surface, (b) 0.53 ML of $H_2{}^{18}O$ on 0.18 ML of ^{16}O covered Au(111) surface, and TPD of D_2O (m/e=20) and $D_2{}^{18}O$ (m/e=22) from (c) 0.53 ML of D_2O on clean Au(111) surface, (d) 0.53 ML of D_2O on 0.18 ML of ^{18}O covered Au(111) surface. All isotopically labeled water and oxygen atoms were dosed at 77 K. Heating rate of β = 1 K/s was used.

Figure 2.2

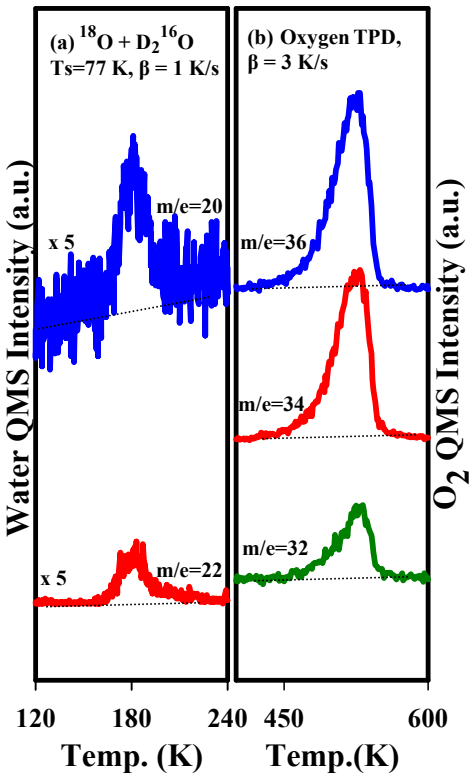

Figure 2.2: TPD of (a) $D_2{}^{16}O$ (m/e=20) and $D_2{}^{18}O$ (m/e=22); and (b) oxygen from 0.08 ML of $D_2{}^{16}O$ on 0.18 ML of ^{18}O covered surface. All isotopically labeled water and oxygen atoms were dosed at 77 K. Heating rate of β = 1 K/s was used.

Figure 2.3

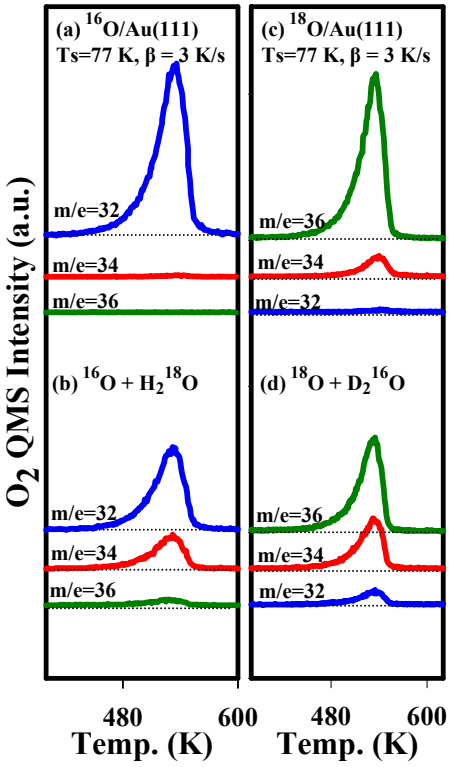

Figure 2.3: TPD spectra of oxygen from Au(111) after dosing (a) 0.37 ML of ^{16}O, (b) 0.53 ML of $H_2{}^{18}$O on top of 0.37 ML of ^{16}O, (c) 0.37 ML of ^{18}O, and (d) 0.53 ML of D_2O on top of 0.37 ML of ^{18}O. All isotopically labeled water and oxygen atoms were dosed at 77 K. A heating rate of β = 3 K/s was used.

Figure 2.4

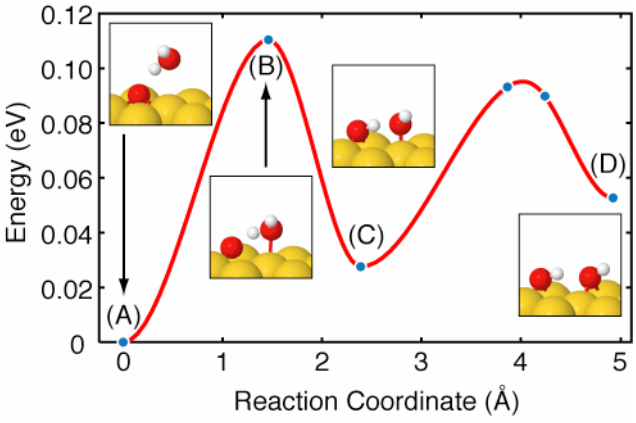

Figure 2.4: (A) H_2O hydrogen bonds to an oxygen atom adsorbed at the fcc site. From this initial state, a hydrogen atom can transfer (B) to the oxygen atom, forming (C) two hydroxyl groups bound in adjacent hollow sites. The low barrier and similar initial and final state energies make this reaction both fast and reversible.

Figure 2.5

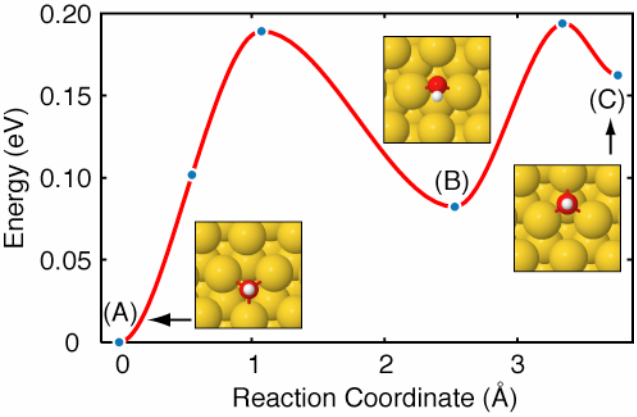

Figure 2.5: Hydroxyl diffuses from (A) a fcc site, (B) over a bridging transition state, (C) into an hcp hollow. The barrier for this process is 0.19 eV.

Figure 2.6

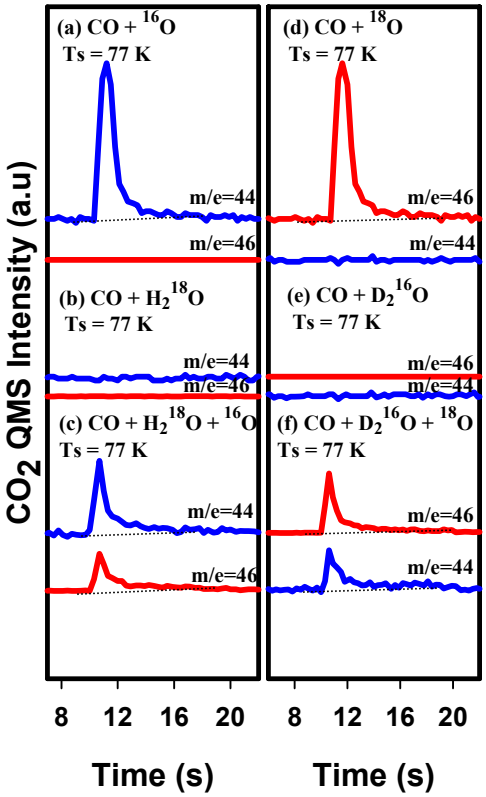

Figure 2.6: Evolution of CO_2 from Au(111) surface, while impinging a continuous CO beam (from 10 to 20 sec.) at the surface with (a) 0.11 ML of ^{16}O atoms preadsorbed, (b) 0.11 ML of $H_2{}^{18}O$ preadsorbed, (c) 0.11 ML of $H_2{}^{18}O$ in addition to 0.11 ML of ^{16}O atoms preadsorbed, (d) 0.11 ML of ^{18}O atoms preadsorbed, (e) 0.11 ML of D_2O preadsorbed, and (f) 0.11 ML of D_2O in addition to 0.11 ML of ^{18}O atoms preadsorbed on the surface. All procedures were performed holding the surface temperature at 77 K.

Figure 2.7

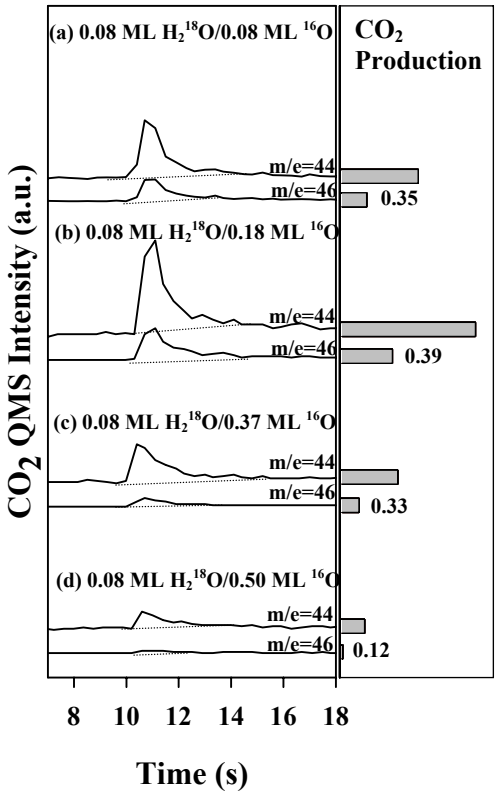

Figure 2.7: Evolution of CO_2 at 77 K while impinging a continuous CO beam (from 10 to 20 sec.) at four different surfaces following oxygen coverages of (a) 0.08 ML, (b) 0.18 ML, (c) 0.37 ML, and (d) 0.50 ML (respectively) to which 0.08 ML of $H_2{}^{18}O$ is added in each case. The bar charts on the right are relative amounts of CO_2 produced in each case as shown next to the corresponding QMS spectra. The ratio of mass 46/44 produced is shown as number labels beside each bar chart.

Figure 2.8

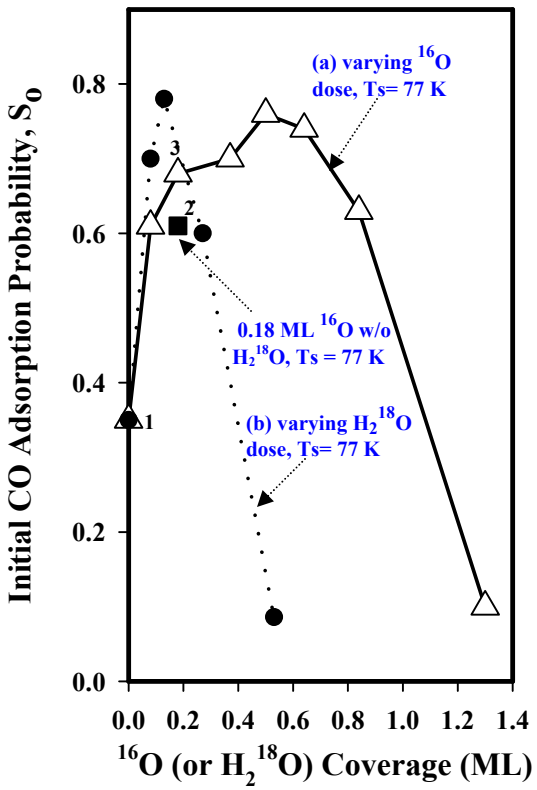

Figure 2.8: Initial CO adsorption probability (S_o) at 77 K using the method of King and Wells. 2.0 sec CO pulse was dosed on Au(111) with (a) varying ^{16}O coverages (0.08 ML, 0.18 ML, 0.37 ML, 0.5 ML, 0.64 ML and 0.84 ML) followed by 0.08 ML $H_2{}^{18}O$ dose in each case [triangles]; (b) 0.37 ML ^{16}O to which varying $H_2{}^{18}O$ coverages (0.08 ML, 0.13 ML, 0.27 ML and 0.53 ML) were added [solid circles]. Data points labeled 1, 2 and 3 represent S_o values measured on clean Au(111)(1), 0.18 ML ^{16}O covered Au(111)(2) and 0.18 ML ^{16}O with 0.08 ML $H_2{}^{18}O$ added prior to CO dose(3).

Figure 2.9

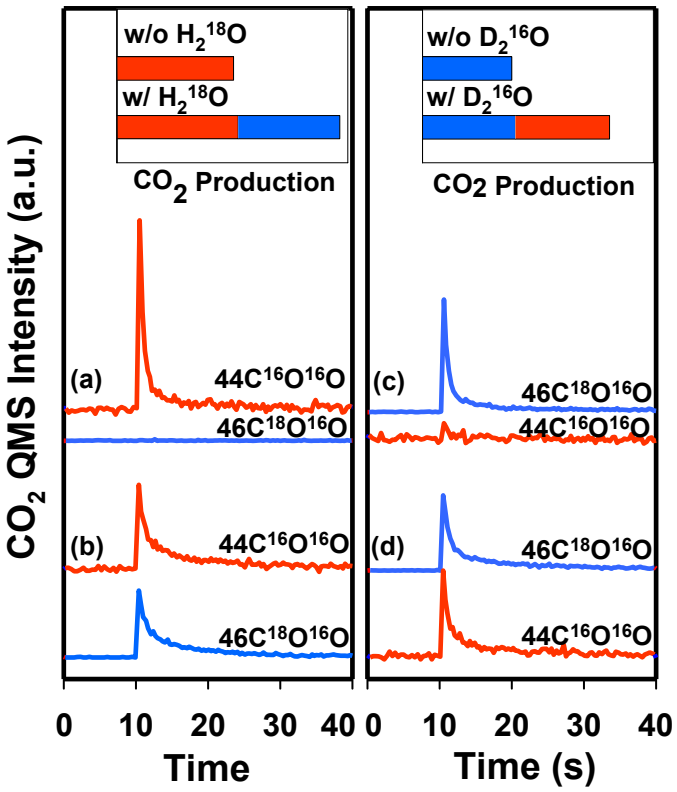

Figure 2.9: Evolution of CO_2 at 140 K while impinging a continuous CO beam (from 10 to 40 sec.) at the surface. (a) 0.11 ML of ^{16}O preadsorbed without $H_2{}^{18}O$, (b) 0.14 ML $H_2{}^{18}O$ in addition to 0.11 ML of ^{16}O atoms preadsorbed on Au(111) at 77 K, (c) 0.11 ML of ^{18}O preadsorbed without D_2O, and (d) 0.14 ML D_2O in addition to 0.11 ML of ^{18}O atoms preadsorbed at 77 K. The area underneath the plots between 10 and 40 seconds represent the amount of CO_2 produced as shown in the insets.

Figure 2.10

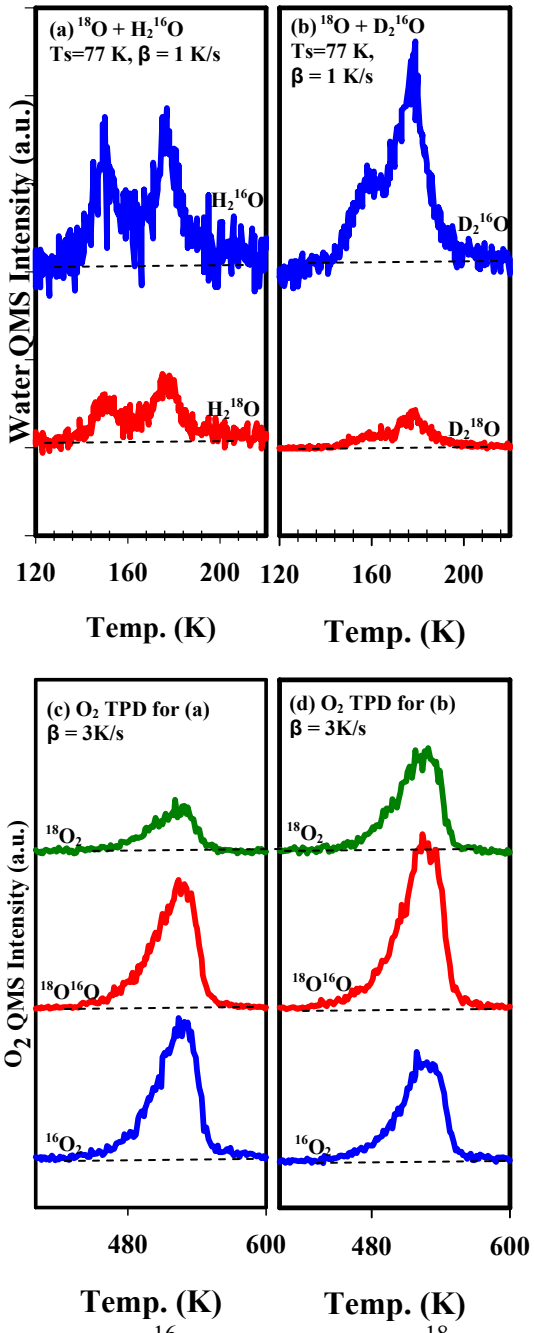

Figure 2.10: (a) TPD of $H_2{}^{16}O$ (m/e=18) and $H_2{}^{18}O$ (m/e=20) from 0.27 ML of $H_2{}^{16}O$ on 0.18 ML of ^{18}O covered Au(111) surface. (b) TPD of $D_2{}^{16}O$ (m/e=20) and $D_2{}^{18}O$ (m/e=22) from 0.27 ML of $D_2{}^{16}O$ on 0.18 ML of ^{18}O covered Au(111) surface. (c) and (d) are the corresponding oxygen TPD spectra from (a) and (b) respectively. All isotopically labeled water and oxygen atoms were dosed at 77 K. Heating rate of β = 1 K/s was used for water and 3 K/s for oxygen.

Figure 2.11

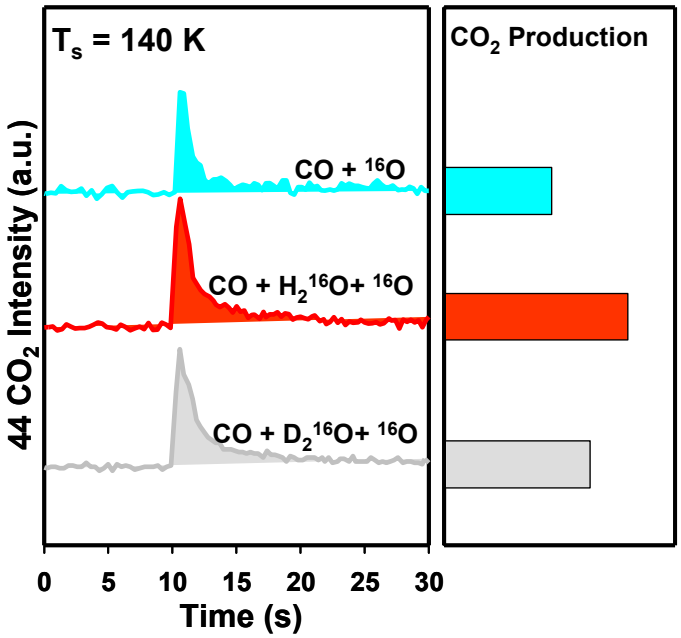

Figure 2.11: Mass 44 CO_2 evolution at 140 K while impinging a continuous CO beam (from 10 to 40 sec.) on a Au(111) with (a) 0.08 ML of ^{16}O atoms preadsorbed at 77 K without $H_2{}^{16}O$ (b) 0.08 ML $H_2{}^{16}O$ added in addition to 0.08 ML of ^{16}O, and (c) 0.08 ML $D_2{}^{16}O$ added in addition to 0.08 ML of ^{16}O. The bar charts on the right are relative amounts of CO_2 produced in each case as shown next to the corresponding QMS spectra.

Figure 2.12

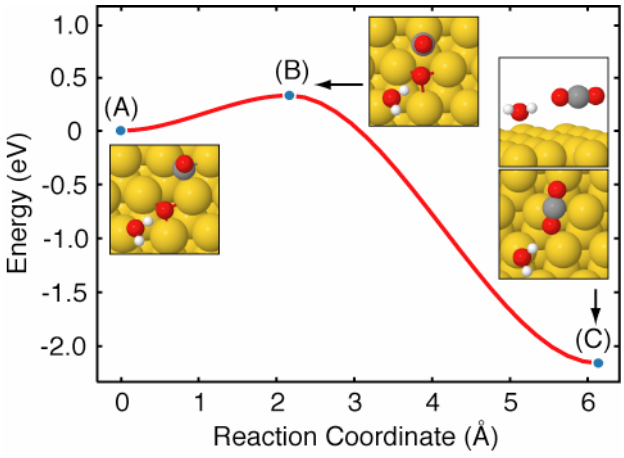

Figure 2.12: H_2O acting as a spectator in the CO oxidation reaction (A-C). The barrier of 0.33 eV is higher than for the reaction without water molecules present.

Figure 2.13

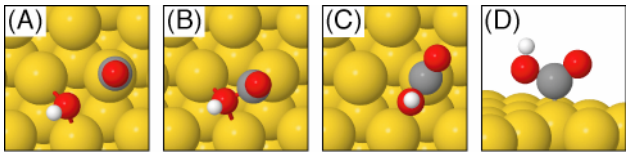

Figure 2.13: Formation of carboxylate (OCOH) from the reaction of CO with OH. The barrier for this reaction is 0.32 eV.

Figure 2.14

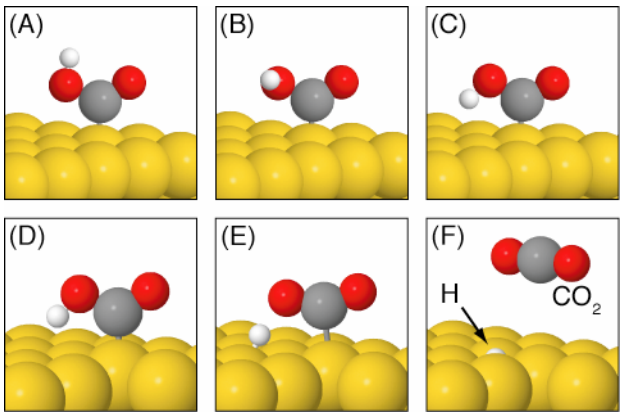

Figure 2.14: When carboxylate (OCOH) forms from the reaction of CO with OH, the hydrogen is positioned away from the surface (A). In order to form CO_2, the molecule must first undergo a conformational change (B-C), with a barrier of 0.44eV, so that the

hydrogen atom can then transfer to the surface (D-F). The hydrogen transfer process occurs with a prohibitively high barrier of 0.93 eV.

Figure 2.15

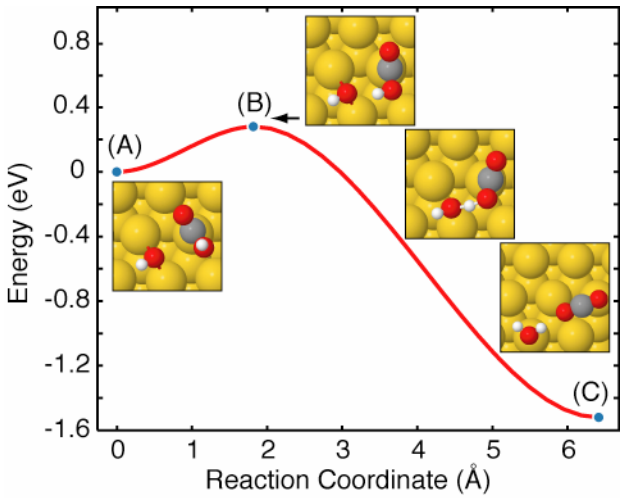

Figure 2.15: Hydrogen transfer from OCOH to OH (A), over a barrier of 0.28 eV (B), to form H_2O and CO_2 (C).

Figure 2.16

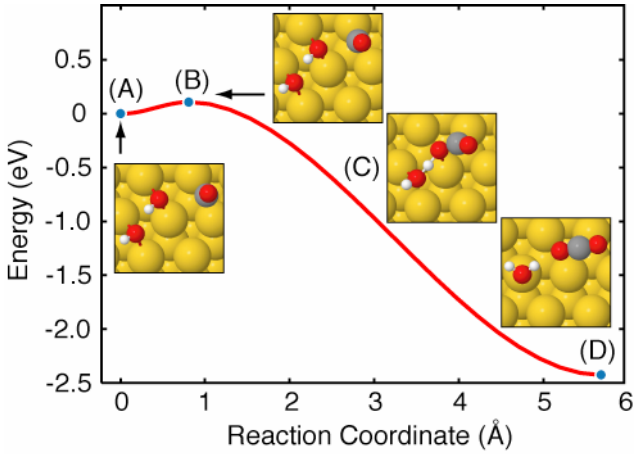

Figure 2.16: (A) Initial state configuration (after H_2O dissociation) with two OH groups bound to the surface. (B) The transition state of the reaction is due to the 0.11 eV diffusion barrier of CO. (C) Intermediate configuration in which the hydrogen in one hydroxyl is spontaneously transferred to the other hydroxyl to form H_2O and CO_2. (D) The final transition state of the reaction with H_2O is bound to the surface and CO_2 has desorbed.

Figure 2.17

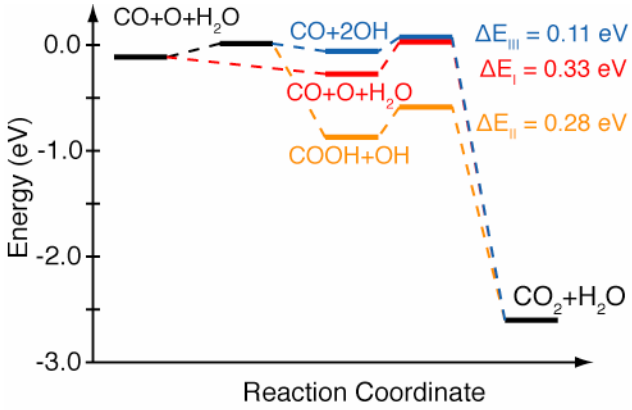

Figure 2.17: Energy landscape for three reaction mechanisms of CO oxidation in the presence of H_2O. In pathway I (red), there is no hydrogen transfer from H_2O. In pathway II (orange), hydrogen transfer occurs before CO oxidation. In pathway III (blue), hydrogen transfer occurs concertedly with CO oxidation, leading to the lowest overall barrier for CO oxidation (0.11 eV).

Chapter 3: Carbonate Formation and Decomposition on Atomic Oxygen Pre-covered Au(111)

INTRODUCTION

The carbonate formation and decomposition ($CO_3 \leftrightarrow CO_2 + O_a$) reaction on gold is important from the point of view of low-temperature CO oxidation. Carbonate formation has been proposed as a possible reaction intermediate in CO oxidation in several investigations of supported and unsupported gold clusters.[1-4] Therefore, an understanding of this reaction on Au(111) may provide additional insight. Carbonate formation and decomposition went undetected in previous studies on Au(110)[5] and Au(111)[6]. However, a surface carbonate was readily formed when oxygen pre-covered Ag(110) was exposed to CO_2 at 300 K.[7-10] This surface carbonate decomposes to produce CO_2 at 485 K and the remaining oxygen atoms recombinatively desorbed at 590 K.[7-10] Due to its' similarity with silver we would anticipate equally facile carbonate formation and decomposition reactions on gold. Similar reactions have also been reported on other surfaces.[11-13]

Here we present experimental evidence with supporting density functional theory calculations (*all DFT calculations were performed by Dr. Graeme Henkelman and Nathan S. Froemming*) of carbonate formation and decomposition from the adsorption of oxygen-labeled carbon dioxide ($C^{18}O_2$) on an atomic oxygen (^{16}O) pre-covered Au(111) surface. We studied the effects of CO_2 exposure, surface temperature, and oxygen coverage on carbonate formation and decomposition and also estimated reaction probabilities ($\sim 10^{-3}$-10^{-4}) and activation energies as a function of conditions.

EXPERIMENTAL

Our experiments were performed in a UHV chamber that has been described elsewhere,[14-17] but details specific to this study are briefly summarized here. The Au(111) single crystal sample is mounted to a tantalum plate that can be resistively heated and is in thermal contact with a liquid nitrogen bath. Oxygen (^{16}O) atoms were deposited using a radio frequency (RF) plasma-jet source. The $^{16}O_a$/Au(111) surface was exposed to $C^{18}O_2$ by backfilling the chamber and carbonate $^{16}OC^{18}O^{18}O$ was formed. The surface carbonate decomposes to form either $C^{18}O_2$ or ^{16}O $C^{18}O$ leaving $^{18}O_a$ or $^{16}O_a$ adatoms on the surface. Upon heating, the oxygen atoms undergo recombinative desorption to produce $^{16}O_2$ (mass 32) and $^{16}O^{18}O$ (mass 34), as observed in TPD. Thus, carbonate formation and decomposition were detected via the increased presence of mass 34 $^{18}O^{16}O$ in a temperature programmed desorption (TPD) spectrum after the $^{16}O_a$ covered Au(111) surface was exposed to $C^{18}O_2$. We did not observe $^{18}O_2$ (mass 36) in the oxygen TPD since the surface concentration of ^{18}O (from carbonate decomposition) is very small.

RESULTS AND DISCUSSION

Figure 3.1 (a) displays TPD spectra of $^{16}O^{18}O$ (m/e=34) produced from exposure of the $^{16}O_a$/Au(111) surface to $C^{18}O_2$. The amount of $^{16}O^{18}O$ produced increases with $C^{18}O_2$ exposure at 167 K (and all temperatures studied). Two control experiments were performed to ascertain the source of $^{16}O^{18}O$. First, no mass 34 was produced when the Au(111) surface was exposed to $C^{18}O_2$ *without* pre-adsorbed atomic oxygen. Second, only ~0.5% of the total amount of oxygen desorbs as mass 34 when the Au(111) surface is pre-covered with ^{16}O but with no exposure to $C^{18}O_2$ (due to natural isotopic abundance of ^{18}O). As expected, no surface-bound oxygen was lost during carbonate formation and decomposition, in agreement with previous studies.[8-10] For clarity, Figure 3.1 (b) shows the amount of mass 34 produced (from the integrated TPD spectra in Figure 3.1 (a)) as a function of $C^{18}O_2$ exposure.

In order to further examine the role of pre-adsorbed atomic oxygen on carbonate formation, we varied the oxygen pre-coverage (0.18 ML – 2.1 ML) while keeping both $C^{18}O_2$ exposure (30 L) and surface temperature (167 K) constant (Figure 3.2). Mass 34 production increases with increasing $^{16}O_a$ coverage, likely because more reactive oxygen is accessible to $C^{18}O_2$ on the surface. Similar results were obtained employing surface temperatures of 220 K and 300 K.

We estimated the reaction probability of carbonate formation assuming a statistical distribution[7] in the decomposition of the surface-bound carbonate $^{16}OC^{18}O_2$ and obtained values of ~10^{-3}-10^{-4} (uncertainties of ± 50%). These small values are likely part of the reason why an earlier study on Au(111)[6] reported undetectable surface carbonate formation. An Arrhenius plot of the reaction probability for two oxygen coverages (0.5

and 1.0 ML) is shown in Figure 3.3. The inverse relationship between reaction probability and temperature, with negative apparent activation energy E_a = -0·15 eV, is suggestive of a competition between carbonate formation and $C^{18}O_2$ desorption on the O/Au(111) surface.

Compared to Au(111), the carbonate formation reaction on Ag(110) is very facile.[10] Using density functional theory (DFT) we have calculated the difference in energetics for CO_3 formation on Au(111), Au(110), Ag(111), and Ag(110)**.** The metal surfaces were modeled with 4 (for 111) and 6 (for 110) layers, allowing the top two layers to relax. A vacuum gap of 10 Å separated the slabs. A plane wave basis set with a 274 eV cutoff was found to be sufficient for the PAW based pseudopotentials**,**[18] with a 4x4x1 Monkhost-Pack k-point sampling of the Brillouin zone. All calculations were based upon the PW91 GGA functional.[19]

Figure 3.4 shows calculated reaction paths for CO_2 bound to an adsorbed O atom on the surface forming a CO_3 species. Ag is more reactive than Au, binding CO_2 with over 1 eV before it spontaneously reacts to form CO_3. The initial CO_2 binding is weaker on Au, and there is a significant barrier to CO_3 formation– particularly on the (111) surface. Our calculations suggest that CO_3 is bound much stronger to Ag than Au, consistent with our experimental results on Au(111) in which CO_3 decomposition and CO_2 desorption appear to occur in an overlapping temperature range (~120-140K) while on Ag(110), the carbonate decomposes near 485 K and CO_2 desorbs below 160 K.

Our DFT calculations are consistent with a negative apparent activation energy E_a for CO_3 formation on Au(111). From an initial state with CO_2 bound to an adsorbed O atom, there is a competition between desorption (0.72 eV) and carbonate formation (0.32

eV). Our calculations suggest that carbonate formation is favored at low temperature with E_a = -0.4 eV.

CONCLUSIONS

In summary, we have shown evidence for carbonate formation and reaction on atomic oxygen pre-covered Au(111). Oxygen mixing was observed when $^{16}O_a$ pre-covered Au(111) was exposed to isotopically labeled CO_2 ($C^{18}O_2$) at surface temperatures ranging from 77 – 400 K and initial oxygen coverages ranging from 0.18 ML – 2.1 ML. Subsequent desorption of isotopically mixed oxygen ($^{16}O^{18}O$, mass 34) is observed as a by-product of carbonate formation and decomposition on the surface. TPD spectra showed more mass 34 as more oxygen is pre-adsorbed on the surface likely due to an increase in carbonate formation. Carbonate formation occurs with a very small reaction probability (~ 10^{-4} - 10^{-5}) and is most favorable at low surface temperatures.

REFERENCES

(1) Date, M.; Haruta, M. J. Catal. 2001, 201, 221.
(2) Daté, M.; Okumura, M.; Tsubota, S.; Haruta, M. Angew. Chem. Int. Edit 2004, 43, 2129.
(3) Hakkinen, H.; Landman, U. J. Am. Chem. Soc. 2001, 123, 9704.
(4) Konova, P.; Naydenov, A.; Venkov, C.; Mehandjiev, D.; Andreeva, D.; Tabakova, T. J. Mol. Catal. A 2004, 213, 235.
(5) Outka, D. A.; Madix, R. J. Surf. Sci. 1987, 179, 351.
(6) Lazaga, M. A.; Wickham, D. T.; Parker, D. H.; Kastanas, G. N.; Koel, B. E. ACS Symposium Series 1993, 523, 90.
(7) Barteau, M. A.; Madix, R. J. J. Chem. Phys. 1981, 74, 4144.
(8) Bowker, M.; Barteau, M. A.; Madix, R. J. Surf. Sci. 1980, 92, 528.
(9) Campbell, C. T.; Paffett, M. T. Surf. Sci. 1984, 143, 517.
(10) Guo, X. C.; Madix, R. J. J. Phys. Chem. B 2001, 105, 3878.
(11) Behm, R. J.; Brundle, C. R. Surf. Sci. 1991, 255, 327.
(12) Felter, T. E.; Weinberg, W. H.; Lastushkina, G. Y.; Boronin, A. I.; Zhdan, P. A.; Boreskov, G. K.; Hrbek, J. Surf. Sci. 1982, 118, 369.
(13) Wang, Y.; Kovacik, R.; Meyer, B.; Kotsis, K.; Stodt, D.; Staemmler, V.; Qiu, H.; Traeger, F.; Langenberg, D.; Muhler, M.; Woll, C. Angew. Chem. Int. Ed. 2007, 46, 5624.
(14) Ojifinni, R. A.; Froemming, N. S.; Gong, J. L.; Pan, M.; Kim, T. S.; White, J. M.; Henkelman, G.; Mullins, C. B. In preparation 2008.
(15) Stiehl, J. D.; Kim, T. S.; McClure, S. M.; Mullins, C. B. J. Am. Chem. Soc. 2004, 126, 13574.
(16) Stiehl, J. D.; Kim, T. S.; McClure, S. M.; Mullins, C. B. J. Am. Chem. Soc. 2004, 126, 1606.
(17) Wheeler, M. C.; Seets, D. C.; Mullins, C. B. J. Chem. Phys. 1996, 105, 1572.
(18) Kresse, G.; Joubert, D. Phys. Rev. B. 1999, 59, 1758.
(19) Perdew, J. P. Electronic structure of solids, Berlin, 1991.

Figure 3.1

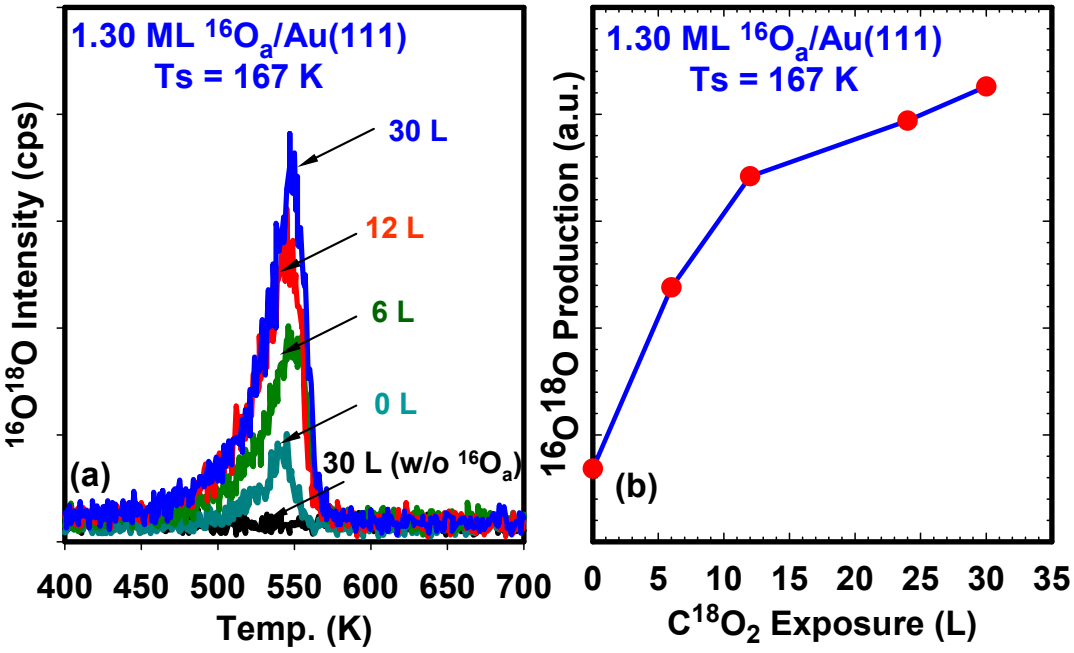

Figure 3.1: (a) shows the TPD of $^{16}O^{18}O$ (m/e=34) after a Au(111) surfaces covered with 1.3 ML ^{16}O at 77 K was exposed to varying amounts (0 – 30 L, where 1 L = 10^{-6} Torr · s) of $C^{18}O_2$ at 167 K. (b) $^{16}O^{18}O$ production as a function of $C^{18}O_2$ exposure.

Figure 3.2

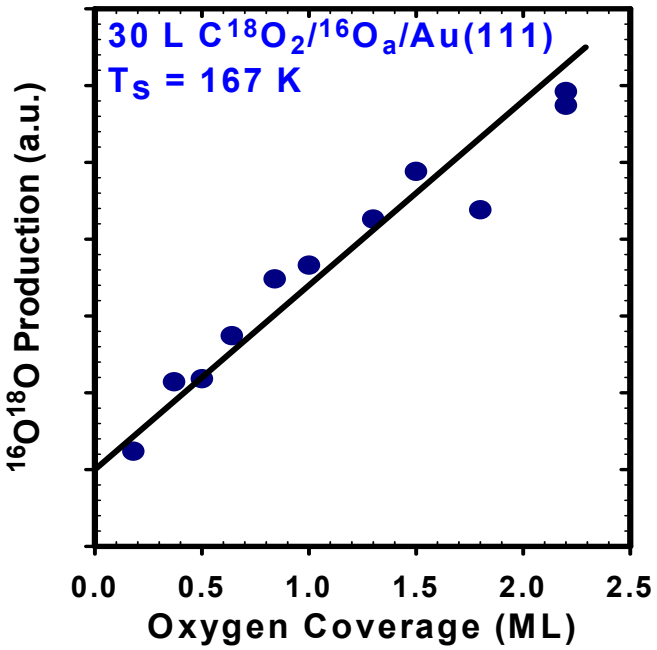

Figure 3.2: Integrated TPD area of $^{16}O^{18}O$ (mass 34) for varying initial oxygen pre-coverages (0.18 ML – 2.1 ML) on which 30 L of $C^{18}O_2$ was reacted at 167 K. The contribution to the signal due to the natural abundance of ^{18}O has been subtracted off.

Figure 3.3

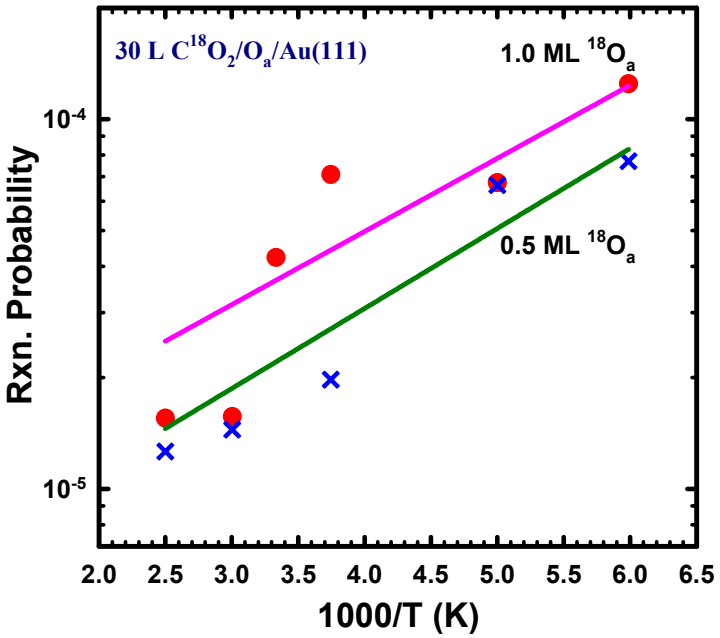

Figure 3.3: Arrhenius plot of $C^{18}O_2$ reaction probability using a constant $C^{18}O_2$ exposure of 30 L for 1.0 ML (upper plot) and 0.5 ML (lower plot) of atomic oxygen on Au(111).

Figure 3.4

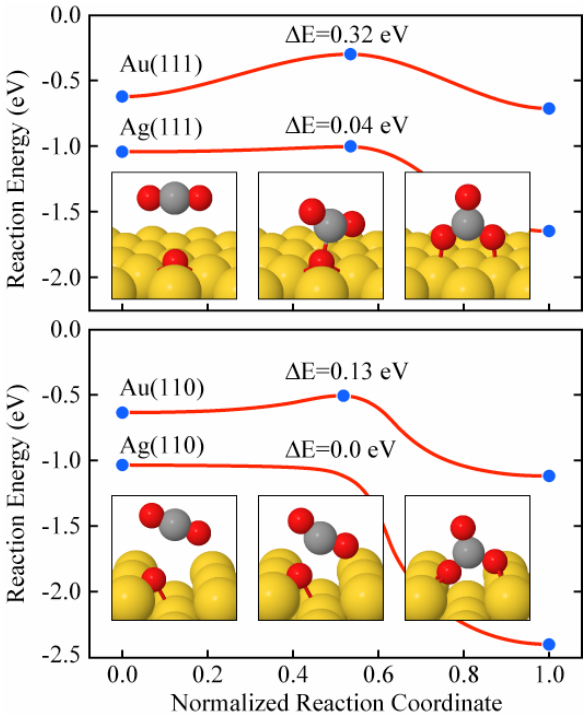

Figure 3.4: Results from DFT calculations of carbonate formation on Au and Ag (111, upper plot) and (110, lower plot) surfaces.

Chapter 4: The Effect of Annealing on Reactivity of Oxygen towards Water, CO and CO_2 on Au(111)

INTRODUCTION

Gold catalysis has drawn tremendous attention since Haruta's discovery[1] of the exceptional catalytic activity of supported nanoparticles (NPs) 2-5 nm in diameter. Several reactions have therefore been shown to be catalyzed on both Au NPs and single crystal Au. Particular attention has been paid to low temperature CO oxidation and other oxidation reactions on Au. However, several questions remain unanswered regarding the details of oxidation reactions on gold. One of these questions is the nature of the reactive oxygen species, an important factor in understanding oxidation reaction mechanisms. Numerous ideas have been proposed in the literature about the reactive state of oxygen on gold. Atomic oxygen has been reported by some authors[2-4] as responsible for reactivity on gold while a case has been made for molecular oxygen being the reactive species by some authors.[5,6] Stiehl et al. have also shown that both molecularly and atomically adsorbed oxygen are active in CO oxidation on Au/TiO_2.[7-11] It has been reported that one of the most fruitful approaches to characterizing oxygen states on metal surfaces is by exploiting their different chemical reactivities using probe molecules.[12] This current work therefore attempts to use simple but important probe reactions to study how annealing affects the reactivity of the atomic oxygen overlayer on gold.

Studies have shown that oxygen reactivity can be changed by controlling its adsorption conditions. For example, an earlier study by Gallagher showed that although an aluminum surface pre-adsorbed with oxygen at 295 K was unreactive towards CO at 80 K, the same surface pre-adsorbed with oxygen at 80 K led to the formation of

carbonates and other products.[13] Similar observations were reported regarding the reactivity of an oxygen pre-covered lead surface at 80 K in which it was unreactive towards water[14] and ethylene[15] when pre-covered with oxygen at 295 K but reactive with both water and ethylene when pre-covered with oxygen at 80 K. On O-covered Zn(0001), hydroxyl formation was observed when oxygen was pre-covered at 80 K.[16,17]

Sueyoshi et al. used the CO oxidation reaction to probe the reactivities of oxygen adsorbed on Cu(110) at 100 K and at 300 K, and reported that the low-temperature species are 25 times more reactive for CO_2 formation.[18-21] All these studies attributed the observed reactivity at low adsorption temperature to the presence of metastable oxygen ($O^{\delta-}$) species.

Regarding gold in particular, understanding the reactivity of oxygen as it pertains to CO oxidation and other oxidation reactions on gold nanoparticles and single crystals have elicited numerous interesting works.[1,3,7,8,22-46] Madix and co-workers[47] showed in early pioneering work that atomic oxygen-covered Au(110) is reactive towards methanol, acetylene and water. They attributed this reactivity to the Brönsted base character of oxygen adatoms on gold as earlier seen on other group 1B metals. Gottfried and co-workers prepared an O/Au(110) surface by electron bombardment (500eV) of O_2/Au(110) at 28 K and reported recombinative desorption of O_2 near 550 K.[33] On Au(111), Lazaga et.al. studied the reactivity of up to 1 ML initial coverage of atomic oxygen with CO, CO_2, NO_2, H_2O, CH_3OH and C_2H_4 using ozone as the atomic oxygen source. Results from this work showed that although CO, NO_2, and CH_3OH reacted with oxygen, H_2O, CO_2 and C_2H_4 did not show any observable reactivity on O/Au(111).[35] In a

recent study, Min et al. (using TPD, XPS and STM) reported the presence of three oxygen states (chemisorbed oxygen, surface oxide and bulk oxide) each showing different reactivity towards CO oxidation on O/Au(111).[40] Recently, we have also shown that on a Au(111) surface populated with atomic oxygen, water, carbon monoxide, carbon dioxide, ammonia and methanol all react.[28,29,48-51] In particular we have demonstrated experimentally that atomic oxygen activates water as seen by oxygen exchange between ^{16}O and $H_2{}^{18}O$.[49,50] We also showed by continuously impinging a CO beam on a surface co-adsorbed with ^{16}O and $H_2{}^{18}O$, that both masses $44C^{16}O^{16}O$ and $46C^{16}O^{18}O$ were produced as an indication of the direct involvement of water in CO oxidation.[49,50]

Previous annealing experiments have been performed to investigate the effect of annealing on clean gold. In one of those experiments, Gottfried et al. reported that annealing causes a decrease in the intensity of the desorption peaks of CO from Au(110).[52] They annealed a Au(110) surface at temperatures between 50 and 900 K and found changes in the CO TPD spectra up to 500 K.[52] This phenomenon was attributed to a reduction in the defect concentration on the clean gold surface.[52] Paul and Bent[53] also investigated the relationship between structure and reactivity on gold using CH_3I as a probe molecule. They reported that methyl group coupling occurred at ~ 270 K on a well annealed Au(111) surface while the reaction occurs at ~ 350 K on an incompletely annealed Au(111) surface following sputtering.[53] Despite all these works, there are no published studies that describe how annealing affects oxygen reactivity on either atomic oxygen pre-covered single crystal gold or supported NPs. Here we present experimental data showing that the reactivity of oxygen with CO, H_2O and CO_2 is reduced as a result

of annealing of the oxygen pre-covered Au(111) surface. It is believed that oxygen adsorbed at low temperatures (77 K in the current work) is trapped in a metastable state from which the barrier to further reaction is lowered. Annealing the adsorbed oxygen stabilizes the oxygen overlayer, thereby increasing the barrier to reaction.

EXPERIMENTAL

All experiments reported here were performed in an ultrahigh vacuum (UHV) molecular beam surface scattering apparatus that has been previously described in detail[11,28,34,48,50,54-56] but is briefly summarized here. The UHV chambers are comprised of a scattering/analysis chamber and a quadruply differentially-pumped molecular beam source chamber. The scattering/analysis chamber has a base pressure less than 2.0×10^{-10} Torr and is equipped with standard surface analysis tools such as Auger electron spectrometer (AES), low energy electron diffraction optics (LEED), and a quadrupole mass spectrometer (QMS).

The Au(111) single crystal sample (11mm in diameter, 1.5 mm thick) used for these experiments was mounted to a tantalum plate that can be resistively heated and is in thermal contact with a liquid nitrogen bath for cooling. A type K thermocouple spot-welded to the tantalum plate was used for measuring surface temperature. Oxygen atoms were deposited on the Au(111) surface using a radio frequency (RF) generated plasma-jet source that produces a supersonic beam of O atoms from an 8% (vol.) O_2 in Ar gas mixture.[54,56,57] An oxygen dissociation fraction of ~40%, as measured by time of flight techniques, was achieved. Ions were deflected from the O-atom beam by a charged plate (biased negatively at 3000 V) located below the beam line in one of the differential pumping stages. We have previously shown that adsorbed $O_{2,a}$ is present after exposure to the plasma-jet source but we neglect its presence here because the concentration ($\leq$ 0.02 ML) is very low.[7,8]

Research purity isotopically labeled water [Isotec®, 97.1% $H_2{}^{18}O$ and Spectra®, 99.9% $D_2{}^{16}O$] was used while atomic oxygen (^{16}O and ^{18}O) was generated from research

purity molecular oxygen (from Matheson Trigas™ 99.999% $^{16}O_2$ and Isotec® 99.7% $^{18}O_2$ respectively). The $C^{18}O_2$ (Cambridge Isotopes Inc., 95% $C^{18}O_2$) used for the carbonate experiments was backfilled into the chamber using a leak valve. A typical value for the CO beam flux was ~9×10^{13} molecules / cm^2·

All molecular beams (oxygen, water, and CO) were expanded from the same nozzle through the same apertures to ensure that the beam spots on the gold sample were the same in size and coincident. The RF generator was switched on only when it was necessary to dose atomic oxygen through the nozzle. The beam spot (~3 mm in diameter) was much smaller than the sample size to minimize the effects of scattered gas interacting with other surfaces in the chamber. The Au(111) surface was cleaned by argon ion (1keV, 6μA) sputtering, followed by annealing in UHV (850 K for 10 minutes), a procedure which produces a carbon-free surface as verified by AES. Further cleaning with atomic oxygen is done to ensure that the surface is free of all impurities. Surface crystallinity was verified by LEED.

Oxygen coverages were estimated from the ratio of the dN(E)/dE peak heights, O(503eV)/Au(239eV) AES ratio compared to the O/Pt AES ratio of 0.3 observed for a p(2 × 2) oxygen adlayer on Pt(111) which corresponds to 3.9×10^{14} O atoms/cm^2. Using a Au(239eV)/Pt(237eV) AES ratio of 0.95 as a conversion factor,[47] a O/Au AES ratio of 0.3 corresponds to 4.1×10^{14} oxygen atoms cm^{-2} (0.29 ML). Here, 1ML of oxygen is defined as 1.39×10^{15} atoms/cm^2 and refers to a single atomic layer of close-packed gold. Water coverages were determined from a mass balance on a CO oxidation experiment involving co-adsorbed water as previously described in details.[50] $C^{18}O_2$ exposures are reported in Langmuir (L) where 1 L corresponds to 10^{-6} Torr·s.

Two types of surfaces were used for these experiments. The unannealed surface described in this work refers to a Au(111) pre-covered with atomic oxygen at 77 K without annealing to higher temperatures before dosing probe molecules (water, CO and $C^{18}O_2$). The annealed surface on the other hand was prepared by first pre-covering the Au(111) with atomic oxygen at 77 K. The surface is then annealed to a higher temperature (as desired) and cooled back down to 77 K before dosing probe molecules.

RESULTS AND DISCUSSION

The temperature programmed desorption (TPD) spectra of water are displayed in Figures 4.1 (a) (unannealed surface) and (b) (annealed surface), with corresponding oxygen TPD spectra shown in Figures 4.1 (c) and (d) respectively, when a 0.18 ML ^{16}O pre-covered Au(111) at 77 K was dosed with 0.53 ML $H_2{}^{18}O$ at 77 K. In Figure 4.1 (a) the oxygen pre-covered surface was unannealed prior to exposure to water while in Figure 4.1 (b) the oxygen pre-covered surface was annealed to 300 K and then cooled back down to 77 K before dosing water.

The water TPD spectra of both Figure 4.1 (a) and (b) show two peaks. The 155 K peak corresponds to water desorption from clean Au(111) and the 175 K desorption peak is due to the water-oxygen interaction.[50] The intensity of the higher temperature feature gives a good measure of the interaction of the co-adsorbed water and oxygen. Integrating the area under the higher temperature feature in Figure 4.1 (a) corresponds to 29% of the total amount of water but only 18% on the annealed surface [Figure 4.1 (b)]. Similarly, in Figure 4.1 (d), the amount of unscrambled $^{16}O_2$ (78% of the total oxygen on the annealed surface) desorbing is much greater than that in Figure 4.1 (c) (43% of the total oxygen on the unannealed surface). This indicates that more of the atomic oxygen reacted and exchanged oxygen with water on the unannealed surface. We also note that the amounts of oxygen exchange products i.e. $^{16}O^{18}O$ and $^{18}O_2$ on the annealed surface (20% and 2% respectively) in Figure 4.1 (c) are visibly less than on the unannealed surface (42% and 15% respectively) in Figure 4.1 (d). Mass balance for both oxygen and water shows that there was no loss of oxygen or water upon annealing.

Experiments similar to those described above were also performed using $D_2{}^{16}O$ and ^{18}O. The experiments in Figures 4.1 (a), (b), (c) and (d) were repeated using ^{18}O and $D_2{}^{16}O$, and the results are shown in Figures 4.1(e), (f), (g) and (h) respectively. Comparing Figure 4.1 (e), the unannealed surface with Figure 4.1 (f), the annealed surface, we also see less of the higher temperature water desorption feature from the annealed surface (16% compared to 23% from the unannealed surface). There is also more unscrambled $^{18}O_2$ (62% of total adsorbed oxygen) desorbing from the annealed surface [Figure 4.1 (h)] than from the unannealed surface [Figure 4.1 (g) which has only 24%].

To further determine the effect of surface annealing on water reactivity with different oxygen coverages, we measured the amount of mass 32 oxygen desorption from surfaces with varying oxygen (^{16}O) adatom coverages to which a fixed amount of water had been added (in this case 0.53 ML of $H_2{}^{18}O$). For example, the experiment shown in Figure 4.1 (a) has an initial coverage of 0.18 ML ^{16}O to which 0.53 ML of $H_2{}^{18}O$ is added. The value of the area underneath the m/e=32 TPD spectrum in Figure 4.1 (c) divided by the value of the area underneath the mass 32 oxygen feature (TPD not shown) from a Au(111) covered with solely 0.18 ML ^{16}O gives the fraction of remaining oxygen (subsequently referred to as unscrambled oxygen) on the unannealed surface. Similarly on the annealed surface, the area underneath the mass 32 oxygen feature in Figure 4.1 (d) was divided by the area underneath the mass 32 oxygen feature (TPD not shown) from a surface covered with solely 0.18 ML ^{16}O. These provide quantitative measures of how much oxygen scrambling occurred for a given oxygen dose and annealing treatment. If the fraction of mass 32 remaining on the surface is high, it indicates a small degree of

exchange between water and surface oxygen adatoms, and conversely a low fraction indicates a high degree of oxygen scrambling. Figure 4.2 shows data for several different initial oxygen coverages on annealed (upper curve) and unannealed (lower curve) surfaces. The lower curve shows the fraction of mass 32 oxygen desorbing with $H_2{}^{18}O$ on the surface when it was held at 77 K throughout the entire oxygen and water dose. The upper curve in Figure 4.2 shows the fraction of mass 32 oxygen when the oxygen overlayer was annealed to 300 K and then cooled to 77 K prior to adding $H_2{}^{18}O$ to the surface. We clearly observe a smaller degree of mixing for the surface that has been annealed to 300 K prior to the water dose.

Studies of metastable oxygen on metal surfaces have been reviewed by Carley et al.[12] They cite several examples demonstrating that oxygen reactivity can be modified by changing the conditions under which oxygen is exposed to the metal surface. By changing the adsorption conditions, oxygen can be kinetically trapped in a metastable state so that the barrier to reaction is decreased. We believe that this metastable oxygen contributes to the increased reactivity observed regarding water on oxygen pre-covered Au(111). Regarding water-oxygen interaction, water is less likely to interact dissociatively with the more stable oxygen overlayer created once the surface is annealed to 300 K, and this leads to less oxygen scrambling on the surface. For example with an initial oxygen coverage of 0.18 ML, the fraction of unscrambled oxygen on the unannealed surface (lower plot of Figure 4.2) is about 0.18 while this value is about 0.48 for the annealed surface (upper plot of Figure 4.2) In both cases (with and without annealing to 300 K), the fraction of unscrambled oxygen increases with the oxygen ^{16}O dose. This behavior is ascribed to the fact that as the surface is covered with more atomic

oxygen, fewer adsorption sites are available for water to interact with the oxygen adatoms and hence less oxygen scrambling. For instance as the initial oxygen coverage increases from 0.18 ML to 0.37 ML while keeping the water coverage fixed at 0.53 ML, the fraction of unscrambled mass 32 increases from 0.18 to 0.30, for the unannealed surface.

To determine if temperature-induced oxygen stabilization also applies to CO oxidation reactions, we pre-covered our Au(111) surface with 0.37 ML ^{16}O at 77 K, followed by a 10 second CO dose (via molecular beam from 10 to 20 sec on the plot) at 77 K, as shown by the family of curves in the lower portion of Figure 4.3 (a). Figure 4.3 (b) shows the corresponding oxygen TPD spectra for each annealing temperature as labeled and represents the oxygen remaining on the surface. There is a decrease in CO_2 production with increasing annealing temperature, with the highest CO_2 production occurring when there was no surface annealing (lowest curve). For clarity, the inset in Figure 4.3 (a) shows the relative amount of CO_2 produced as a function of annealing temperature. For each annealing temperature in Figure 4.3 (a), the relative amount of CO_2 was calculated by dividing the CO_2 TPD area for that annealing temperature by the CO_2 TPD area of the lowest curve (no anneal). According to the inset in Figure 4.3 (a), the relative amount of CO_2 decreases with increasing annealing temperature. The inset in Figure 3 (b) which gives the relative amount of oxygen was obtained for each case by dividing the area beneath the oxygen TPD in each case by the area beneath an oxygen TPD from a Au(111) surface pre-covered with 0.37 ML ^{16}O at 77 K. We noted that the amount of unreacted oxygen increases with increasing annealing temperature of the oxygen overlayer prior to CO dose, an observation consistent with the measurements shown in Figure 4.3 (a). The inset in Figure 4.3 (b) gives a quantitative measure of the

amount of unreacted oxygen as a function of annealing temperature. In an XPS and UPS study by Felter et al,[58] the presence of two types (active and inactive oxygen) of atomic oxygen species on Ag(111) were reported. The active oxygen was characterized by an O 1s peak at 528.5 eV while the inactive specie was seen at 530 eV. CO exposure followed by XPS showed that the oxygen with a peak at 530 eV was less reactive in oxidizing CO than the oxygen with its O 1s peak at 528.5 eV.[58] Again, our observation on Au(111) is similar to those results on Ag(111). We note that CO accumulates on the surface at 77 K and that annealing the surface to higher temperatures allows some of these accumulated CO to scrub off some of the remaining oxygen on the surface. Therefore the oxygen shown in the TPD of Figure 4.3 (b) might be smaller than it should have been if no CO_2 formed from the accumulated CO on the surface reacting with adsorbed atomic oxygen.

Another measure of the effect of annealing on oxygen reactivity is the carbonate formation and decomposition reaction previously reported on oxygen covered Au(111).[51] Figure 4.4 shows reaction probability for surface carbonate on atomic oxygen (^{16}O) pre-covered Au(111) surface that has been pre-annealed to different temperatures. In each annealing experiment, we pre-covered the Au(111) surface with 0.64 ML of ^{16}O then annealed to higher temperatures (150 K, 300 K and 400 K) and later exposed to 30 L $C^{18}O_2$ after the surfaces have cooled down to 77 K. A similar experiment was performed on a Au(111) surface pre-covered with 0.64 ML of ^{16}O at 77 K without any subsequent annealing prior to 30 L $C^{18}O_2$ exposure at 77 K. A sizeable decrease in reaction probability was observed with increasing annealing temperature as shown in Figure 4.3. The reaction probability of the surface annealed to 400 K is 9.2 times smaller than that of the unannealed surface. Annealing the oxygen pre-covered surface to 300 K results in a

reduction in carbonate formation probability by a factor of four relative to the unannealed surface. There was no oxygen loss in these reactions as determined from the areas underneath both the mass 32 and mass 34 oxygen TPD spectra. Oxygen mixing was used as a measure of carbonate formation and decomposition as earlier reported on oxygen pre-covered Au(111).[51] A surface carbonate is formed when atomic oxygen (^{16}O) pre-covered Au(111) is exposed to oxygen-labeled carbon dioxide ($C^{18}O_2$). This surface carbonate decomposes leaving behind $^{18}O_a$ and $^{16}O_a$ which recombine to form $^{16}O^{18}O$. Pre-annealing the oxygen covered surface reduces the reactivity of the oxygen adlayer on the surface. In the case of pre-annealing to 300 K and 400 K, we anticipate a decrease in the concentration of surface carbonates formed as there are less reactive oxygen species available to react with adsorbed $C^{18}O_2$. This in turn leads to fewer $^{18}O_a$ on the surface. This reported reduction the reaction probability further supports our claim that most of the surface oxygen species that could have reacted with probe molecules are present in an thermally-induced stable (less reactive) state from which the barrier to reaction is quite high. It is worthwhile to compare our carbonate formation results to a previous report[59] on the formation of surface carbonate from the reaction of $C^{16}O_2$ (T_s = 300 K) with $^{18}O_2$ pre-covered Ni(100) at 135 K, 300 K and 370 K using XPS and TPD. Negligible carbonate formation was observed on the surface pre-covered with oxygen at 370 K even with CO_2 exposures of up to 100 L while the maximum rate of carbonate formation was attained for the surface exposed to oxygen at 135 K.[59] A reduction (by a factor of 3) in the rate of carbonate formation was reported for the surface pre-exposed to oxygen at 300 K.[59] The reactivity of Ni(100) in the experiments conducted at 135 K and 300 K was attributed to the reaction of CO_2 with an activated form of oxygen that were made

available to the Ni(100) at these adsorption conditions.[59] According to this study, the presence of stable or ordered oxygen species is responsible for the lack of reactivity observed at 370 K. These results on oxygen pre-covered Ni(100) are similar to our observations regarding surface carbonate formation and decomposition on atomic oxygen pre-covered Au(111).

It is therefore evident from our results that the surface reactivity of atomic oxygen can be maximized when it is adsorbed at low temperatures (77 K n this case). At these low temperatures, adsorbed atomic oxygen exists in a metastable and reactive state from which the barrier to further reaction is quite low. By annealing, this reactive oxygen state becomes thermally stabilized and trapped in a chemisorbed state from which the barrier to further reaction is higher than the unannealed state. This work therefore further provides experimental evidence that atomic oxygen is a reactive species on gold and that its reactivity can be altered by changing the adsorption conditions on the surface.

CONCLUSIONS

Based on our investigation of the effect of annealing on the reactivity of oxygen on Au(111) using temperature-programmed desorption and reactivity measurements of probe molecules, we observed significant reduction in oxygen reactivity on all annealed surfaces. These results are confirmed by previous studies on other metal surfaces where the reactivity of oxygen was changed by varying its adsorption conditions on those surfaces. On Au(111), TPD results of water-oxygen interaction on an annealed surface indicates that the reactive oxygen state is the unannealed oxygen state. We observed that there is a reduction in the higher temperature water desorption peak (~ 175 K) from the annealed surface. Corresponding oxygen TPD spectra also showed less oxygen scrambling on the annealed surface.

Comparing CO titration experiments from annealed and unannealed oxygen pre-covered Au(111) surfaces shows more CO_2 being produced on the unannealed surface. Subsequent oxygen TPD spectra after each CO_2 titration experiment showed that there was an increasing amount of unreacted oxygen as annealing temperature increased.

The surface carbonate formation experiments on atomic oxygen pre-covered Au(111) surface pre-annealed before CO_2 dose also showed significantly lower reaction probability. Since oxygen mixing is due to carbonate formation and decomposition, less carbonate seems to be formed on the annealed surface to begin with. This also further reiterates our previous report that the carbonate formation and decomposition reaction on oxygen pre-covered Au(111) originates from $C^{18}O_2$ reacting with adsorbed atomic oxygen to form surface carbonate ($C^{18}O^{18}O^{16}O$). Upon heating the surface during TPD, the surface carbonate decomposes into $^{18}CO_2$ and adsorbed atomic oxygen ($^{18}O_a$ and

$^{16}O_a$). We hypothesize that the observed reduction in reactivity is due to thermal stabilization of metastable oxygen species as a result of pre-annealing the oxygen covered Au(111) surfaces reported in this work. These metastable oxygen species are responsible for the higher reactivity observed on the unannealed surfaces.

REFERENCES

(1) Haruta, M.; Kobayashi, T.; Sano, H.; Yamada, N. *Chem. Lett.* **1987**, 405.
(2) Bondzie, V. A.; Parker, S. C.; Campbell, C. T. *Catal Lett.* **1999**, *63*, 143.
(3) Grunwaldt, J. D.; Baiker, A. *J. Phys. Chem. B* **1999**, *103*, 1002.
(4) Schubert, M. M.; Hackenberg, S.; van Veen, A. C.; Muhler, M.; Plzak, V.; Behm, R. J. *J. Catal.* **2001**, *197*, 113.
(5) Hakkinen, H.; Landman, U. *J. Am. Chem. Soc.* **2001**, *123*, 9704.
(6) Konova, P.; Naydenov, A.; Venkov, C.; Mehandjiev, D.; Andreeva, D.; Tabakova, T. *J. Mol. Catal. A* **2004**, *213*, 235.
(7) Stiehl, J. D.; Gong, J. L.; Ojifinni, R. A.; Kim, T. S.; McClure, S. M.; Mullins, C. B. *J. Phys. Chem. B* **2006**, *110*, 20337.
(8) Stiehl, J. D.; Kim, T. S.; McClure, S. M.; Mullins, C. B. *J. Am. Chem. Soc.* **2004**, *126*, 13574.
(9) Stiehl, J. D.; Kim, T. S.; McClure, S. M.; Mullins, C. B. *J. Am. Chem. Soc.* **2004**, *126*, 1606.
(10) Stiehl, J. D.; Kim, T. S.; McClure, S. M.; Mullins, C. B. *J. Phys. Chem. B* **2005**, *109*, 6316.
(11) Stiehl, J. D.; Kim, T. S.; Reeves, C. T.; Meyer, R. J.; Mullins, C. B. *J. Phys. Chem. B* **2004**, *108*, 7917.
(12) Carley, A. F.; Davies, P. R.; Roberts, M. W. *Curr. Opin. Solid St. Mat. Sci.* **1997**, *2*, 525.
(13) Gallagher, D. E. Photoelctron spectroscopic studies of aluminum and chromium surfaces, University of Wales, 1987.
(14) Carley, A. F. R., S.; and Roberts, M.W. *Surf. Sci.* **1983**, *135*, 35.
(15) Carley, A. F.; Roberts, M. W. Unpublished results.
(16) Au, C. T.; Roberts, M. W.; Zhu, A. R. *Proc. R. Soc. London, Ser. A* **1984**, *396*, 165.
(17) Au, C. T.; Roberts, M. W.; Zhu, A. R. *J. Chem. Soc. -Chem. Commun.* **1984**, 737.
(18) Sueyoshi, T.; Sasaki, T.; Y., I. *Chem. Phys. lett.* **1995**, *241*, 189.
(19) Sueyoshi, T.; Sasaki, T.; Y., I. *Surf. Sci.* **1995**, *343*, 1.
(20) Sueyoshi, T.; Sasaki, T.; Y., I. *J. Phys. Chem.* **1996**, *100*, 1048.
(21) Sasaki, T.; Sueyoshi, T.; Y., I. *Surf. Sci.* **1994**, *316*, L1081.
(22) Boyen, H. G.; Kastle, G.; Weigl, F.; Koslowski, B.; Dietrich, C.; Ziemann, P.; Spatz, J. P.; Riethmuller, S.; Hartmann, C.; Moller, M.; Schmid, G.; Garnier, M. G.; Oelhafen, P. *Science* **2002**, *297*, 1533.
(23) Canning, N. D. S.; Outka, D. A.; Madix, R. J. *Surf. Sci.* **1984**, *141*, 240.
(24) Choudhary, T. V.; Goodman, D. W. *Top. Catal.* **2002**, *21*, 25.
(25) Daniells, S. T.; Makkee, M.; Moulijn, J. A. *Catal. Lett.* **2005**, *100*, 39.
(26) Date, M.; Haruta, M. *J. Catal.* **2001**, *201*, 221.
(27) Davis, K. A.; Goodman, D. W. *J.Phys. Chem. B* **2000**, *104*, 8557.
(28) Gong, J. L.; Ojifinni, R. A.; Kim, T. S.; Stiehl, J. D.; McClure, S. M.; White, J. M.; Mullins, C. B. *Top. Catal.* **2007**, *44*, 57.
(29) Gong, J. L.; Ojifinni, R. A.; Kim, T. S.; White, J. M.; Mullins, C. B. *J. Am. Chem. Soc.* **2006**, *128*, 9012.
(30) Gong, X. Q.; Hu, P.; Raval, R. *J. Chem.Phys.* **2003**, *119*, 6324.

(31) Gottfried, J. M.; Elghobashi, N.; Schroeder, S. L. M.; Christmann, K. *Surf. Sci.* **2003**, *523*, 89.
(32) Gottfried, J. M.; Schmidt, K. J.; Schroeder, S. L. M.; Christmann, K. *Surf. Sci.* **2002**, *511*, 65.
(33) Gottfried, J. M.; Schmidt, K. J.; Schroeder, S. L. M.; Christmann, K. *Surf. Sci.* **2003**, *525*, 184.
(34) Kim, T. S.; Stiehl, J. D.; Reeves, C. T.; Meyer, R. J.; Mullins, C. B. *J. Am. Chem. Soc.* **2003**, *125*, 2018.
(35) Lazaga, M. A.; Wickham, D. T.; Parker, D. H.; Kastanas, G. N.; Koel, B. E. *ACS Symposium Series* **1993**, *523*, 90.
(36) Liu, Z. P.; Hu, P.; Alavi, A. *J. Am. Chem. Soc.* **2002**, *124*, 14770.
(37) Liu, Z.-P.; Jenkins, S. J.; King, D. A. *Phys. Rev. Lett.* **2005**, *94*, 196102.
(38) Lopez, N.; Norskov, J. K. *J. Am. Chem. Soc.* **2002**, *124*, 11262.
(39) Mills, G.; Gordon, M. S.; Metiu, H. *J. Chem. Phys.* **2003**, *118*, 4198.
(40) Min, B. K.; Alemozafar, A. R.; Pinnaduwage, D.; Deng, X.; Friend, C. M. *J. Phys. Chem. B* **2006**, *110*, 19833.
(41) Outka, D. A.; Madix, R. J. *Surf. Sci.* **1987**, *179*, 351.
(42) Parker, D. H.; Koel, B. E. *J. Vac. Sci. Tech. A* **1990**, *8*, 2585.
(43) Pireaux, J. J.; Chtaib, M.; Delrue, J. P.; Thiry, P. A.; Liehr, M.; Caudano, R. *Surf. Sci.* **1984**, *141*, 211.
(44) Saliba, N.; Parker, D. H.; Koel, B. E. *Surf. Sci.* **1998**, *410*, 270.
(45) Schrader, M. E. *Surf. Sci.* **1978**, *78*, L227.
(46) Trapnell, B. M. W. *Proceedings of the Royal Society, A*. **1952**, *218*, 566.
(47) Outka, D. A.; Madix, R. J. *J. Am. Chem. Soc.* **1987**, *109*, 1708.
(48) Gong, J. L.; Flaherty, D. W.; Ojifinni, R. A.; White, J. M.; Mullins, C. B. *J. Phys Chem. C Submitted for publication*.
(49) Kim, T. S.; Gong, J.; Ojifinni, R. A.; White, J. M.; Mullins, C. B. *J. Am. Chem. Soc.* **2006**, *128*, 6282.
(50) Ojifinni, R. A.; Froemming, N. S.; Gong, J. L.; Pan, M.; Kim, T. S.; White, J. M.; Henkelman, G.; Mullins, C. B. *In preparation* **2008**.
(51) Ojifinni, R. A.; Gong, J. L.; Flaherty, D. W.; Pan, M.; Mullins, C. B. *In preparation* **2008**.
(52) Gottfried, J. M.; Schmidt, K. J.; Schroeder, S. L. M.; Christmann, K. *Surf. Sci.* **2003**, *536*, 206.
(53) Paul, A. M.; Bent, B. E. *J. Catal.* **1994**, *147*, 264.
(54) Wheeler, M. C.; Reeves, C. T.; Seets, D. C.; Mullins, C. B. *J. Chem. Phys.* **1998**, *108*, 3057.
(55) Wheeler, M. C.; Seets, D. C.; Mullins, C. B. *J. Chem. Phys.* **1996**, *105*, 1572.
(56) Wheeler, M. C.; Seets, D. C.; Mullins, C. B. *J. Chem. Phys.* **1997**, *107*, 1672.
(57) Pollard, J. E. *Rev. Sci. Instru.* **1992**, *63*, 1771.
(58) Felter, T. E.; Weinberg, W. H.; Lastushkina, G. Y.; Boronin, A. I.; Zhdan, P. A.; Boreskov, G. K.; Hrbek, J. *Surf. Sci.* **1982**, *118*, 369.
(59) Behm, R. J.; Brundle, C. R. *J. Vac. Sci. Tech. A 1* **1983**, *1*, 1223.

Figure 4.1

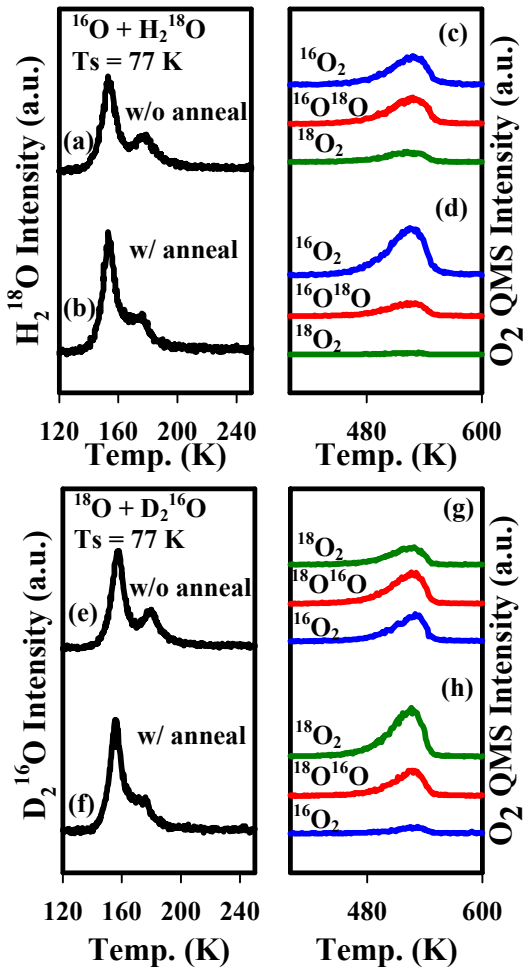

Figure 4.1: TPD Spectra of $H_2{}^{18}O$ after dosing (a) 0.53 ML of $H_2{}^{18}O$ in addition to 0.18 ML of ^{16}O on Au(111); (b) 0.18 ML of ^{16}O on Au(111) at 77 K, and annealing the surface to 300 K (β = 1 K/s) followed by 0.53 ML of $H_2{}^{18}O$ dose at 77 K. Figures 1 (c) and (d) represent the corresponding oxygen TPD for (a) and (b) respectively.
TPD spectra of $D_2{}^{16}O$ from (e) a surface similar to [1 (a)], but with $D_2{}^{16}O$ and ^{18}O; (f) a surface similar to [1 (b)], but with D_2O and ^{18}O. Figure 1 (g) and (h) represent the corresponding oxygen TPD spectra for 1 (e) to (f) respectively. All doses are done at 77 K and the heating ramps are 1 K/s for water and 3 K/s for oxygen.

Figure 4.2

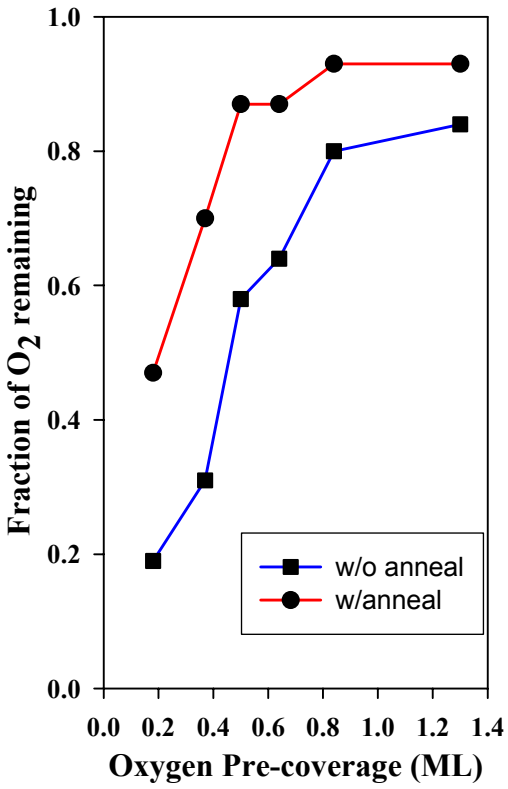

Figure 4.2: Fraction of mass 32 oxygen remaining on the Au(111) surface from TPD taken after dosing 0.53 ML of $H_2{}^{18}O$ on top of six different amounts (0.18 ML, 0.37 ML, 0.50 ML, 0.64 ML, 0.84 ML and 1.30 ML) of ^{16}O. The lower plot shows the fraction of mass 32 oxygen remaining on the unannealed surface, while upper plot shows the fraction of mass 32 oxygen remaining on the surface that was annealed to 300 K after oxygen dose and cooled back to 77 K before $H_2{}^{18}O$ dose. All isotopically labeled water and oxygen atoms were dosed at 77 K. A heating rate of β = 1K/s was used for water and β = 3 K/s was used for oxygen.

Figure 4.3

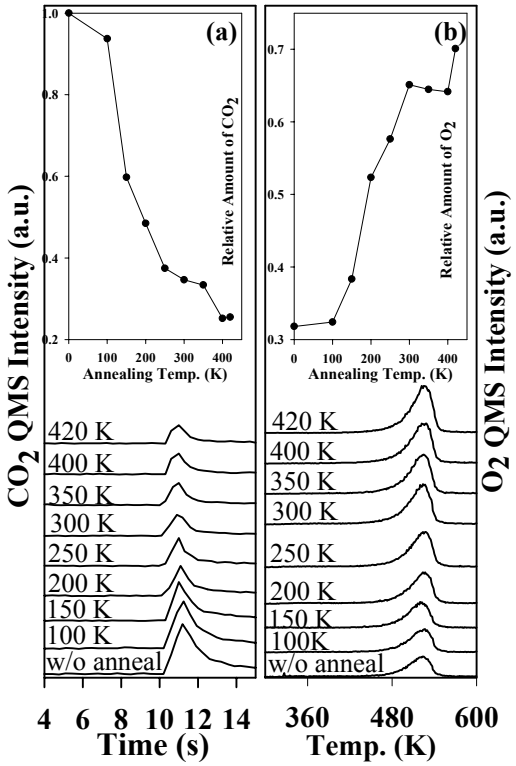

Figure 4.3: (a) CO_2 evolution at 77 K from eight different 0.37 ML ^{16}O covered Au(111) surfaces annealed to varying temperatures (100 K, 150 K, 200 K, 250 K, 300 K, 350 K, 400 K , 420 K respectively) at β=1K/s and cooled to 77 K in each case before 10sec CO dose. The ninth curve (lowest curve) represents CO_2 evolution from an unannealed surface. The inset in the upper portion of the panel shows the normalized amount of CO_2 evolved as a function of annealing temperature. (b) TPD spectra showing unreacted O_2 remaining on the Au(111) surface after CO oxidation in each of the above case. Again, the lowest curve represents TPD of the remaining oxygen on the unannealed surface. The inset in the upper portion of panel shows the normalized amount of O_2 remaining on the surface as a function of annealing temperature.

Figure 4.4

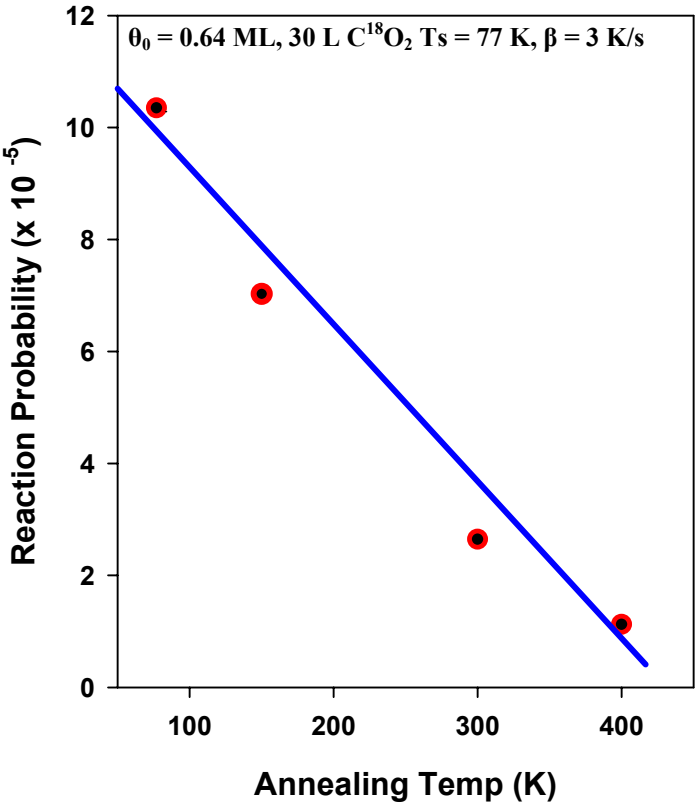

Figure 4.4: Reaction probability of carbonate formation as a function of annealing temperature on 0.64 ML ^{16}O pre-covered Au(111) surface at 77 K followed by exposure to 30 L $C^{18}O_2$ at 77 K. The surface was annealed to higher temperatures 150 K, 300 K and 400 K before $C^{18}O_2$. The leftmost point represents carbonate formation probability from a surface that was not annealed prior to $C^{18}O_2$ exposure. All surface doses and exposures were done at 77 K and a heating ramp of 3 K/s was used in all cases.

Chapter 5 Concluding Remarks

There is no doubt that more is known today about gold catalysis than was known twenty years ago. Haruta's pioneer work[1] on gold NPs supported on metal oxides has sensitized the catalysis and surface science community to the great potential of gold in catalyzing reactions that are useful for both fundamental and industrial applications. Despite the wealth of information from several studies[2-14] about gold catalysis in general and in particular, about low temperature CO oxidation, this subject area is far from being completely understood. Several aspects of gold catalysis are still debated in literature. Issues pertaining to the mechanistic details of low temperature CO oxidation such as the nature of active sites, the nature of the reactive oxygen species, the role of support and the role of moisture, all require further studies. This dissertation has therefore focused on a number of these issues mentioned above.

In general, the use of single crystal Au(111) can help to understand how important the metal oxide support is in gold catalysis. For all the experiments shown in this dissertation, the Au(111) surface was pre-covered with atomic oxygen using an RF plasma jet. Similar reactions to those reported by classical catalytic studies on supported gold NPs were also observed on oxygen pre-covered Au(111). For example, Date and Haruta showed that water promoted CO oxidation on well-prepared Au/TiO_2,[15,16] this same phenomenon was observed by impinging CO on atomic oxygen pre-covered Au(111) to which water was added. This shows that not only is gold NPs (with or without support) reactive, bulk gold can also be reactive given the right conditions like pre-covering with atomic oxygen. Atomic oxygen is necessary because the dissociative adsorption of molecular oxygen on Au(111) is a highly activated reaction. Another issue

is that the lifetime of molecular oxygen on Au(111) is very short as it desorbs at temperatures lower than 77 K which is the lowest temperature used in this work.

In Chapter 2, experimental evidence and DFT calculations were presented to show that water enhances CO oxidation on Au(111) by water and oxygen first forming hydroxyls followed by CO reacting with these hydroxyls to form CO_2. It was shown that water is directly involved in CO oxidation reactions contrary to previous reports that water is acting as a spectator molecule. Using isotopically labeled water ($H_2{}^{18}O$) co-adsorbed with atomic oxygen (^{16}O), water was shown to react with water to form hydroxyls. DFT calculations showed that the hydroxyl formation was rapid and facile because the kinetic barrier to the reaction is only 0.11 eV (45 K). The oxygen exchange observed in TPD further proves that the hydroxyls formed from water-oxygen reaction recombine very rapidly and reversibly with only 0.05 eV energy difference between the O/H_2O initial state and 2OH final state. Impinging $C^{16}O$ on the Au(111) co-adsorbed with $H_2{}^{18}O$ and ^{16}O produced 46 $^{18}OC^{16}O$ (in addition to 44 $^{16}OC^{16}O$). The ^{18}O undoubtedly originated from water and proves the direct involvement of the adsorbed water in CO oxidation. It was noted however, that impinging $C^{16}O$ a Au(111) surface pre-covered with only $H_2{}^{18}O$ did not oxidize CO to produce CO_2. Hence, hydroxyls are the active species in water assisted CO oxidation. Isotope effects were observed as differences in oxygen scrambling and in CO_2 production between co-adsorbing H_2O and D_2O. These isotope effects reinforced the proposed model of CO oxidation by hydroxyls formed by water reacting with co-adsorbed oxygen.

In Chapter 3, the formation of surface carbonate on oxygen pre-covered Au(111) was investigated. Experimental results supported by DFT calculations were presented to

show that surface carbonate can be formed on oxygen pre-covered Au(111). $^{16}O^{18}O$ (mass 34) was used as the signature for carbonate formation and decomposition when a Au(111) surface pre-covered with ^{16}O was exposed to $C^{18}O_2$. A fascinating observation was that mass 34 production increased as the surface was exposed to more $C^{18}O_2$ while holding oxygen coverage and surface temperature fixed. There was no detectable $^{16}O^{18}O$ formation when a clean Au(111) surface was exposed to $C^{18}O_2$. Interestingly, an oxygen-coverage dependent carbonate formation and decomposition was observed as more and more mass 34 was produced with increasing oxygen pre-coverage until saturation coverage of oxygen on Au(111) was reached. $C^{18}O_2$ was reported to first react with adsorbed atomic oxygen to form surface carbonate species, $C^{18}O^{18}O^{16}O$. This carbonate species decompose upon heating and leaving $^{16}O_a$ and $^{18}O_a$ on the surface. $^{16}O^{18}O$ was produced from the recombinative desorption of the $^{16}O_a$ and $^{18}O_a$ left on the surface. Chapter 3 also reported that there was no oxygen loss during the carbonate formation and decomposition reaction, an important observation made previously about carbonate formation and decomposition reaction on Ag(110).[17] One significant observation from Chapter 3 is that surface carbonates can be formed on gold and the claim by some studies[18,19] that carbonate formation is an important step during CO oxidation might be true.

The nature of the reactive oxygen species on gold has drawn some attention as it is believed to be important in determining the mechanistic details of many oxidation reactions. Chapter 4 is a presentation of results showing the effect of annealing on the reactivity of atomic oxygen pre-covered Au(111). Results are presented to show the annealing effect on the reactivity of oxygen using water, carbon monoxide and carbon

dioxide as probe molecules. Chapter 4 examines the previously believed notion that the reactivity of oxygen can be changed by changing the adsorption conditions of oxygen on the surface. On Au(111), TPD results of water-oxygen interaction on an annealed surface indicates that the reactive oxygen state is the unannealed oxygen state. Experimental results showed less water-oxygen interaction on the annealed surface as evident in both the water and oxygen TPD spectra. CO titration experiments from annealed and unannealed oxygen pre-covered Au(111) surfaces also showed more CO_2 being produced on the unannealed surface. There was an increase in the amount of unreacted oxygen as annealing temperature increased showing stabilization of the oxygen overlayer as a result of annealing. Results were also presented showing that the surface carbonate formation on annealed and unannealed oxygen pre-covered Au(111) surfaces are different. Significantly less $^{16}O^{18}O$ (mass 34) was produced on the annealed surfaces. Chapter 4 concludes that metastable oxygen is the reactive oxygen species on our Au(111) sample similar to observations on other metal surfaces.[20-23] Annealing is believed to stabilize these reactive oxygen species thereby making them less reactive to probe molecules on the surface. This work therefore further provides experimental evidence that atomic oxygen is a reactive species on gold and that its reactivity can be altered by changing the adsorption conditions on the surface.

RECOMMENDATIONS FOR FUTURE RESEARCH

Gold catalysis continues to draw attention as more energy and resources are focused on understanding the mechanistic details of the unique reactivity of metal-oxide supported Au NPS < 5 nm in diameter. On one hand, the provision of a complete picture for the surprising activity of Au NPs towards low temperature CO oxidation is a motivating factor for doing more work on gold catalysis. Another motivating factor is exploring areas of possible future research and applications that are currently being catalyzed by other metals. The use of Au in bimetallic catalysis is a new and growing area of interest. Goodman and co-workers reported in a recent publication that Au can be used as a promoter in a bimetallic Au-Pd catalyst.[24] This and other results continue to emerge about the enormous potentials of gold catalysis. Although I have presented experimental results and DFT calculations to shed more light on some of the controversial issues pertaining to low temperature CO oxidation and some other aspects of gold catalysis, more work still needs to be done in order to move closer to a position where there is a vivid picture of the mechanistic details of gold catalysis.

Pertaining to the role of moisture in low temperature CO oxidation, I suggest two additional experiments. The first experiment is to use other surface spectroscopy tools to determine the intermediates that are formed during the water-oxygen interactions and CO oxidation in the presence of co-adsorbed water and oxygen. Using Infra red Adsorption Spectroscopy (IRAS) is a possible way to confirm the formation of OH or OD as the vibrational modes can be observed and differentiated. IR spectra from co-adsorbing a Au(111) surface with both water and oxygen can be used to garner information about the species available on the surface under different reaction conditions. Experimental results

and DFT calculations presented in Chapter 2 suggested that COOH and OHCOOH are both possible intermediate during CO oxidation. IR spectra during CO impingement on a Au(111) surface co-adsorbed with water and oxygen might provide very useful information about the presence of COOH or other intermediates during this reaction.

Another useful experiment to complement my work on water enhanced CO oxidation on Au(111) is the use of metal oxide supported Au NPs. Since the (111) surface is the most predominant surface of supported gold NPs, impinging a CO beam after co-adsorbing water and oxygen on oxide-supported Au NPs will help confirm results from the Au(111) surface. Using oxide-supported Au NPs will also mimic Date and Haruta's classical catalysis work[15,16] on CO oxidation by water under clean UHV conditions.

The effect of nanoparticle size on reactivity can also be studied using methods that can allow the deposition of size-controlled metal NPs. Our lab has the capability of making size-selected metal nanoparticles using a commercial nanocluster deposition

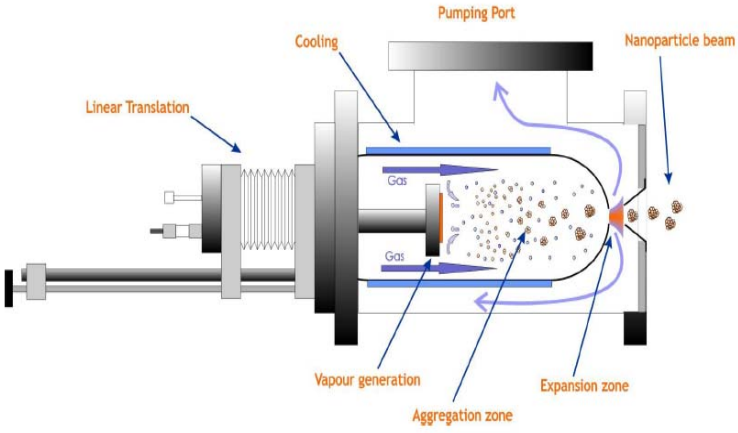

Figure 5.1: Schematic illustration of NP formation.

system Nanogen50 (Figure 5.1) placed in line with a quadrupole mass filter (MesoQ) both purchased from Mantis Deposition Limited, UK. The nanocluster deposition system

works by using a dc magnetron sputtering discharge. By striking a plasma of Ar carrier gas at high voltage (typically > 500V, and > 100mA current), a magnetron discharge formed and is directed towards the 2" diameter sputter target (cathode) where it sputters off the target metal into the aggregation zone. The cluster vapor is condensed and agglomerated by gases (usually Ar or He) in the aggregation zone. The aggregated clusters (both ionized and neutral species) are introduced into the quadrupole where they are size-selected based on the input into the computer software. Figure 5.2 shows a typical mass distribution of unfiltered NPs.

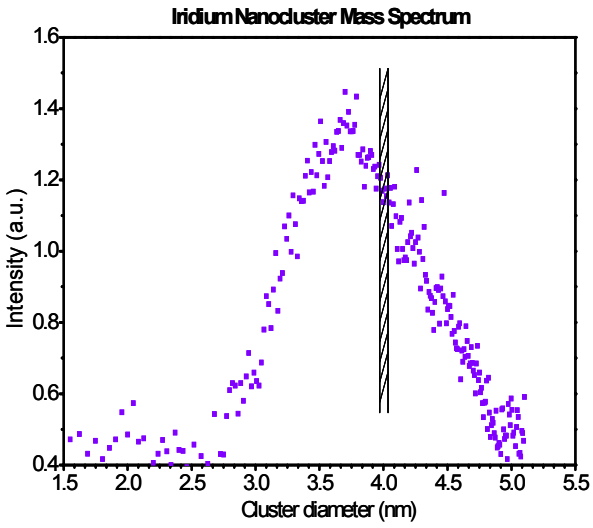

Figure 5.2: Example of size distribution spectrum of Ir nanoclusters without mass filtering.

Having presented a brief account about the concept of carbonate formation on oxygen pre-covered Au(111), I recommend a full-scale study using both experiments and calculations. A more systematic approach incorporating experiments and DFT calculations might be able to explain the difference in reactivity between single crystal Ag(110) and results presented in Chapter 3 on Au(111). I am also curious about how the chemistry might differ due to possible structural effects on the more corrugated single

crystal Au(110) surface. A structural effect on reactivity has been seen as differences carbonate formation on Ag(110) and Ag(111) where the reaction is very facile on the (110) surface of silver. An extension of this study on supported NPs might also provide useful information in understanding the surface chemistry of carbonate formation and decomposition on gold.

REFERENCES

(1) Haruta, M.; Kobayashi, T.; Sano, H.; Yamada, N. *Chem. Lett.* **1987**, 405.
(2) Bond, G. C.; Thompson, D. T. *Catal. Rev.* **1999**, *41*, 319.
(3) Chen, M. S.; Goodman, D. W. *Science* **2004**, *306*, 252.
(4) Chen, M. S.; Goodman, D. W. *Acc. Chem. Res.* **2006**, *39*, 739.
(5) Haruta, M. *Catal. Today* **1997**, *36*, 153.
(6) Haruta, M. *Cattech* **2002**, *6*, 102.
(7) Haruta, M.; Date, M. *Appl. Catal. A* **2001**, *222*, 427.
(8) Kim, T. S.; Stiehl, J. D.; Reeves, C. T.; Meyer, R. J.; Mullins, C. B. *J. Am. Chem. Soc.* **2003**, *125*, 2018.
(9) Meyer, R.; Lemire, C.; Shaikhutdinov, S. K.; Freund, H. *Gold Bull.* **2004**, *37*, 72.
(10) Stiehl, J. D.; Gong, J. L.; Ojifinni, R. A.; Kim, T. S.; McClure, S. M.; Mullins, C. B. *J. Phys. Chem. B* **2006**, *110*, 20337.
(11) Stiehl, J. D.; Kim, T. S.; McClure, S. M.; Mullins, C. B. *J. Am. Chem. Soc.* **2004**, *126*, 13574.
(12) Stiehl, J. D.; Kim, T. S.; McClure, S. M.; Mullins, C. B. *J. Am. Chem. Soc.* **2004**, *126*, 1606.
(13) Stiehl, J. D.; Kim, T. S.; McClure, S. M.; Mullins, C. B. *J. Phys. Chem. B* **2005**, *109*, 6316.
(14) Stiehl, J. D.; Kim, T. S.; Reeves, C. T.; Meyer, R. J.; Mullins, C. B. *J. Phys. Chem. B* **2004**, *108*, 7917.
(15) Date, M.; Haruta, M. *J. Catal.* **2001**, *201*, 221.
(16) Daté, M.; Okumura, M.; Tsubota, S.; Haruta, M. *Angew. Chem. Int. Edit* **2004**, *43*, 2129.
(17) Guo, X. C.; Madix, R. J. *J. Phys. Chem. B* **2001**, *105*, 3878.
(18) Hakkinen, H.; Landman, U. *J. Am. Chem. Soc.* **2001**, *123*, 9704.
(19) Konova, P.; Naydenov, A.; Venkov, C.; Mehandjiev, D.; Andreeva, D.; Tabakova, T. *J. Mol. Catal. A* **2004**, *213*, 235.
(20) Carley, A. F.; Davies, P. R.; Roberts, M. W. *Curr. Opin. Solid St. Mat. Sci.* **1997**, *2*, 525.
(21) Carley, A. F.; Davies, P. R.; Roberts, M. W.; Shukla, N.; Song, Y.; Thomas, K. K. *Appl. Surf. Sci.* **1994**, *81*, 265.
(22) Carley, A. F.; Davies, P. R.; Roberts, M. W.; Thomas, K. K. *Surf. Sci.* **1990**, *238*, L467.
(23) Carley, A. F. R., S.; and Roberts, M.W. *Surf. Sci.* **1983**, *135*, 35.
(24) Chen, M. S.; Kumar, D.; Yi, C. W.; Goodman, D. W. *Science* **2005**, *310*, 291.

Bibliography

Bond, G. C.; Thompson, D. T. *Gold Bull.* **2000**, *33*, 41.

Pitzer, K. S. *Acc. Chem. Res.* **1979**, *12*, 272.

Pyykko, P. *Angew. Chem.-Int. Ed.* **2002**, *41*, 3573.

Pyykko, P.; Desclaux, J. P. *Acc. Chem. Res.* **1979**, *12*, 276.

Meyer, R.; Lemire, C.; Shaikhutdinov, S. K.; Freund, H. *Gold Bull.* **2004**, *37*, 72.

Bond, G. C.; Thompson, D. T. *Catal. Rev.-Science and Engineering* **1999**, *41*, 319.

Chen, M. S.; Goodman, D. W. *Science* **2004**, *306*, 252.

Chen, M. S.; Kumar, D.; Yi, C. W.; Goodman, D. W. *Science* **2005**, *310*, 291.

Haruta, M. *Catal. Today* **1997**, *36*, 153.

Stiehl, J. D.; Kim, T. S.; McClure, S. M.; Mullins, C. B. *J. Am. Chem. Soc.* **2004**, *126*, 13574.

Gong, X. Q.; Hu, P.; Raval, R. *J. Chem.Phys.* **2003**, *119*, 6324.

Kim, T. S.; Gong, J.; Ojifinni, R. A.; White, J. M.; Mullins, C. B. *J. Am. Chem. Soc.* **2006**, *128*, 6282.

Min, B. K.; Wallace, W. T.; Goodman, D. W. *Surf. Sci.* **2006**, *600*, L7.

Valden, M.; Lai, X.; Goodman, D. W. *Science* **1998**, *281*, 1647.

Fu, Q.; Saltsburg, H.; Flytzani-Stephanopoulos, M. *Science* **2003**, *301*, 935.

Hayashi, T.; Tanaka, K.; Haruta, M. *J. Catal.* **1998**, *178*, 566.

Mul, G.; Zwijnenburg, A.; van der Linden, B.; Makkee, M.; Moulijn, J. A. *J. Catal.* **2001**, *201*, 128.

Stangland, E. E.; Stavens, K. B.; Andres, R. P.; Delgass, W. N. *J. Catal.* **2000**, *191*, 332.

Andreeva, D.; Idakiev, V.; Tabakova, T.; Ilieva, L.; Falaras, P.; Bourlinos, A.; Travlos, A. *Catal. Today* **2002**, *72*, 51.

Liu, Z.-P.; Jenkins, S. J.; King, D. A. *Phys. Rev. Lett.* **2005**, *94*, 196102.

Ueda, A.; Haruta, M. *Gold Bull.* **1999**, *32*, 3.

Nkosi, B.; Coville, N. J.; Hutchings, G. J.; Adams, M. D.; Friedl, J.; Wagner, F. E. *J. Catal.* **1991**, *128*, 366.

Nkosi, B.; Adams, M. D.; Coville, N. J.; Hutchings, G. J. *J. Catal.* **1991**, *128*, 378.

Guzman, J.; Gates, B. C. *J. Phys. Chem. B* **2002**, *106*, 7659.

Burke, L. D.; Nugent, P. F. *Gold Bull.* **1998**, *31*, 39.

Goodman, D. W. *Catal. Lett.* **2005**, *99*, 1.

Yoon, B.; Hakkinen, H.; Landman, U.; Worz, A. S.; Antonietti, J. M.; Abbet, S.; Judai, K.; Heiz, U. *Science* **2005**, *307*, 403.

Bondzie, V. A.; Parker, S. C.; Campbell, C. T. *J. Vac. Sci. Tech. A* **1999**, *17*, 1717.

Bondzie, V. A.; Parker, S. C.; Campbell, C. T. *Catal Lett.* **1999**, *63*, 143.

Hakkinen, H.; Landman, U. *J. Am. Chem. Soc.* **2001**, *123*, 9704.

Konova, P.; Naydenov, A.; Venkov, C.; Mehandjiev, D.; Andreeva, D.; Tabakova, T. *J. Mol. Catal. A* **2004**, *213*, 235.

Stiehl, J. D.; Kim, T. S.; McClure, S. M.; Mullins, C. B. *J. Am. Chem. Soc.* **2004**, *126*, 1606.

Stiehl, J. D.; Kim, T. S.; McClure, S. M.; Mullins, C. B. *J. Phys. Chem. B* **2005**, *109*, 6316.

Stiehl, J. D.; Kim, T. S.; Reeves, C. T.; Meyer, R. J.; Mullins, C. B. *J. Phys. Chem. B* **2004**, *108*, 7917.

Date, M.; Haruta, M. *J. Catal.* **2001**, *201*, 221.

Daté, M.; Okumura, M.; Tsubota, S.; Haruta, M. *Angew. Chem. Int. Edit* **2004**, *43*, 2129.

Gong, J. L.; Ojifinni, R. A.; Kim, T. S.; Stiehl, J. D.; McClure, S. M.; White, J. M.; Mullins, C. B. *Top. Catal.* **2007**, *44*, 57.

Barth, J. V.; Brune, H.; Ertl, G.; Behm, R. J. *Phys. Rev. B* **1990**, *42*, 9307.

Lazaga, M. A.; Wickham, D. T.; Parker, D. H.; Kastanas, G. N.; Koel, B. E. *ACS Symposium Series* **1993**, *523*, 90.

Carley, A. F.; Davies, P. R.; Roberts, M. W. *Curr. Opin. Solid St. Mat. Sci.* **1997**, *2*, 525.

Carley, A. F.; Davies, P. R.; Roberts, M. W.; Shukla, N.; Song, Y.; Thomas, K. K. *Appl. Surf. Sci.* **1994**, *81*, 265.

Carley, A. F.; Davies, P. R.; Roberts, M. W.; Thomas, K. K. *Surf. Sci.* **1990**, *238*, L467.

Carley, A. F.; Roberts, M. W. Unpublished results.

Carley, A. F. R., S.; and Roberts, M.W. *Surf. Sci.* **1983**, *135*, 35.

Ajo, H. M.; Bondzie, V. A.; Campbell, C. T. *Catal. Lett.* **2002**, *V78*, 359.

Bollinger, M. A.; Vannice, M. A. *Appl. Catal. B* **1996**, *8*, 417.

Bond, G. C.; Thompson, D. T. *Catal. Rev.* **1999**, *41*, 319.

Boyen, H. G.; Kastle, G.; Weigl, F.; Koslowski, B.; Dietrich, C.; Ziemann, P.; Spatz, J.

Chen, M. S.; Goodman, D. W. *Acc. Chem. Res.* **2006**, *39*, 739.

Choudhary, T. V.; Goodman, D. W. *Top. Catal.* **2002**, *21*, 25.

Choudhary, T. V.; Goodman, D. W. *App. Catal. A* **2005**, *291*, 32.

Chusuei, C. C.; Lai, X. F.; Davis, K. A.; Bowers, E. K.; Goodman, D. W.; Omary, M. A.; Rawashdeh-Omary, M. A.; Fackler, J. P.; Bagus, P. S. *Abstracts of Papers of the American Chemical Society* **2000**, *220*, U237.

Crowell, J. E.; Chen, J. G.; Hercules, D. M.; Yates, J. J. T. *J. Chem. Phys.* **1987**, *86*, 5804.

Daniells, S. T.; Makkee, M.; Moulijn, J. A. *Catal. Lett.* **2005**, *100*, 39.

Hodge, N. A.; Kiely, C. J.; Whyman, R.; Siddiqui, M. R. H.; Hutchings, G. J.; Pankhurst, Q. A.; Wagner, F. E.; Rajaram, R. R.; Golunski, S. E. *Catal. Today* **2002**, *72*, 133.

Kolmakov, A.; Goodman, D. W. *Catal. Lett.* **2000**, *70*, 93.

Kolmakov, A.; Goodman, D. W. *Surf. Sci.* **2001**, *490*, L597.

Lin, S. D.; Bollinger, M.; Vannice, M. A. *Catal. Lett.* **1993**, *17*, 245.

Liu, Z. P.; Hu, P.; Alavi, A. *J. Am. Chem. Soc.* **2002**, *124*, 14770.

Lopez, N.; Norskov, J. K. *J. Am. Chem. Soc.* **2002**, *124*, 11262.

Luo, K.; Kim, D. Y.; Goodman, D. W. *J. Mol. Catal. A-Chem* **2001**, *167*, 191.

Mills, G.; Gordon, M. S.; Metiu, H. *J. Chem. Phys.* **2003**, *118*, 4198.

Min, B. K.; Alemozafar, A. R.; Pinnaduwage, D.; Deng, X.; Friend, C. M. *J. Phys. Chem. B* **2006**, *110*, 19833.

Outka, D. A.; Madix, R. J. *J. Am. Chem. Soc.* **1987**, *109*, 1708.

Outka, D. A.; Madix, R. J. *Surf. Sci.* **1987**, *179*, 351.

Schubert, M. M.; Hackenberg, S.; van Veen, A. C.; Muhler, M.; Plzak, V.; Behm, R. J. *J. Catal.* **2001**, *197*, 113.

Schumacher, B.; Plzak, V.; Kinne, M.; Behm, R. J. *Catal. Lett.* **2003**, *V89*, 109.

Stiehl, J. D.; Gong, J. L.; Ojifinni, R. A.; Kim, T. S.; McClure, S. M.; Mullins, C. B. *J. Phys. Chem. B* **2006**, *110*, 20337.

Wallace, W. T.; Min, B. K.; Goodman, D. W. *J. Mol. Catal. A* **2005**, *228*, 3.

Wang, Z. L.; Gao, R. P.; Nikoobakht, B.; El-Sayed, M. A. *J. Phys. Chem. B* **2000**, *104*, 5417.

Yan, Z.; Chinta, S.; Mohamed, A. A.; Fackler, J. P.; Goodman, D. W. *Catal. Lett.* **2006**, *111*, 15.

Gong, J. L.; Ojifinni, R. A.; Kim, T. S.; White, J. M.; Mullins, C. B. *J. Am. Chem. Soc.* **2006**, *128*, 9012.

Grunwaldt, J. D.; Baiker, A. *J. Phys. Chem. B* **1999**, *103*, 1002.

Xu, Y.; Mavrikakis, M. *J. Phys. Chem. B* **2003**, *107*, 9298.

Baltrusaitis, J.; Schuttlefield, J. D.; Zeitler, E.; Jensen, J. H.; Grassian, V. H. *J. Phys. Chem. C* **2007**, *111*, 14870.

Baro, A. M.; Erley, W. *J. Vac. Sci. Tech.* **1982**, *20*, 580.

Callen, B. W.; Griffiths, K.; Norton, P. R.; Harrington, D. A. *J. Phys. Chem. B* **1992**, *96*, 10905.

Jiang, P.; Zappone, M. W.; Bernasek, S. L.; Robertson, J. A. *J. Vac. Sci. Tech. A* **1996**, *14*, 2372.

Shao, Y.; Paul, J. *Appl. Surf. Sci.* **1993**, *72*, 113.

Spitzer, A.; Luth, H. *Surf. Sci.* **1985**, *160*, 353.

Au, C. T.; Carley, A. F.; Pashuski, A.; Read, S.; Roberts, M. W.; Zeini-Isfahan, A. *Springer Series in Surface Sciences* **1993,** *33*, 241.

Bedurftig, K.; Volkening, S.; Wang, Y.; Wintterlin, J.; Jacobi, K.; Ertl, G. *J. Chem. Phys.* **1999**, *111*, 11147.

Creighton, J. R.; White, J. M. *Surf. Sci.* **1984**, *136*, 449.

Klaua, M.; Madey, T. E. *Surf. Sci.* **1984**, *136*, L42.

Seitsonen, A. P.; Zhu, Y.; Bedurftig, K.; Over, H. *J. Am. Chem. Soc.* **2001**, *123*, 7347.

Bange, K.; Madey, T. E.; Sass, J. K.; Stuve, E. M. *Surf. Sci.* **1987**, *183*, 334.

Fisher, G. B.; Sexton, B. A. *Phys. Rev. Lett.* **1980**, *44*, 683.

Kubota, J.; Kondo, J.; Domen, K.; Hirose, C. *Surf. Sci.* **1993**, *295*, 169.

Nyberg, C.; Tengstl, C. G. *J. Chem. Phys.* **1984**, *80*, 3463.

Henderson, M. A. *Surf. Sci. Rep.* **2002**, *46*, 1.

Doering, D. L.; Madey, T. E. *Surf. Sci.* **1982**, *123*, 305.

Kretzschmar, K.; Sass, J. K.; Hofmann, P.; Ortega, A.; Bradshaw, A. M.; Holloway, S. *Chem. Phys. Lett.* **1981**, *78*, 410.

Madey, T. E.; Yates, J. J. T. *Chem. Phys. Lett.* **1977**, *51*, 77.

Pache, T.; Steinruck, H. P.; Huber, W.; Menzel, D. *Surf. Sci.* **1989**, *224*, 195.

Schulze, M.; Reißner, R.; Bolwin, K.; Kuch, W. *Fresenius J. Anal. Chem.* **1995**, *V353*, 661.

Thiel, P. A.; Hoffmann, F. M.; Weinberg, W. H. *Phys. Rev. Lett.* **1982**, *49*, 501.

Wheeler, M. C.; Seets, D. C.; Mullins, C. B. *J. Chem. Phys.* **1996**, *105*, 1572.

Pollard, J. E. *Rev. Sci. Instru.* **1992**, *63*, 1771.

Wheeler, M. C.; Reeves, C. T.; Seets, D. C.; Mullins, C. B. *J. Chem. Phys.* **1998**, *108*, 3057.

Wheeler, M. C.; Seets, D. C.; Mullins, C. B. *J. Chem. Phys.* **1997**, *107*, 1672.

Perdew, J. P. *Electronic structure of solids* Berlin, 1991.

Kresse, G.; Joubert, D. *Phys. Rev. B* **1999**, *59*, 1758.

Monkhorst, H. J.; Pack, J. D. *Phys. Rev. B* **1976**, *13*, 5188.

Henkelman, G.; Jonsson, H. *J. Chem. Phys.* **2000**, *113*, 9978.

Henkelman, G.; Uberuaga, B. P.; Jonsson, H. *J. Chem. Phys.* **2000**, *113*, 9901.

Henkelman, G.; Jonsson, H. *J. Chem. Phys.* **1999**, *111*, 7010.

Olsen, R. A.; Kroes, G. J.; Henkelman, G.; Arnaldsson, A.; Jonsson, H. *J. Chem. Phys.* **2004**, *121*, 9776.

Kay, B. D.; Lykke, K. R.; Creighton, J. R.; Ward, S. J. *J. Chem. Phys.* **1989**, *91*, 5120.

Sueyoshi, T.; Sasaki, T.; Iwasawa, Y. *J. Phys. Chem. B* **1997**, *101*, 4648.

Gorte, R. J.; Zhao, S. *Catal. Today* **2005**, *104*, 18.

Grenoble, D. C.; Estadt, M. M.; Ollis, D. F. *J. Catal.* **1981**, *67*, 90.

Salmi, T.; Hakkarainen, R. *Appl. Catal.* **1989**, *49*, 285.

Vanherwijnen, T.; Dejong, W. A. *J. Catal.* **1980**, *63*, 83.

Bunluesin, T.; Gorte, R. J.; Graham, G. W. *Appl. Catal. B* **1998**, *15*, 107.

Chinchen, G. C.; Spencer, M. S. *J. Catal.* **1988**, *112*, 325.

Rodriguez, J. A.; Ma, S.; Liu, P.; Hrbek, J.; Evans, J.; Perez, M. *Science* **2007**, *318*, 1757.

Erdohelyi, A.; Fodor, K.; Suru, G. *App. Catal. A* **1996**, *139*, 131.

Wang, J. G.; Hammer, B. *J. Catal.* **2006**, *243*, 192.

Lester, M. I.; Pond, B. V.; Anderson, D. T.; Harding, L. B.; Wagner, A. F. *J. Chem. Phys.* **2000**, *113*, 9889.

Rockmann, T.; Brenninkmeijer, C. A. M.; Saueressig, G.; Bergamaschi, P.; Crowley, J. N.; Fischer, H.; Crutzen, P. J. *Science* **1998**, *281*, 544.

Bergeld, J.; Kasemo, B.; Chakarov, D. V. *Surf. Sci.* **2001**, *495*, L815.

Hayden, B. E.; Rendall, M. E.; South, O. *J. Am. Chem. Soc.* **2003**, *125*, 7738.

Lei, T.; Zei, M. S.; Ertl, G. *Surf. Sci.* **2005**, *581*, 142.

Wieckowski, A. *J. Electroanal. Chem.* **1977**, *78*, 229.

Melander, L.; Saunders, W. H. J. *Reaction Rates of Isotopic Molecules*, 2nd ed.; Wiley, New York, 1980.

Bowker, M.; Barteau, M. A.; Madix, R. J. Surf. Sci. 1980, 92, 528.

Barteau, M. A.; Madix, R. J. J. Chem. Phys. 1981, 74, 4144.

Barteau, M. A.; Madix, R. J. J. Electron Spectrosc. Relat. Phenom. 1983, 31, 101.

Campbell, C. T.; Paffett, M. T. Surf. Sci. 1984, 143, 517.

Constant, L.; Krenzer, B.; Stenzel, W.; Conrad, H.; Bradshaw, A. M. Surf. Sci. 1999, 428, 262.

Guo, X. C.; Madix, R. J. J. Phys. Chem. B 2001, 105, 3878.

Krenzer, B.; Constant, L.; Conrad, H. Surf. Sci. 1999, 443, 116.

Madix, R. J.; Solomon, J. L.; Stohr, J. Surf. Sci. 1988, 197, L253.

Okawa, Y.; Tanaka, K. Surf. Sci. 1995, 344, L1207.

Prince, K. C.; Bradshaw, A. M. Surf. Sci. 1983, 126, 49.

Prince, K. C.; Paolucci, G. J. of Electron Spectrosc. and Relat. Phenom. 1985, 37, 181.

Ricken, D. E.; Somers, J. S.; Robinson, A. W.; Bradshaw, A. M. J. Chem. Phys. 1991, 94, 8592.

Stensgaard, I.; Laegsgaard, E.; Besenbacher, F. J. Chem. Phys. 1995, 103, 9825.

Stuve, E. M.; Madix, R. J.; Sexton, B. A. Chem. Phys. Lett. 1982, 89, 48.

Ojifinni, R. A.; Froemming, N. S.; Gong, J. L.; Pan, M.; Kim, T. S.; White, J. M.; Henkelman, G.; Mullins, C. B. In preparation 2008.

Gottfried, J. M.; Elghobashi, N.; Schroeder, S. L. M.; Christmann, K. *Surf. Sci.* **2003**, *523*, 89.

Gottfried, J. M.; Schmidt, K. J.; Schroeder, S. L. M.; Christmann, K. *Surf. Sci.* **2002**, *511*, 65.

Gottfried, J. M.; Schmidt, K. J.; Schroeder, S. L. M.; Christmann, K. *Surf. Sci.* **2003**, *525*, 184.

Gottfried, J. M.; Schmidt, K. J.; Schroeder, S. L. M.; Christmann, K. *Surf. Sci.* **2003**, *536*, 206.

Paul, A. M.; Bent, B. E. *J. Catal.* **1994**, *147*, 264.

Behm, R. J.; Brundle, C. R. *J. Vac. Sci. Tech. A 1* **1983**, *1*, 1223.

Vita

Rotimi Ayodele Ojifinni was born in Ijare, Nigeria on Sunday, August 10, 1975; the son of Abosede Rachel Ojifinni and Adebayo Cornelius Ojifinni. He attended St. Michael's Primary School and then Unity Secondary School, Ado Ekiti for elementary and secondary schools respectively. In September 1993, Rotimi began his undergraduate studies at the Obafemi Awolowo University, Ile – Ife and received a Bachelor of Science in Metallurgical and Materials Engineering in the Spring of 2000. Rotimi joined Andersen and KPMG in August 2000, where he worked as a Business Consultant before he entered the Graduate School of the University of Texas in August 2003.

Permanent Address: 1618 W. 6th Street, Apt. F, Austin, TX 78703

This dissertation was typed by the author